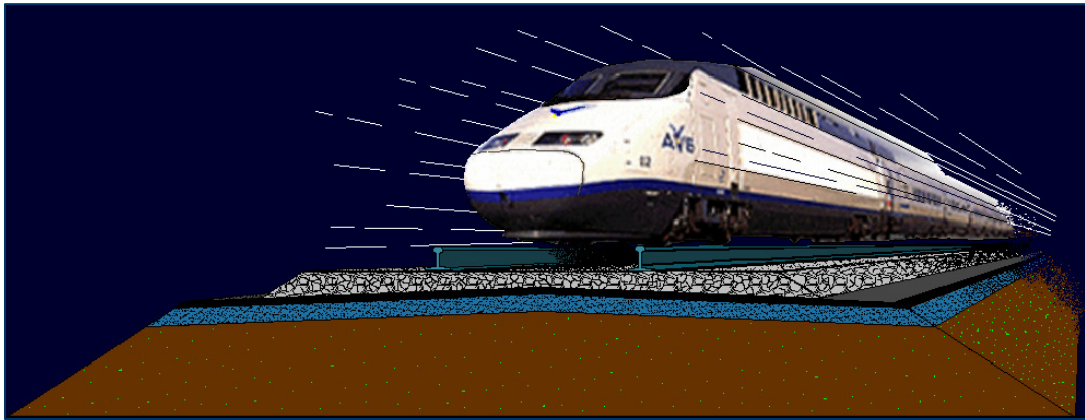




INSTITUTO SUPERIOR TÉCNICO  
Universidade Técnica de Lisboa



# **INFLUENCE OF INCORPORATING A BITUMINOUS SUB-BALLAST LAYER ON THE DEFORMATIONS OF RAILWAY TRACKBED**

**Tiago Moço Ferreira**

M.Sc Thesis in  
**Civil Engineering**

President:	Prof. Carlos dos Santos Pereira
Supervisor:	Prof. Paulo Manuel da Fonseca Teixeira
Co-supervisor:	Eng <sup>a</sup> . Maria Rafaela Pinheiro Cardoso
Member:	Prof. Emanuel José Leandro Maranha das

**Novembro de 2007**

# Acknowledgments

The author would like to thank the great encouragement, collaboration and motivation given since the beginning by Prof. Paulo F. Teixeira (supervisor), whose persistent guidance in sharing his valuable knowledge in this specific theme gave great support and confidence through the development of this work.

Special thanks to Prof. M. Rafaela Cardoso (co-supervisor) for the constant availability, continuous attendance, patience, persistence and positive attitude along the whole process.

The assistance with the finite elements program CODE\_BRIGHT provided by Dr. S. Olivella is greatly acknowledged.

## **Abstract**

The increase of high-speed traffic, the development of new commercial scenarios and the raise of maximum speeds to 350 km/h in the close future require the development of new low maintenance substructural solutions for high-speed ballasted tracks. Track design plays an important part in the performance of high-speed rail service.

This paper analyses theoretically the performance of a bituminous sub-ballast against environmental actions as an alternative to the conventional sub-ballast granular layers. The comparison between both designs is made in terms of the vertical displacements and its seasonal variation as well as the capability of maintaining the moisture content along the year.

The control of the displacements and their annual amplitude plays a central role when high-speed railway lines are considered. From a trackbed design perspective, the use of a bituminous sub-ballast as an alternative to the granular one, may improve the geometric performance of the railway infrastructure and contribute to an effective reduction of track maintenance needs.

From the different approaches developed, it is found that the bituminous sub-ballast may allow an important reduction in the seasonal vertical displacements, up to 50% or more under poor drainage conditions.

The cyclic nature of the vertical displacements leads to fatigue problems in the infrastructure as well as an increase in the number of maintenance operations. Being almost completely water-resistant, bituminous sub-ballast offers a higher protection of the formation along its life-time, increasing the trackbed life cycle.

## **Keywords**

High speed railway

Bituminous sub-ballast

Railway infrastructure

Railway trackbed deformations

## Resumo

O aumento do tráfego ferroviário de alta velocidade, o desenvolvimento de novos cenários comerciais e o incremento das velocidades máximas para os 350 km/h num futuro próximo, requerem o desenvolvimento de novas soluções de baixa manutenção para a infraestrutura de vias balastradas de alta velocidade. O dimensionamento das vias férreas desempenha um papel importante na performance do serviço de alta velocidade.

O presente artigo analisa de um ponto de vista teórico o comportamento de uma camada de sub-balastro betuminoso sob acções ambientais como alternativa às convencionais camadas de sub-balastro granulares. A comparação entre ambos os dimensionamentos é feita em termos dos deslocamentos verticais e da sua variação sazonal bem como pela sua capacidade de manter o teor em água ao longo do ano.

Em linhas de alta velocidade, verifica-se que o controlo dos deslocamentos e da sua amplitude anual é de extrema importância. Do ponto de vista do dimensionamento das camadas de assentamento, o uso de um sub-balastro betuminoso como alternativa às granulares, pode significar uma melhoria da qualidade geométrica da infraestrutura ferroviária e contribuir para uma redução efectiva nas necessidades de manutenção das vias.

Tendo em conta as diferentes abordagens desenvolvidas, é possível concluir que o sub-balastro betuminoso pode permitir uma importante redução ao nível dos deslocamentos verticais sazonais, superior a 50%, em más condições de drenagem.

A natureza cíclica dos deslocamentos verticais é responsável por problemas de fadiga ao nível da infra-estrutura e pelo aumento do número das operações de manutenção. Graças ao elevado nível de impermeabilização conferido pelo sub-balastro betuminoso, este oferece uma maior protecção das camadas de assentamento ao longo do seu período de vida levando a um aumento do ciclo de vida da infra-estrutura.

## Palavras-chave

Alta velocidade ferroviária

Sub-balastro betuminoso

Infraestrutura ferroviária

Deformações em plataformas ferroviárias

## Symbols

$e$	void ratio
$E$	Young modulus
$g$	gravity
$i_g^w$	non-advective water mass flux in gas phase
$n$	porosity
$N(s)$	specific volume at $p = p^c$
$p$	excess of mean stress over air pressure (net mean stress)
$p_{at}$	atmospheric pressure
$p_l$	liquid pressure
$p_g$	gas pressure
$p_0$	preconsolidation stress
$p_0^*$	preconsolidation stress for saturated conditions
$p^c$	reference stress
$q_l$	liquid advective flux
$r$	parameter defining the maximum soil stiffness
$RH$	relative humidity
$S_r$	degree of saturation
$s$	suction ( $= u_a - u_w$ )
$s_0$	hardening parameter of the suction increase yield curve
$T$	temperature
$u_a$	air pressure
$u_w$	water pressure
$v$	specific volume
$\omega_g^w$	mass fraction of water in gas phase
$\beta$	parameter controlling the rate of increase of soil stiffness with suction
$\varepsilon_v, \varepsilon_v^e, \varepsilon_v^p$	total, elastic and plastic volumetric strains
$\varepsilon_{vp}^e$	elastic volumetric strain induced by changes in net mean stress
$\varepsilon_{vp}^p$	plastic volumetric strain associated with the LC yield surface
$\varepsilon_{vp}$	$(\varepsilon_{vp}^e + \varepsilon_{vp}^p)$
$\varepsilon_{vs}^e$	elastic volumetric strain induced by changes in suction
$\varepsilon_{vs}^p$	plastic volumetric strain associated with the SI yield surface

$\varepsilon_{vs}$	$(\varepsilon_{vs}^e + \varepsilon_{vs}^p)$
$k$	elastic stiffness parameter for changes in net mean stress
$k_s$	elastic stiffness parameter for changes in suction
$\lambda(s)$	stiffness parameter for changes in net mean stress for virgin states of the soil
$\lambda_s$	stiffness parameter for changes in suction for virgin states of the soil
$\mu_l$	liquid viscosity
$\nu$	Poisson coefficient
$\rho_l$	liquid density

# Contents

<b>Acknowledgments</b> .....	1
<b>Abstract</b> .....	2
Keywords.....	2
<b>Resumo</b> .....	3
Palavras-chave.....	3
Symbols.....	4
Contents.....	6
List of Figures.....	8
List of Tables.....	11
<b>1. Introduction</b> .....	12
<b>2. Suction due to weather effects</b> .....	15
<b>3. Calculation of soil deformations by using the Barcelona Basic Model (BBM)</b> .....	17
3.1 Introduction.....	17
3.2 Description of BBM for Isotropic Stress States.....	17
3.3 Application of BBM to the case study.....	24
<b>4. Description of the analyzed cases</b> .....	28
4.1 Introduction.....	28
4.2 Case studies analyzed.....	28
4.3 Characteristics of the materials.....	30
4.4 Weather actions considered.....	31
<b>5. Simplified calculation</b> .....	32
5.1 Calculation procedure.....	32
5.2 Granular vs. Bituminous: parametric analysis.....	37
<b>6. CODE_BRIGHT description</b> .....	44
6.1 Introduction.....	44
6.2 Basic principles of the formulation.....	45
6.2.1 Water Mass Balance.....	46
6.2.2 Air Mass Balance.....	49
6.2.3 Energy Balance.....	51
6.2.4 Mechanical balance equations.....	52

<b>7. Models description and CODE_BRIGHT calibration.....</b>	<b>55</b>
7.1 Introduction .....	55
7.2 Cross Sections .....	55
7.3 Weather action considered .....	57
7.4 Materials constitutive models calibration.....	57
7.5 Boundary Conditions.....	60
7.6 Initial Unknowns.....	62
<b>8. Study on the performance of the two trackbed solutions for five years under poor     drainage conditions .....</b>	<b>63</b>
8.1 Introduction .....	63
8.2 Results for Bituminous and Granular sub-ballast designs.....	64
8.2.1 Temperature .....	64
8.2.2 Relative Humidity .....	65
8.2.3 Liquid Saturation .....	66
8.2.4 Vertical Displacements.....	70
8.3 Geometry influence in the hydraulic boundary conditions .....	74
8.3.1 Models considered .....	74
8.3.2 Extended cross sections .....	76
8.3.3 Lower cross sections.....	78
8.4 Conclusions about the performance of Original, Lower and Extended cross sections.....	79
8.5 Considerations on the drainage system.....	83
<b>9. Considerations regarding the Geometric Quality of high-speed railway track .....</b>	<b>84</b>
<b>10. Conclusions and Current Research .....</b>	<b>88</b>
<b>11. Bibliographic References .....</b>	<b>91</b>
<b>12. Annexes.....</b>	<b>93</b>

# List of Figures

<b>Fig.1</b> – Relationship between preconsolidation stresses $p_0$ and $p_0^*$ : (a) compression curves for saturated and unsaturated soil; (b) stress path and yield curve in $(p, s)$ stress plane .....	19
<b>Fig. 2</b> – Loading-collapse (LC) and suction increase (SI) yield curves Alonso et al., 1990). .....	22
<b>Fig. 3</b> – Initial conditions (stress and suction) in a representative point (A) – space $(p, s)$ . .....	24
<b>Fig. 4</b> – Independent paths in the $(p, s)$ plane - Plastic Deformations. ....	25
<b>Fig. 5</b> – Independent paths in the $(p, s)$ plane- Suction changes in the Elastic Region. ....	26
<b>Fig. 6</b> – Cross sections: (a) Granular sub-ballast; (b) Bituminous sub-ballast. ....	29
<b>Fig. 7</b> – Climates data: (a) Tropical (Moa, Cuba); (b) Mediterranean (Tarragona, Spain); (c) Subalpine (Camprodón, Spain). ....	31
<b>Fig. 8</b> – Line Control – Point A: (a) Granular Sub-ballast; (b) Bituminous Sub-ballast.....	33
<b>Fig. 9</b> – Relative Humidity registered on control points for a granular sub-ballast cross section (values calculated with CODE_BRIGHT). ....	34
<b>Fig. 10</b> – Example for RH reduction (30%). ....	37
<b>Fig. 11</b> – Example for Maximum amplitude of Vertical Displacements. ....	37
<b>Fig. 12</b> – Parametric Analysis for $\lambda$ – Tropical (Moa, Cuba): (a) $\lambda$ 's range 0-100%; (b) $\lambda$ 's range 50-100% .....	39
<b>Fig. 13</b> – Parametric Analysis for $\lambda$ – Mediterranean (Tarragona): (a) $\lambda$ 's range 0-100%; (b) $\lambda$ 's range 50-100% .....	40
<b>Fig. 14</b> – Parametric Analysis for $\lambda$ – Subalpine (Camprodón, Spain): (a) $\lambda$ 's range 0-100%; (b) $\lambda$ 's range 50-100% .....	41
<b>Fig. 15</b> – Bituminous reduction for maximum vertical displacements .....	43
<b>Fig. 16</b> – Bituminous sub-ballast cross section: (a) general design; (b) mesh (CODE_BRIGHT).....	55
<b>Fig. 17</b> – Granular sub-ballast cross section: (a) general design; (b) mesh (CODE_BRIGHT). ....	56
<b>Fig. 18</b> – Atmospheric variables of average representative year in Tarragona, Spain.....	57
<b>Fig. 19</b> – Boundary flow rate conditions.....	60
<b>Fig. 20</b> – Control Points: (a) Granular Sub-ballast; (b) Bituminous Sub-ballast. ....	63
<b>Fig. 21</b> – Temperature evolution during first year (Original Granular cross section $\alpha = 15\%$ ).....	64
<b>Fig. 22</b> – Temperature evolution on Points D, E and F along five years (Original Granular cross section) .....	65
<b>Fig. 23</b> – Relative Humidity evolution on Points D, E and F during five years (Original Granular cross section ( $\alpha = 15\%$ )).....	65

<b>Fig. 24</b> – Liquid Saturation evolution during 5 years (Original Bituminous cross section ( $\alpha = 15\%$ ))	66
<b>Fig. 25</b> – Liquid Saturation evolution on control points (Original Bituminous cross section ( $\alpha = 15\%$ ))	67
<b>Fig. 26</b> – Liquid Saturation evolution during 5 years (Original Granular cross section ( $\alpha = 15\%$ ))	68
<b>Fig. 27</b> – Liquid Saturation evolution on control points (Original Granular cross section ( $\alpha = 15\%$ ))	68
<b>Fig. 28</b> – Liquid Saturation evolution during 5 years (Original Granular cross section ( $\alpha = 30\%$ ))	69
<b>Fig. 29</b> – Liquid Saturation evolution on control points (Original Granular cross section ( $\alpha = 30\%$ ))	69
<b>Fig. 30</b> – Vertical Displacements variation on control points (Original Bituminous cross section ( $\alpha = 15\%$ ))	71
<b>Fig. 31</b> – Vertical Displacements variation on control points (Original Granular cross section ( $\alpha = 15\%$ ))	71
<b>Fig. 32</b> – Vertical Displacements variation on control points (Original Granular cross section ( $\alpha = 30\%$ ))	71
<b>Fig. 33 (a)</b> – Extended granular sub-ballast cross section: general design	74
<b>Fig. 33 (b)</b> – Extended granular sub-ballast cross section: mesh (CODE_BRIGHT)	75
<b>Fig. 34</b> – Low bituminous sub-ballast cross section: (a) general design; (b) mesh (CODE_BRIGHT)	75
<b>Fig. 35</b> – Relation between original and alternative designs using bituminous sub-ballast	82
<b>Fig. 36</b> – Track defects: a) Track gauge; b) Horizontal defect; c) Longitudinal defect; d) Transverse defect; e) Local distortion	85
<b>Fig. 37</b> – Recording vehicle (Mauzin) – register for the longitudinal defects	85
<b>Fig. 38</b> – Register for Longitudinal defects: Granular vs. Bituminous	87
<b>Fig. A1</b> – Liquid Saturation evolution along 5 years (Extended Bituminous cross section ( $\alpha = 15\%$ ))	93
<b>Fig. A2</b> – Liquid Saturation evolution on control points (Extended Bituminous cross section ( $\alpha = 15\%$ ))	93
<b>Fig. A3</b> – Liquid Saturation evolution during 5 years (Extended Granular cross section ( $\alpha = 15\%$ ))	94
<b>Fig. A4</b> – Liquid Saturation evolution on control points (Extended Granular cross section ( $\alpha = 15\%$ ))	94
<b>Fig. A5</b> – Liquid Saturation evolution during 5 years (Extended Granular cross section ( $\alpha = 30\%$ ))	95
<b>Fig. A6</b> – Liquid Saturation evolution on control points (Extended Granular cross section ( $\alpha = 30\%$ ))	95
<b>Fig. A7</b> – Vertical Displacements variation on control points (Extended Bituminous cross section ( $\alpha = 15\%$ ))	96
<b>Fig. A8</b> – Vertical Displacements variation on control points (Extended Granular cross section ( $\alpha = 15\%$ ))	96
<b>Fig. A9</b> – Vertical Displacements variation on control points (Extended Granular cross section ( $\alpha = 30\%$ ))	96
<b>Fig. A10</b> – Liquid Saturation evolution along 5 years (Lower Bituminous cross section ( $\alpha = 15\%$ ))	97

<b>Fig. A11</b> – Liquid Saturation evolution on control points (Lower Bituminous cross section ( $\alpha = 15\%$ )).....	97
<b>Fig. A12</b> – Liquid Saturation evolution during 5 years (Lower Granular cross section ( $\alpha = 15\%$ )).....	98
<b>Fig. A13</b> – Liquid Saturation evolution on control points (Lower Granular cross section ( $\alpha = 15\%$ )). .....	98
<b>Fig. A14</b> – Liquid Saturation evolution during 5 years (Lower Granular cross section ( $\alpha = 30\%$ )). .....	99
<b>Fig. A15</b> – Liquid Saturation evolution on control points (Lower Granular cross section ( $\alpha = 30\%$ )).....	99
<b>Fig. A16</b> – Vertical Displacements variation on control points (Lower Bituminous cross section ( $\alpha = 15\%$ )). .....	100
<b>Fig. A17</b> – Vertical Displacements variation on control points (Lower Granular cross section ( $\alpha = 15\%$ ))....	100
<b>Fig. A18</b> – Vertical Displacements variation on control points (Lower Granular cross section ( $\alpha = 30\%$ )).. ..	100

## List of Tables

<b>Table 1</b> – Model Parameters for different types of soil (from Alonso, 1998) .....	30
<b>Table 2</b> – Relative Humidity reductions with depth (Granular Sub-ballast).....	35
<b>Table 3</b> – Relative Humidity reductions with depth (Bituminous Sub-ballast). .....	36
<b>Table 4</b> – Properties and parameters for flow, temperature and deformation analysis (Alonso, 1998). .....	54
<b>Table 5</b> – Material Models and Parameters.....	58
<b>Table 6</b> – Numerical values for boundary flow rate. ....	62
<b>Table 7</b> – Initial unknowns: Porosity, Liquid Pressure, Temperature and Stress.....	62
<b>Table 8</b> – Vertical Displacements (Original Bituminous cross section ( $\alpha = 15\%$ )).....	72
<b>Table 9</b> – Vertical Displacements (Original Granular cross section ( $\alpha = 15\%$ and $\alpha = 30\%$ )).....	73
<b>Table 10</b> – Ranges for Qualitative reduction performed by bituminous sub-ballast – Displacements. ....	73
<b>Table 11</b> – Vertical Displacements (Extended Bituminous cross section ( $\alpha = 15\%$ )).....	77
<b>Table 12</b> – Vertical Displacements (Extended Granular cross section ( $\alpha = 15\%$ and $\alpha = 30\%$ )).....	77
<b>Table 13</b> – Ranges for Qualitative reduction performed by bituminous sub-ballast – Displacements (Extended cross section).....	77
<b>Table 14</b> – Vertical Displacements (Lower Bituminous cross section ( $\alpha = 15\%$ )).....	79
<b>Table 15</b> – Vertical Displacements (Lower Granular cross section ( $\alpha = 15\%$ and $\alpha = 30\%$ )).....	79
<b>Table 16</b> – Ranges for Qualitative reduction performed by bituminous sub-ballast – Displacements (Lower cross section).....	79
<b>Table 17</b> – Ranges for Vertical Displacements and Liquid Saturation on interior control points (Bituminous cross sections ( $\alpha = 15\%$ )).....	80
<b>Table 18</b> – Ranges for Vertical Displacements and Liquid Saturation on interior control points (Granular cross sections ( $\alpha = 15\%$ and $\alpha = 30\%$ )).....	80
<b>Table 19</b> – Ranges for Qualitative reduction performed by bituminous sub-ballast Displacements and Liquid Saturation.....	81
<b>Table 20</b> – Limits for corrective operations – Influence of speed in Geometric Quality. ....	86
<b>Table 21</b> – Longitudinal defects – Standard deviation and Maximum values on isolated points. ....	87

# 1. Introduction

Since the first high-speed railway lines, high speed rail has proved to be one of the most competitive on intercity medium distances. The improvements made on the railway track design, among other aspects, have played an important role on the development of the performance of this transport mean.

In recent years, the maximization of the use of the infrastructure with the development of new commercial situations (very high-speeds, mixed traffic, the network effect on European scale) seem to lead the conventional ballasted configuration to a certain limit requiring higher maintenance needs and lower maintenance intervals. These factors are responsible for a general increase of track maintenance costs.

Important improvements were performed both on the superstructure (rail, fastenings, sleepers and ballast) and on the infrastructure (sub-ballast-subgrade system). Different granular sub-ballast layers enable to achieve a good structural behaviour suitable for high-speed traffic have been introduced.

Almost all European high-speed ballasted tracks built so far use granular material (sand and gravel). In some cases, the difficulties to accomplish the stiffness standards led to the use of cement-treated soils and cement treated gravels instead of the traditional granular layers. Moreover, in certain Railway Administrations an asphalt trackbed is used as an alternative to these granular solutions. Furthermore, an asphalt trackbed was applied in the first high-speed tracks in Japan and in Italy.

The interest of this alternative solution (bituminous sub-ballast) must be discussed considering the following aspects: the technical feasibility and the design requirements for a solution with this material, in order to fulfill the required standards for the new high-speed lines; the effective role of this solution in the reduction of track maintenance needs.

From a theoretical point of view, a bituminous sub-ballast may perform structural advantages (reductions on tensile strain levels on the sub-ballast and on vertical stresses on the ballast and subgrade) when compared with a granular one.

Nevertheless, the aim of this work is to discuss the importance of a bituminous sub-ballast layer in terms of the protection provided by it against environmental conditions.

Track long-term behaviour highly depends on the evolution of formation quality along its life cycle. The use of sand and gravel layers on conventional high-speeds lines aims to fulfill an accurate protection of the formation not only against traffic load, but also against weather effects. However, it is found that along the track lifetime those layers tend to loose their filter characteristics, reducing the subgrade protection and resulting in possible ballast or subgrade contamination.

Being almost completely water-resistant, the bituminous sub-ballast may offer important comparative advantages from the point of view of long term deterioration of the subgrade, when compared to the granular solutions. Besides these possible advantages, it is intended to analyze its influence in maintaining the moisture content along the year, a very important factor on its deterioration process.

Railway infrastructure is composed by different soil layers, which are generally exposed to seasonal moisture changes due to weather actions. Rainfall, changes in the relative humidity and in temperature lead to water infiltration/evaporation into the ground, resulting in soil moisture fluctuations. The variations in the water content of the soil are associated with volume changes (swelling and shrinking) which are responsible for vertical displacements. Depending on their amplitude, these displacements may cause serious structural problems in the railway infrastructure. Moreover, the seasonal alternate wetting-drying cycles are responsible for alternate displacements, which eventually lead to fatigue problems and to the degradation of the mechanical properties of the soil (mainly strength decrease and compressibility increase).

Wetting and drying cycles, due to weather effects, result in strong changes in suction. The mechanics of partially saturated soils is considered to be appropriate to perform the calculation of displacements due to environmental changes. This calculation it is not a simple task once it is necessary to calculate changes in suction and then the associated soils deformations. The relative humidity (RH) of the air on the soil voids is the one to calculate the associated soil suction and it is used in the Psychrometric Law (Eq. (1)) presented in Chapter 2 where suction is described.

Suitable unsaturated soils constitutive models are required for the calculation of soil deformations due to suction changes. At the present there are available in the bibliography increasing number of unsaturated soil constitutive models (Alonso et al. (1990); Wheeler (1991); Toll (1990); Vanapalli, et al. (1996); Loret et Khalili (2002) among others). The description of these models is out of the scope of this work and any model considered to be adequate to model the soil behavior under suction variation could be chosen. The model used in this work is the Barcelona Basic Model, BBM, proposed by Alonso et al. (1990). The reasons that lead to its choice are its simplicity and also because several geotechnical commercial programs that allow calculations in unsaturated conditions are now including it in their codes (Plaxflow, Abacus, etc).

In this work, two methods are used for the calculation of the relative humidity/suction in the soil. The first one is a very simple approach where it is assumed that the soil would have a given percentage of the relative humidity of the surrounding environment and uses the BBM to calculate the deformations associated to it. Chapters 3, 4 and 5 describe BBM and the way it is used in this work. The second method uses the numerical program for finite elements CODE\_BRIGTH (Olivella et al. (1994)) to perform this calculation and is present in Chapters 6, 7 and 8.

BBM gives an acceptable description of the stress-strain behaviour of partially saturated soils. This model is formulated within the framework of hardening plasticity using total stress over air pressure (net mean stress) and suction as independent set of variables. It allows simulate the different types of deformations (swelling or collapse) occurring on partially saturated soils under suction changes observed in practice, as also as predicting the contribution of suction to stiffening the soil against external loading. This last one is a well proved result when compacted samples either dry or wet of optimum are loaded in compression, as extensively reported in the bibliography (for example, Sivakumar and Wheeler (2000), Alonso (2004)). BBM model and its formulation are presented in Chapter 3. The case studies analyzed with this model are described

in Chapter 4 as well as the materials composing the different layers and the weather actions considered. A simplified calculation is described in Chapter 5, which includes a parametric analysis for the relative humidity reduction performed by the bituminous sub-ballast allowing a direct comparison between the performances of the bituminous and granular solutions in terms of the maximum amplitude of displacements.

The Relative Humidity values in the soil voids are affected by the water supplied from the environment (rainfall and relative humidity of the surrounding air). It is necessary to have an adequate formulation to rule the exchanges of water in both vapour and liquid phases between soil and the environment. The exchange between these two media is ruled by evaporation (therefore by temperature), by the amount of liquid water supplied from rain, by the soil water and air permeability (that changes with the saturation degree) and by the soil water retention properties. This calculation is mathematically complex and requires the use of adequate computational tools. The finite elements program CODE\_BRIGHT presented in Chapter 6 is able to carry out this simulation. This numerical program allows a complete and accurate description of the whole problem. Its formulation considers the hydraulic constitutive equations controlling the balance of water in the liquid and gas phases adopting Darcy's law, Fick's law in the calculation of the diffusive and dispersive fluxes and Fourier's law for the calculation of the conductive flux of heat. The intrinsic permeability is calculated by Kozeny's model and for the definition of the water retention curve it is used the Van Genuchten model (Van Genuchten, (1980)).

The numerical models of the two trackbed solutions analyzed in this work as well as their calibration for CODE\_BRIGHT calculation are presented in Chapter 7. The models are used to carry out sensitivity and evaluation studies for different physical phenomena that drive to moisture changes in trackbed layers. Alternative geometry for cross sections design and different percentages of rain infiltration are also considered and analyzed in Chapter 8, where the results in terms of vertical displacements and their amplitude are presented for all cases as well as the results from calculation used to validate it, namely the seasonal evolution in time of the temperature, degree of saturation and relative humidity.

Chapter 9 describes the most important parameters related with geometric quality of high-speed railway tracks. The importance of the displacements' control provided by possible improvements in the trackbed design as well as its contribution to an effective reduction of track maintenance needs is also discussed in this chapter.

Final considerations to the results obtained for both methods (BBM theoretical approach and CODE\_BRIGHT application) as well as the conclusions and future research on the use of bituminous sub-ballast are presented in Chapter 10.

## 2. Suction due to weather effects

Wetting and drying cycles, controlled by atmospheric changes, result in strong changes in suction. It is necessary to have an adequate formulation to rule the exchanges of water in both vapour and liquid phases between soil and the environment. Compacted soils as well as natural soils near ground surface are not saturated, therefore it is considered appropriate to use concepts associated with the mechanics of unsaturated soils to compute the displacements due to weather effects. The calculation of displacements due to weather actions is a difficult task because it is necessary to calculate suction changes in the soil associated to weather effects and then, with those suction changes, calculate the soil deformations.

Suction can be defined as the free energy state of soil water and can be measured in terms of the partial vapour pressure of the soil water (Fredlund and Rahardjo, 1974). The thermodynamic relationship between total suction and the partial pressure of the pore-water vapour is the Psychrometric Law and can be written as follows:

$$\psi = -\frac{RT}{v_{w0} w_v} \ln\left(\frac{\bar{u}_v}{\bar{u}_{v0}}\right) \quad (1)$$

where

$\psi$  - soil suction or total suction (kPa);

$R$  - universal (molar) gas constant [i.e., 8.31432 J/(mol K)] ;

$T$  - absolute temperature [i.e.,  $T = (273.16 + t^0)$  (K)] ;

$t^0$  - temperature ( $^{\circ}\text{C}$ );

$v_{w0}$  - specific volume of water or the inverse of the density of water [i.e.  $1/\rho_w$  ( $\text{m}^3/\text{kg}$ )];

$\rho_w$  - density of water [i.e., 998 kg/m<sup>3</sup> at  $t^0 = 20^{\circ}\text{C}$ ] -  $\rho_w = 1007,9 \exp^{-4,573 \times 10^{-4} T}$  ;

$w_v$  - molecular mass of water vapour (i.e., 18.016 kg/kmol);

$\bar{u}_v$  - partial pressure of pore-water vapour (kPa);

$\bar{u}_{v0}$  - saturation pressure of water vapour over a flat surface of pure water at the same temperature (kPa);

The term  $\bar{u}_v/\bar{u}_{v0}$  is the relative humidity, RH (%). For a selected temperature of 20 $^{\circ}\text{C}$ , the equation can be written to give a fixed relationship between total suction and relative vapour pressure:

$$\psi = -135002 \cdot \ln(RH) \quad (2)$$

An accurate calculation of suction implies considering temperature. Suction is affected by temperature in a non linear way: explicitly in Equation (1) and also in the calculation of the density of water,  $\rho_w$ , as express in Equation 3:

$$\rho_w = 1007,9 \exp^{-4,573 \times 10^{-4} T} \quad (3)$$

The soil suction,  $\psi$ , is equal to 0.0 MPa when the relative humidity, RH, is equal to 100%. A relative humidity value less than 100% indicates the presence of suction in the soil.

Except in the arid regions, the range of suctions of interest in geotechnical (and railway) engineering will correspond to high relative humidity since the water tables in the soils are near the surface, indicating high degrees of saturation.

Total suction,  $\psi$ , is made up of two components, namely, the matric suction,  $(u_a - u_w)$ , and the osmotic suction,  $\pi$ :

$$\psi = (u_a - u_w) + \pi \quad (4)$$

Matric suction (associated with capillary phenomenon) is known to vary with time due to environmental changes and any change affects the overall equilibrium of the soil mass. Osmotic suction is related to the salt content in the pore-water and can control the mechanical behavior of a soil in case of changes on the chemical composition of the capillary water.

Measurements of total, matric and osmotic suction (Krahn and Fredlund, 1972) show that matric suction is the main responsible in total suction variations, particularly in the higher water content range. In other words, a change in total suction is essentially equivalent to a change in the matric suction (Eq. (5)):

$$\Delta \psi \approx \Delta(u_a - u_w) \quad (5)$$

Since the deformations due to alternate wetting and drying cycles are related to suction changes, Equation (5) justified the use in this work of the word suction to represent both total and matric suctions.

Finally, soil and the surrounding air exchange water in the gas (vapour) and/or in the liquid phase but the amounts exchanged depend on the soil's water retention capability. In fact, the water in the liquid phase present in the soil (with a given pressure named liquid pressure,  $u_w$ ) depends on many factors such as soil grading size and soil density (pore dimensions and geometry). To use Equation (1) in a realistic way, the relative humidity considered must be the one of the air from the soil voids (in equilibrium with the water in the liquid phase of the soil), and not the one of the atmosphere.

### 3. Calculation of soil deformations by using the Barcelona Basic Model (BBM)

#### 3.1 Introduction

This chapter describes the Barcelona Basic Model, BBM, (Alonso et al., 1990) and the way it is used in this work to calculate the deformations of the soil due to suction changes.

BBM is a hardening elastoplastic constitutive model appropriated to model the behaviour of slightly or moderately expansive soils. It provides the mathematical formulation to calculate the soil deformations due to suction changes and/or stress changes and tries to incorporate some features of the behaviour of partially saturated soils that have been supported by experimental results, such as:

- Partially saturated soils may either expand or collapse on wetting, depending on the confining stress (low stress leads to expansion; high stress leads to soil collapse);
- During the wetting process, if samples are subjected to a suction reduction from a relatively high initial value they may first show some expansion followed by collapse;
- Paths which involve loading steps and non-increasing suction or an increasing in suction for a constant load are essentially path independent; the volumetric response of unsaturated soils depends not only on the initial and final stress and suction values but on the particular path followed from the initial to the final state;
- An increase in suction may result in irrecoverable deformation;
- An increase in suction results in an increase in effective cohesion while maintaining constant the (saturated) friction angle  $\phi$ ; increasing suction leads to a non-linear increasing of strength and a tendency towards a maximum at some given (high) suction.

In this work, due to the nature of the case studied, relevance will be given only to the application of the model to simulate the volumetric response of the soil when loaded isotropically or in oedometric conditions. In this work it will be referred the BBM formulation considering isotropic stress states, which is easily extended to oedometric conditions.

#### 3.2 Description of BBM for Isotropic Stress States

BBM is based in two independent sets of stress variables: the excess of total stress over air pressure,  $p$ , and suction,  $s$ , defined according to Equations (6) and (7), respectively:

$$p = \sigma_m - u_a \quad (6)$$

$$s = u_a - u_w \quad (7)$$

where

$\sigma_m$  - excess of mean stress

$u_a$  - air pressure

$u_w$  - water pressure

In accordance with saturated soils behavior, the specific volume,  $v = 1 + e$ , for  $p$ -load increments along virgin states at a given suction (normal compression line, NCL), will be given by Equation (8):

$$v = N(s) - \lambda(s) \ln \frac{p}{p^c} \quad (8)$$

where  $p^c$  is a reference stress state for which  $v = N(s)$  and  $\lambda(s)$  is the soil compressibility for isotropic stress changes under constant suction  $s$ . On unloading and reloading (at constant  $s$ ) the soil is supposed to behave elastically with compressibility,  $k$ , which is assumed to be independent from suction as presented in Equation (9):

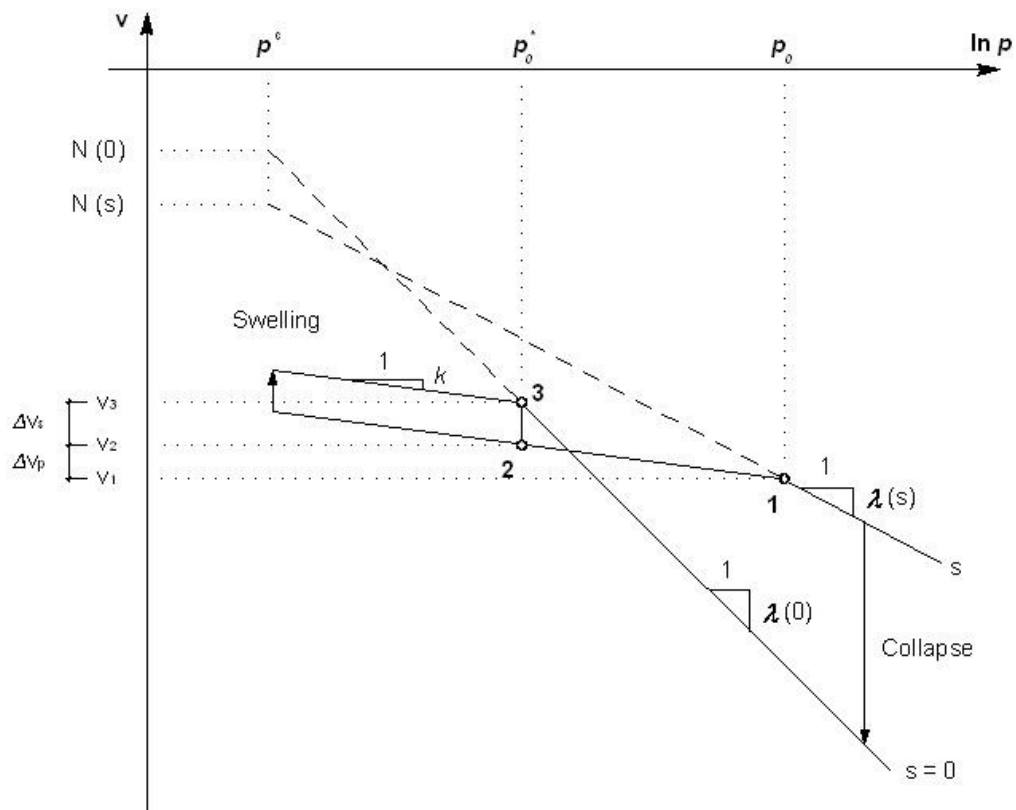
$$dv = -k \frac{dp}{p} \quad (9)$$

A schematic representation of Equations (8) and (9) is given in Figure 1.a, and the contribution of suction to stiffening the soil against external loads (increase in  $p$ ) can be observed since the slope of the NCL for suction  $s$ ,  $\lambda(s)$ , is lower than the one of the NCL for the saturated state,  $\lambda(0)$ .

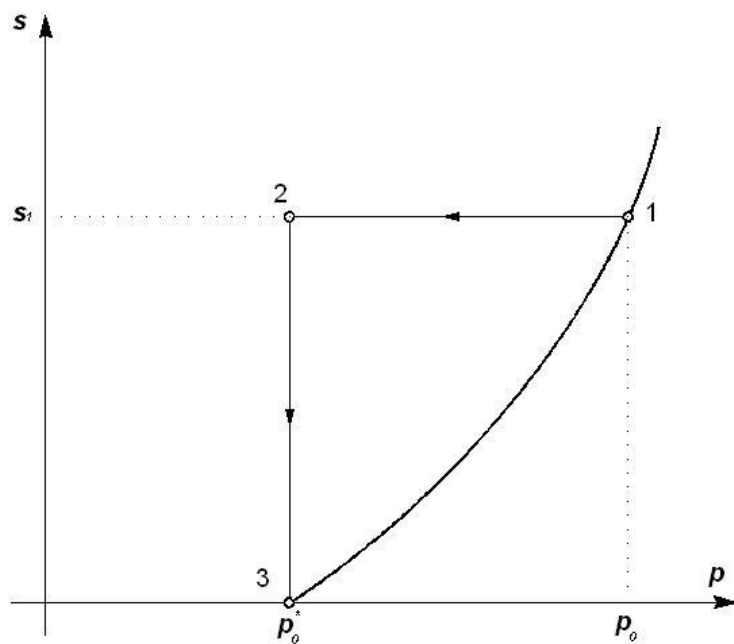
The changes in soil compressibility due to different suctions,  $\lambda(s)$ , can be calculated with Equation (10), where  $\lambda(0)$  is the compressibility for saturated conditions.

$$\lambda(s) = \lambda(0)[(1 - r) \cdot e^{-\beta s} + r] \quad (10)$$

In Equation (10),  $r$  is a constant related to the maximum stiffness of the soil (for an infinite suction),  $r = \lambda(s \rightarrow \infty) / \lambda(0)$ , and  $\beta$  is a parameter which controls the rate of increase of soil stiffness with suction. Parameters  $r$  and  $\beta$  are usually adjusted from experimental data.



(a)



(b)

**Fig.1 – Relationship between preconsolidation stresses  $p_0$  and  $p_0^*$ : (a) compression curves for saturated and unsaturated soil; (b) stress path and yield curve in  $(p, s)$  stress plane (Alonso et al., 1990).**

In Figure 1 is represented the response to isotropic loading of two samples subjected to different suctions:  $s = 0$  (saturated case) and a larger suction  $s_1$  (driest sample). The saturated preconsolidation stress (first yield stress for the saturated sample) is labeled  $p_0^*$  (point 3 in Figure 1). The driest sample (suction  $s_1$ ) will yield at a larger isotropic stress  $p_0$  (point 1 in Figure 1).

If points 1 and 3 belong to the same yield curve in a  $(p, s)$  stress plane (Figure 1.b), it is possible to obtain a relationship between the generic yield stress,  $p_0$ , and the saturated value,  $p_0^*$ , by relating their specific volumes through a virtual path (path 1-2-3 in Figure 1). This path involves an initial unloading from  $p_0$  to  $p_0^*$  at constant suction (path 1-2), followed by wetting from  $s_1$  to zero at constant stress ( $p_0^*$ ) (path 2-3). The change in the specific volume along the path 1-2-3 is given by Equation (11):

$$v_1 + \Delta v_p + \Delta v_s = v_3 \quad (11)$$

where the different quantities are indicated in Figure 1.a.

According to Figure 1, the path from 2 to 3 (wetting) occurs in the elastic domain and gives origin to a reversible swelling,  $\Delta v_s$  (logarithmic expression similar to Equation (9)), where  $k_s$  is the elastic compressibility for changes in suction and  $p_{at}$  is the atmospheric pressure ( $p_{at} = 0.1MPa$ ).

$$dv_s = -k_s \frac{ds}{(s + p_{at})} \quad (12)$$

A relationship between  $p_0$  and  $s$  as a function of some reference stress values ( $p_0^*$ ,  $p^c$ ) and selected soil parameters ( $N(s)$ ,  $\lambda(s)$ ,  $k$ ,  $k_s$ ) is provided when Equations (8), (9) and (12) are taking into account:

$$N(s) - \lambda(s) \ln \frac{p_0}{p^c} + k \ln \frac{p_0}{p_0^*} + k_s \ln \frac{s + p_{at}}{p_{at}} = N(0) - \lambda(0) \ln \frac{p_0}{p^c} \quad (13)$$

A convenient choice of  $p^c$  and  $N(s)$  simplifies Equation (13) (Figure 1.a):

$$\Delta v(p^c) \Big|_s^0 = N(0) - N(s) = k_s \ln \frac{s + p_{at}}{p_{at}} \quad (14)$$

that means that  $p^c$  is the net mean stress at which one may reach the saturated virgin state, starting at an unsaturated condition, through a wetting path which involves only swelling.

Introducing Equation (14) in Equation (13) is possible to obtain Equation (15) that corresponds to the equation of the curve from Figure 1.b that starts in  $p_0^*$  and where points 1 and 3 are represented. This curve is named LC curve (from loading collapse, as following explained):

$$\left(\frac{p_0}{p^c}\right) = \left(\frac{p_0^*}{p^c}\right)^{[\lambda(0)-k]/[\lambda(s)-k]} \quad (15)$$

With Equation (15) it is possible to calculate the yield stress  $p_0$  corresponding to any isotropic loading under constant suction,  $s$ , if the preconsolidation net mean stress for saturated conditions,  $p_0^*$ , is known. Assuming isotropic loading at constant suction for stresses higher than the yielding stress, hardening will occur because the new yield stress will be the higher isotropic stress ever reached along loading. This corresponds to a translation of the curve to the right, increasing the elastic range. Since all the yielding stresses for any suction are related by Equation (15) and  $p_0^*$  is the one value they have in common, this stress can be used as hardening parameter.

Assuming now that wetting was done under constant mean stress inferior to  $p_0^*$  (path 2-3, for example), since point 3 is inside the elastic range defined by the LC curve, the volumetric deformations would be elastic (swelling deformations) and given by Equation (12). If wetting would be done under constant mean stress superior to  $p_0^*$  the saturated point would be out of the elastic range and plastic or irrecoverable deformations (collapse deformations) would occur; the LC curve would have to translate to include all the points. Yielding will occur and  $p_0^*$  will increase to the value of the maximum saturated mean stress reached.

As mentioned in the introduction of this chapter, an increase in suction may also induce irrecoverable strains. In this model, Alonso et al. (1990) proposed that whenever the soil reaches a maximum previously attained value of the suction  $s_0$ , irreversible strains will begin to develop. The yield condition from Equation (16) is adopted, where  $s_0$  has the meaning of the maximum past suction ever experienced by the soil and bounds the transition from the elastic state to the virgin range when suction is increased. Equation (16) defines the yield locus named SI (after suction increase).

$$s = s_0 = \text{constant} \quad (16)$$

If a linear dependence between the void ratio ( $v$ ) and suction ( $\ln(s + p_{at})$ ) is assumed, the elasto-plastic volumetric deformations (for virgin states) can be described by Equation (17) and the elastic volumetric deformations can be described by Equation (12) previously presented.

$$dv_s = -\lambda_s \frac{ds}{(s + p_{at})} \quad (17)$$

Finally, in the  $(p, s)$  plane, both, LC and SI yield loci enclose an elastic region, as presented in Figure 2. The evolution of LC and SI yield surfaces with loading (net mean stress increase, suction increase or stress loading with changes in suction) is ruled by hardening laws, whose expressions must be defined for each one of them. The deduction of these laws is presented in the following paragraphs.

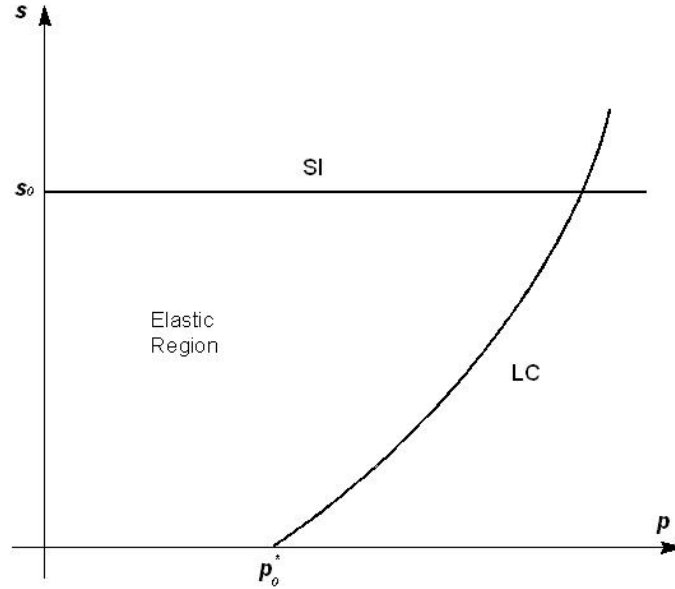


**Fig. 2 – Loading-collapse (LC) and suction increase (SI) yield curves Alonso et al., 1990).**

For LC yield curve, volumetric deformation for an increase of  $p$  in the elastic region can be defined by Equation (18) (similar to Eq. (9)). Knowing that the total volumetric deformation is given by Equation (19), the plastic component of volumetric strain (the difference between the total and the elastic volumetric deformation) is given by Equation (20).

$$d\epsilon_{vp}^e = -\frac{dv}{v} = \frac{k}{v} \frac{dp}{p} \quad (18)$$

$$d\epsilon_{vp} = \frac{\lambda(s)}{v} \frac{dp_0}{p_0} \quad (19)$$

$$d\epsilon_{vp}^p = \frac{\lambda(s) - k}{v} \frac{dp_0}{p_0} \quad (20)$$

Equation (20) can be written for the saturated state taking into account Equation (15) and the volumetric plastic deformation in the saturated state is given by Equation (21).

$$d\epsilon_{vp}^p = \frac{\lambda(0) - k}{v} \frac{dp_0^*}{p_0^*} \quad (21)$$

For SI yield curve, an increase in suction within the elastic region will lead to a volumetric strain defined by Equation (22) (similar to Eq. (12)). Knowing that the total volumetric deformation is given by Equation (23), the plastic volumetric strain (the difference between the total and the elastic volumetric ones) is given by Equation (24).

$$d\epsilon_{vs}^e = \frac{k_s}{v} \frac{ds}{(s + p_{at})} \quad (22)$$

$$d\epsilon_{vs} = \frac{\lambda_s}{v} \frac{ds_0}{(s_0 + p_{at})} \quad (23)$$

$$d\epsilon_{vs}^p = \frac{\lambda_s - k_s}{v} \frac{ds_0}{(s_0 + p_{at})} \quad (24)$$

Finally, LC and SI yield curves are coupled assuming that their position is controlled by the total plastic volumetric deformation,  $d\epsilon_v^p = d\epsilon_{vs}^p + d\epsilon_{vp}^p$ . Then, from Equations (21) and (24) the proposed hardening laws are Equations (25) and (26).

$$\frac{dp_0^*}{p_0^*} = \frac{v}{\lambda(0) - k} d\epsilon_v^p \quad (25)$$

$$\frac{ds_0}{s_0 + p_{at}} = \frac{v}{\lambda_s - k_s} d\epsilon_v^p \quad (26)$$

### 3.3 Application of BBM to the case study

The behaviour of partially saturated slightly or moderately expansive soils under paths which involve wetting and increase or decrease in mean stress may be modeled by BBM, which includes the LC yield curve and the associated yield surface in the  $(p, s)$  plane. This chapter presents the application of BBM to the calculation of the deformations observed in the foundation of railway infrastructure due to traffic loads and to soil suction changes due to weather.

Figure 3 presents the external actions in the foundation of railway infrastructure considered in this work. Traffic loads (mean stress increment) would be represented by a horizontal stress path ( $A_0 \rightarrow A_1$ ) and moisture changes (suction changes), at constant mean stress, would be represented by a vertical stress path ( $A_0 \rightarrow A_s$  for drying and  $A_0 \rightarrow A_h$  for wetting).

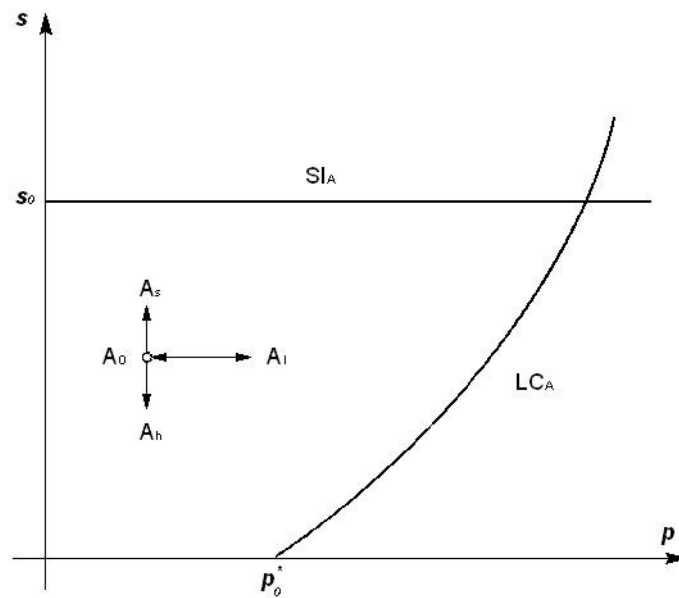


**Fig. 3 – Initial conditions (stress and suction) in a representative point (A) – space  $(p, s)$ .**

When using BBM, the initial state of a given compacted material involves the definition of its initial conditions such as the position of the yielding surfaces in  $(p, s)$  plane by  $p_0^*$  and  $s_0$  definition – range of the elastic domain – and the definition of other parameters necessary to calibrate the constitutive model adopted for that material.

According to BBM, plastic deformations may occur by following the independent paths in the  $(p, s)$  plane presented in Figure 4:

- (A) increase in  $p$ -load, at constant suction - (loading);
- (B) increase in suction, at constant stress - (drying);
- (C) decrease in suction, at a constant stress greater than  $p_0^*$  - (wetting);

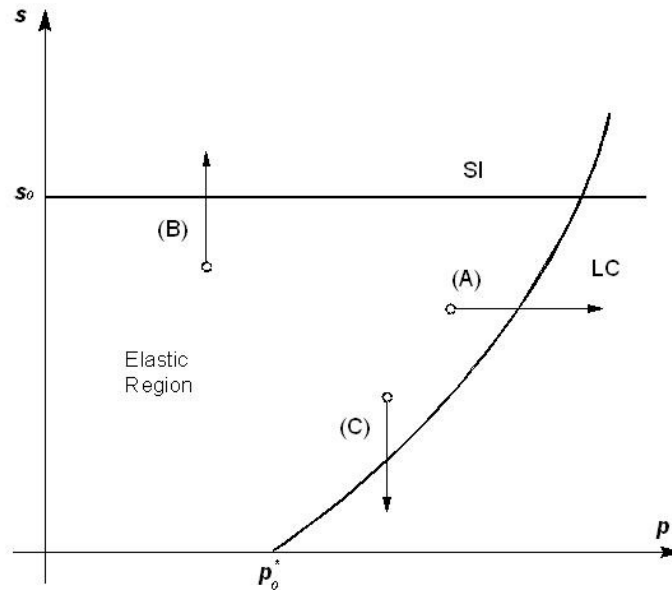


**Fig. 4 – Independent paths in the  $(p, s)$  plane - Plastic Deformations.**

Loading paths that lead to mean stresses or suction values out of the Elastic domain will lead to Plastic Deformations, therefore to a new definition of the LC and/or SI yield curves according to the hardening laws.

An adequate compaction is necessary to prevent the development of plastic deformations in service. A value for preconsolidation greater than the design loads in service (train, rails, sleepers, track support etc.) must be achieved to ensure that plastic deformations will not occur due to a LC translation (A) or wetting paths (C). An accurate description of the compaction process and previous studies on residual stresses induced by compaction has been addressed by many authors (Broms, 1971; Ingold, 1979; Jiménez Salas, 1980; Uzan, 1985; Seed and Duncan, 1986; Duncan et al., 1992).

In a railway infrastructure, the concerns with compaction and preconsolidation values to guarantee adequate performance levels, such the limitation of the deformations, are generally settled in the design and construction of the infrastructure, which include the definition of the compaction method adopted and the tests performed before the exploration of the railway. The future development of irrecoverable (plastic) deformations is intended to be avoided by the construction methods usually adopted once soil is exposed to high loads. In fact, usually the compaction process is done with heavy energy and the loads applied by auxiliary trains used in superstructure construction are similar to those applied in service. Moreover, before the railway opening to traffic, it is exposed to several tests from the point of view of the train utilization. All the reasons presented justified that the value of the preconsolidation stress of the soil,  $p_0^*$ , as well as

the correspondent LC yield curve will be fixed right after the construction, with a reduced probability to be reached higher values during exploration. This fact reduces the risk of a future collapse by a  $p$ -load independent path (A) as previously presented in Figure 4. The independent path (C) from Figure 4 leads to plastic deformations associated to wetting. This path has a very low or even null probability to occur because it corresponds to a decrease in suction under stress greater than  $p_0^*$  and this value is assumed to be fixed during the construction once the most unfavorable conditions are tested (highest vertical stresses applied to the soil almost saturated).

The value of the suction in the soil right after compaction depends on the compaction variables dry unit weight and water content ( $\gamma_d, w$ ). In standard compaction practice for formation layers and subgrades, moisture contents are close to optimum, which implies a degree of saturation in the range of 0.8 - 0.9, that corresponds to relatively low levels of suction (Alonso, 2004). A particular analysis of the railway infrastructure problem in terms of moisture content, may assume that the SI yield curve is defined during in the construction in Summer time, when soil dries. It seems reasonable to assume that the highest levels of suction ever reached by the soil would be at this stage and, if so, the SI yield curve will be defined during this period. The plastic deformations eventually developed in the construction may be recovered by appropriate equipment. For this reason it will be assumed in this work that the load path (B) previously presented in Figure 4 will not occur during exploration.

The reasons presented lead to the conclusion that the paths in the  $(p, s)$  space associated only to suction changes (under constant stress) to be considered in this work are in the elastic domain, as presented in Figure 5. Therefore, the Equation (22) presented in the last section will be the one used in the calculation of the deformations due to suction changes.

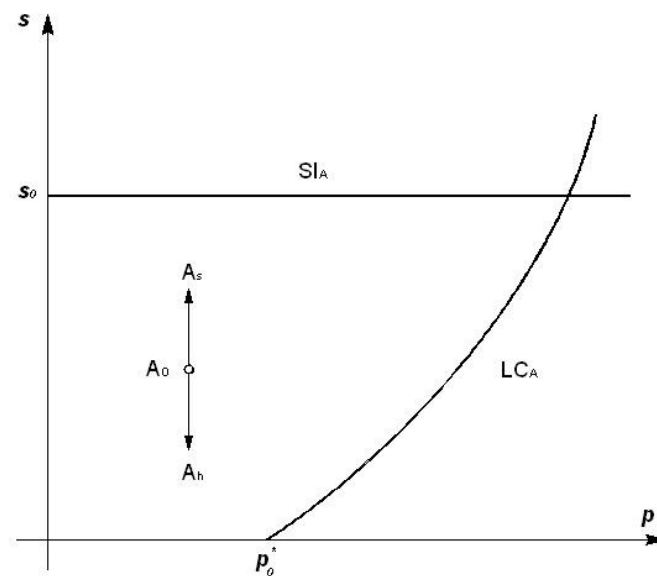


**Fig. 5 – Independent paths in the  $(p, s)$  plane- Suction changes in the Elastic Region.**

In spite of their reversible characteristics, elastic deformations have an important role in railway operation. Seasonal distributions as well as an irregular evolution are responsible for great implications in the railway maintenance costs once these elastic deformations can be considered irreversible (plastic) for small periods of time (associated to maintenance intervals). From this perspective, the understanding of elastic deformations and its control may lead to an improvement of the trackbed quality long term behaviour and the consequent reduction in maintenance costs.

## 4. Description of the analyzed cases

### 4.1 Introduction

Traditional sand and gravel sub-ballast can assure a good performance in the protection of the formation layers not only against traffic loads, but also against environmental conditions. However, its properties and filter characteristics tend to a degradation process along the track lifetime; this may lead to a reduction in the subgrade protection and to a possible ballast contamination.

The use of a bituminous sub-ballast may represent a significant improvement in the long term behaviour of the infrastructure because of its waterproofing properties, which helps to maintain the moisture content along the year. Changes in the moisture content have a negative impact in the railway since they are associated with alternate vertical displacements (swelling in winter and shrinkage in summer), even if their amplitude is considered to be small compared with service tolerances. The limitation of these displacements, however, may contribute to prevent the deterioration process of the formation layer and subgrade due to fatigue and to other effects associated to cyclic loading of the soils.

The evaluation of the possible advantages of using a bituminous sub-ballast layer instead of using a granular one can be done by comparing the long term performance of similar track characteristics in similar environmental conditions with the two different trackbed designs.

The comparison between the use of Granular or Bituminous sub-ballast considering their effects in the moisture content changes of the soil along the year can be done by evaluating the amplitude of the displacements calculated for each case. The calculation of these displacements can be made with the unsaturated soil constitutive model BBM (Alonso et al., 1990) that was presented in Chapter 3, where the expressions used to calculate the deformations due to changes in suction can be found. To allow this calculation it is necessary to relate the moisture content of the soil with the suction in it, which can be done with the knowledge of the soil's water retention curve. This curve, for each soil water content, allows determining the relative humidity of the air in the voids of the soil taken into account its nature, voids size and geometry. This implies that the Psychrometric Law (Eq. (1) previously presented in Chapter 2) can be used to convert relative humidity into suction installed in the soil only if the relative humidity of the air in the voids of the soil is used.

### 4.2 Case studies analyzed

The design of the cross sections, defined to compare both trackbed solutions mentioned in the introduction of this chapter, is made in order to simulate a 5 m high embankment and is based in typical geometry, material and thicknesses of trackbed layers. To reach an equivalent structural behaviour of a granular sub-ballast layer with 30 cm of thickness, a conventional

bituminous mix sub-ballast layer is design with 12 cm (as proposed by P.F. Teixeira et al. – “Optimization of high-speed ballasted tracks: the interest of using a bituminous sub-ballast layer”, 2005). Granular and Bituminous cross sections design are presented in Figure 6. The characteristics of the materials will be presented in next section.

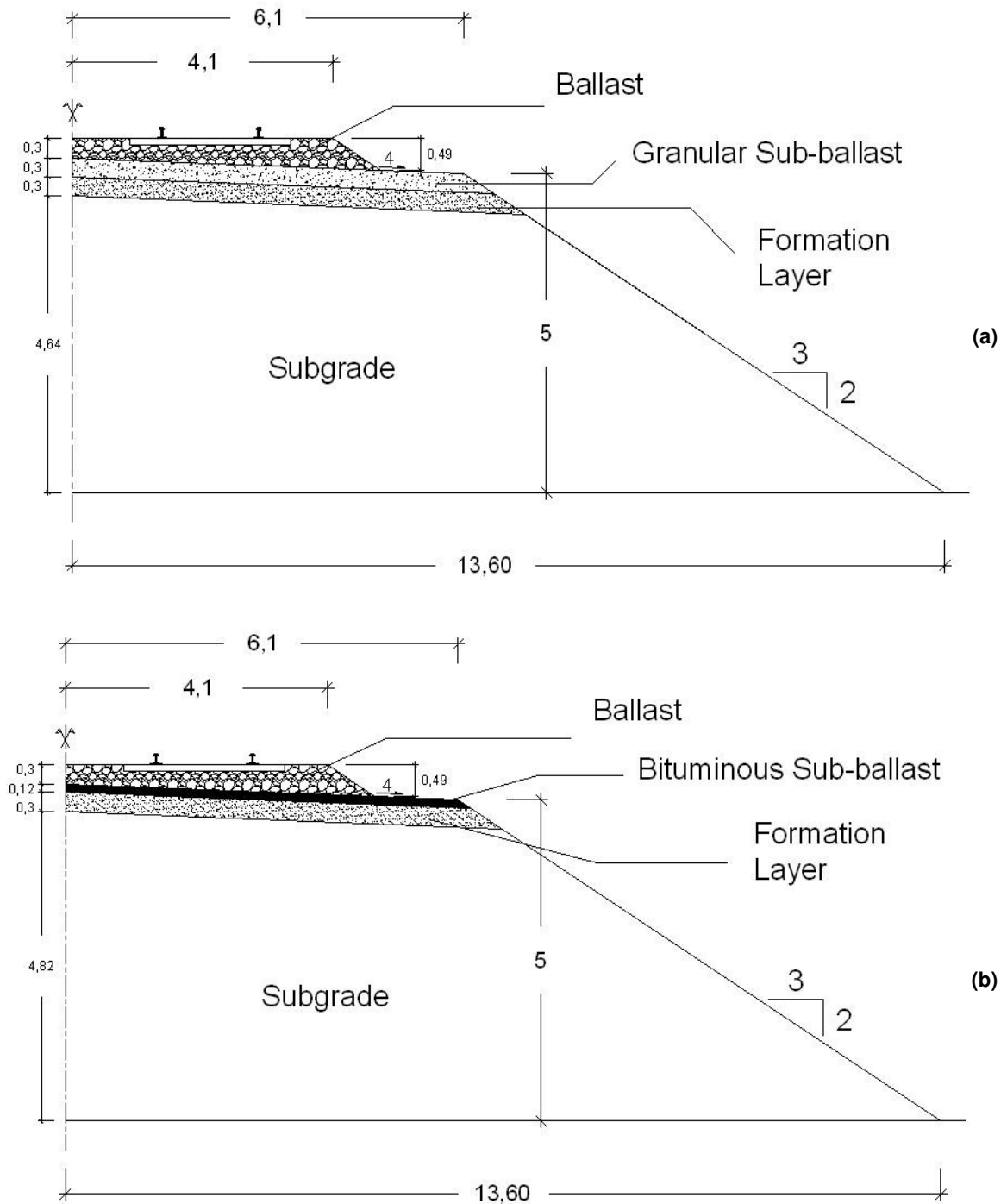


Fig. 6 – Cross sections: (a) Granular sub-ballast; (b) Bituminous sub-ballast.

### 4.3 Characteristics of the materials

The initial state of the formation layer and of the subgrade is controlled by the compaction conditions of the materials that compose each one of them. In a granular material (here granular means that it is not bituminous and should not be confused with the grading size), its initial state can be characterized by the dry density and water content, as also as by its initial stress state. All these variables define the initial properties of the granular layers: permeability, compressibility, strength and water retention properties.

For the calibration of BBM it is required the definition of the parameters of each material ( $p^c$ ,  $\lambda(0)$ ,  $k$ ,  $r$ ,  $\beta$  and  $k_s$ ). These parameters are related only with the elastic volumetric behavior of the soil, as previously explained in Chapter 3. Table 1 shows the parameters adopted for the soils considered in the cross sections presented in last section.

**Table 1 – Model Parameters for different types of soil**  
(from *Alonso, 1998*)

	Model Parameters						
	$\lambda(0)$	$k$	$r$	$\beta$ (MPa <sup>-1</sup> )	$p^c$ (MPa)	$\lambda_s$	$k_s$
(1) Reference Soil	0.200	0.020	0.75	12.5	0.100	0.080	0.008
(2) Compacted silty soil	0.140	0.015	0.26	16.4	0.043	0.050	0.010
(3) Lower Cromer till	0.066	0.008	0.25	20.0	0.012	-	0.001
(4) Compacted silty soil	0.065	0.011	0.75	20.0	0.010	0.025	0.005

The values presented in Table 1 were obtained from *Alonso, 1998*, for soils that can be currently found and often used in embankment constructions due to their low plasticity properties and low compressibility/adequate strength when compacted by standard compaction methods. These materials are described as follows:

**(1) Reference Soil** –Clayey soil (classification ML), moderately expansive, with low plasticity and with low compressibility when compacted ( $w_L = 29\%$  and  $IP = 18\%$ );

**(2) Compacted silty soil** – silty soil (classification ML) moderately expansive and with low compressibility when compacted ( $w_L = 39\%$  and  $IP = 12\%$ );

**(3) Lower Cromer till** – low plasticity sandy clay (classification SC, with clay fraction 15% in mass) (fines classification: ML;  $w_L = 25\%$  and  $IP = 15\%$ ) with compressibility when compacted lower that the one of soils (1) and (2);

**(4) Compacted Kaolin** – silty soil with clay (classification ML, with clay fraction 22% in mass) moderately expansive ( $w_L = 37\%$  and  $IP = 28\%$ ) with compressibility when compacted lower that the one of soils (1) and (2), and also less expansive than them.

## 4.4 Weather actions considered

In this work, three reference climates have been simulated (from *Alonso, 1998*):

- A **Tropical climate** (Figure 7.a) characterized by an uniform high Temperature ( $T_{av}=25.1^{\circ}\text{C}$ ) and high Relative Humidities ( $RH_{av} = 83.2\%$ );

- A **Mediterranean climate** (Figure 7.b) characterized by warm and dry summers and moderate winters ( $T_{av}=18^{\circ}\text{C}$ ). The Relative Humidity has an irregular distribution ( $RH_{av} = 71.3\%$ ). High Temperatures in summer enhance evaporation. The climate corresponds to the coastal city of Tarragona in Spain;

- A **Subalpine climate** (Figure 7.c) typical of a Pre-Pyrenean environment. The average Relative Humidity ( $RH_{av} = 74.5\%$ ) is relatively high and the mean Temperature is moderate ( $T_{av}=11.5^{\circ}\text{C}$ ).

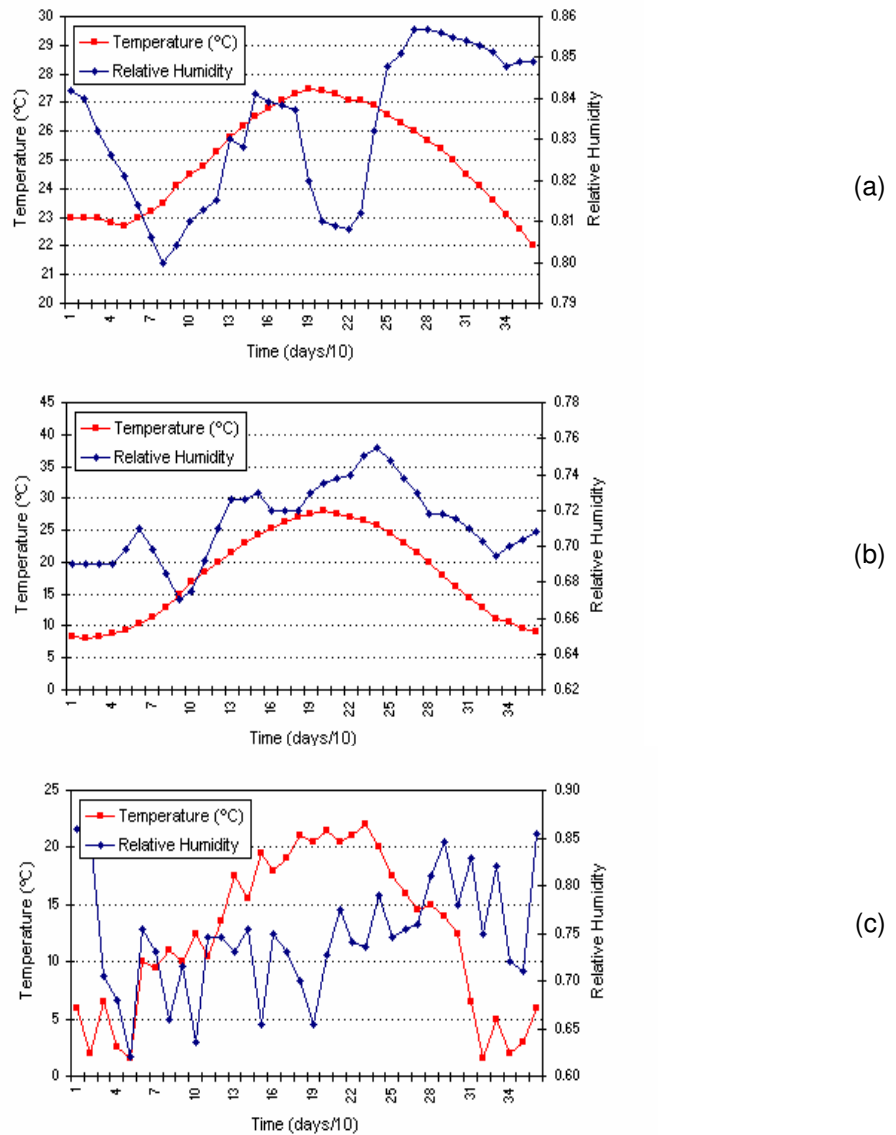


**Fig. 7 – Climates data: (a) Tropical (Moa, Cuba); (b) Mediterranean (Tarragona, Spain); (c) Subalpine (Camprodón, Spain).**

## 5. Simplified calculation

### 5.1 Calculation procedure

As proposed in the beginning of this work, a comparison will be made between the performances of two different cross sections, one using Granular sub-ballast and the other using Bituminous sub-ballast. This comparison will be based on the amplitude values of the seasonal vertical displacements due to water exchanges between the soil and the environment.

As presented in Chapter 3, with BBM (Alonso et al., 1990) it is possible to calculate the volumetric strain associated to a change in suction within the Elastic Domain. Constant stress levels will be assumed. This hydraulic loading has a mechanical effect in the soil once deformations are observed. Their calculation depends on the soil parameter  $k_s$  according to Equation (22) previously presented in Chapter 3, section 2.

$$d\epsilon_{vs}^e = \frac{k_s}{v} \frac{ds}{(s + p_{at})} \quad (22)$$

The integration of Equation (22) gives Equation (27) that can be used to calculate the volumetric strain due to the changes in suction from  $s_0$  to  $s_1$  in distinct time intervals  $t_0$  and  $t_1$ :

$$\epsilon_s^e(t_1) = k_s \ln\left(\frac{s_0 + p_{at}}{p_{at}}\right) - k_s \ln\left(\frac{s_1 + p_{at}}{p_{at}}\right) = \kappa_s \ln\left(\frac{s_0 + p_{at}}{s_1 + p_{at}}\right) \quad (27)$$

The comparison between the Granular and the Bituminous solutions is made by comparing the displacements/deformations calculated with the volumetric strain occurred due to suction changes (Eq. 27).

The global displacement is calculated as the sum of the displacements calculated in specific points of the layers that compose each cross section. These layers and the points used in the calculation, named control points (placed in the rail axis line), are identified in Figure 8. To obtain a more accurate result, the subgrade is divided into two layers named Subgrade 1 and Subgrade 2. In each layer it is assumed a given relative humidity constant along its thickness.

For each soil, it is considered that all layers below the point A are composed by the same material. This is not an exact description of the reality but in terms of comparison as similar results.

For the calculation of the suction in the soil with Equation (1), the relative humidity considered is obtained from the reduction of the atmospheric value. The value found in the calculation is reduced in depth from layer to layer (Layers' RH reduction – Tables 2 and 3) to consider the fact that atmosphere affects more significantly the soil in the surface.

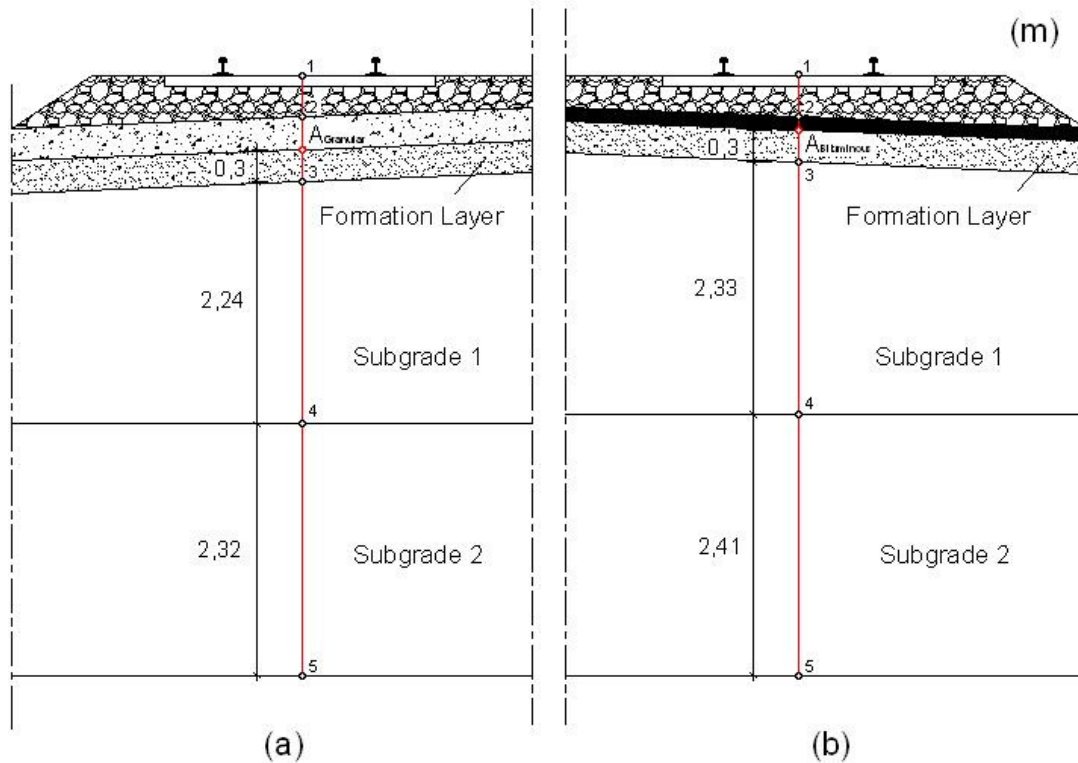


**Fig. 8 – Line Control – Point A: (a) Granular Sub-ballast; (b) Bituminous Sub-ballast.**

Equation (28) is the sum of the vertical displacements calculated in each layer below a given point. For the comparison of both solutions it was used the values of the displacements calculated in Point A.

$$\Delta A = \sum_i \varepsilon_i h_i \quad (28)$$

$\Delta A$  - total vertical displacement in point A [m];

$\varepsilon_i$  - volumetric strain associated to layer  $i$  (calculated with Eq. (27)), equal to linear strain because plane deformation is assumed);

$h_i$  - thickness of layer  $i$  [m] (Figure 8).

For the calculation of the deformations ( $\varepsilon_i$ ) from Equation (28) it is necessary to evaluate how changes in the atmospheric relative humidity and temperature affect the soil. This evaluation must take into account the water supplied from the environment (rainfall and relative humidity of

the surrounding air) and its exchanges in both vapor and liquid phases with the soil (affected by temperature, soil permeability and water retention properties).

To allow a theoretical approach, a simplified method is adopted, where for each layer (Figure 8) it is assumed a given reduction of the relative humidity (RH) of the air from the atmosphere. This reduction is dependent of the depth of the layer (points 1, 2, A, 3, 4 and 5) and increases with it. For the purposes of this exercise the RH reduction associated to each layer is considered to be independent from the type of soil adopted (soils (1), (2), (3) or (4) described in Chapter 4, section 3). The calibration of the RH reduction values for each layer was performed for a general granular sub-ballast cross section (not related with any specific referred soil) and assumed to be equal for all the soils considered. This calibration was computed by CODE\_BRIGHT (a program for finite elements – Chapter 6) recurring to the same procedure used for the results presented in Chapter 8.2.2 concerning the evolution of Relative Humidity.

For the cross section that considers the Granular sub-ballast (presented in Chapter 4), these relations are indicated in Table 2 associated to the control points 1, 2, A, 3, 4 and 5 represented in Figure 8.

The evolution of the Relative Humidity evolution in each control point, the relation between their values in depth and the correspondent reductions of the different layers for the Granular sub-ballast cross section can be found in Figure 9:

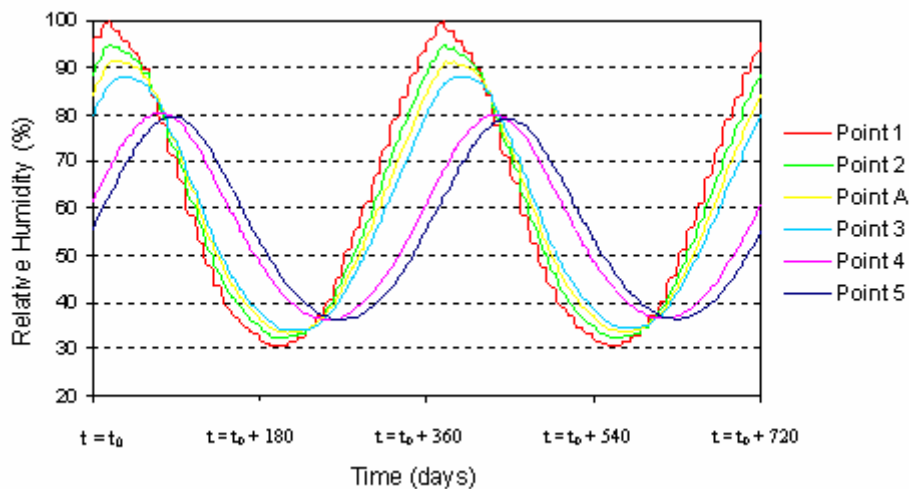


**Fig. 9 – Relative Humidity registered on control points for a granular sub-ballast cross section (values calculated with CODE\_BRIGHT).**

In Figure 9, the difference in time between maximum RH calculated in each control point indicates that the total amount of water in vapour phase does not reach depth. In fact, the relative humidity calculated in points 4 and 5 in the subgrade has values smaller than those calculated in the more superficial layers.

According to Figure 11, the values of RH change along the year, changing the relation between the maximum values found in each control point. However this relation is not very different if the time lag between the maximum values found would be eliminated. Considering only the maximum values found, it is possible to calculate the Relative Humidity reduction associated to each layer by relating the RH reduction in depth from point to point. The application of this procedure for RH definition in depth for other time instants than those where the maximum were registered will be explained later in this section.

Table 2 presents the maximum values found in the calculation for the RH in the control points. In this table, the column “Points RH” presents the RH measured in each control point. For simplicity, the distribution of the RH in each layer is assumed to be uniform in depth therefore it is adopted for the layer the average between the values measured in the border points (presented in the column named “Layer RH”). For example, considering saturation in point 1,  $RH = 100\%$ , the value registered in point 2 is  $RH = 95\%$  so the RH retained in this layer is assumed to 97.5%. Therefore the RH reduction to be considered in this layer is 2.5% (column “RH reduction” in Table 2).

**Table 2 – Relative Humidity reductions with depth (Granular Sub-ballast).**

Granular Sub-ballast cross section					
Layer	Points	Points RH (%)	Layer RH (%)	Layers' RH reduction (%)	
Ballast	1	100	97.5	2.5	10.5
	2	95		93.0	
Sub-ballast	A	91	89.5	3.5	
Formation Layer	3	88	84.5	5.0	
Subgrade 1	4	81		4.0	
Subgrade 2	5	80			

For the cross section that considers the Bituminous sub-ballast, the relations are indicated in Table 3. The meaning of the values presented in this table is equal to the one previously presented in Table 2.

According to Table 3, for the subgrade layers 1 and 2 it is assumed a RH reduction equal to the one found for the granular cross section because this reduction depends only on the characteristics of the materials adopted and not on the input RH (the materials adopted for this two layers are identical in both cross sections. In order to allow a parametric study, once the Bituminous sub-ballast RH reduction is unknown, a new variable is defined,  $\lambda$ , and corresponds to the RH reduction from the top of Ballast into the bottom of the Formation Layer (point A). This parameter will be changed allowing performing a sensitivity test to the bituminous properties.

**Table 3 – Relative Humidity reductions with depth (Bituminous Sub-ballast).**

<b>Bituminous Sub-ballast cross section</b>	
Layer	Layers' RH reduction (%)
Ballast	λ
Sub-ballast	
Formation Layer	
Subgrade 1	5.0
Subgrade 2	4.0

Figure 9 had shown that the RH measured in each point depends on the instant of the year, however an equal reduction is considered along time and for both cross sections analyzed. This assumption will lead to amplitudes of the RH slightly higher than the real ones for time instants far from those where the maximum values were registered, therefore to higher suction changes and to higher displacements. Since this procedure is adopted for both cross sections analyzed it will allow their comparison.

However, the seasonal changes in the RH from the environment (input RH) are considered by maintaining the annual average value,  $RH_{ave}^{atm}$ , and reducing it from a given percentage. This percentage is given in Tables 2 and 3 and the reduction considered is the distance between the RH measured in each time interval and the annual average value (see example in Figure 10). The RH calculation for Formation Layer in the Bituminous sub-ballast cross section is presented in Equation 29:

$$RH_{FL}^{Bit} = RH_{ave}^{atm} \pm |RH_i - RH_{ave}^{atm}| \quad (29)$$

$RH_{FL}^{Bit}$  - RH associated to the Formation Layer on the bituminous cross section;

$RH_{ave}^{atm}$  - annual average for RH;

$RH_i$  - RH associated to time interval  $i$ .

The reductions in the average values of RH,  $RH_{ave}^{atm}$ , are not analyzed in this exercise. This procedure for RH calculation in each layer is conservative in terms of the displacements found for Bituminous sub-ballast cross section (leads to higher ones) because the effects of relative humidity reduction will not only affect the amplitude of RH values but also the average value itself. It is worth to note that an equivalent reduction in suction depends on the interval of the RH in question because the relation between suction changes and relative humidity changes (Eq. (1)) is not linear. Therefore, a reduction in RH from 75% to 70% is responsible for a higher strain than a reduction from 70% to 65%.

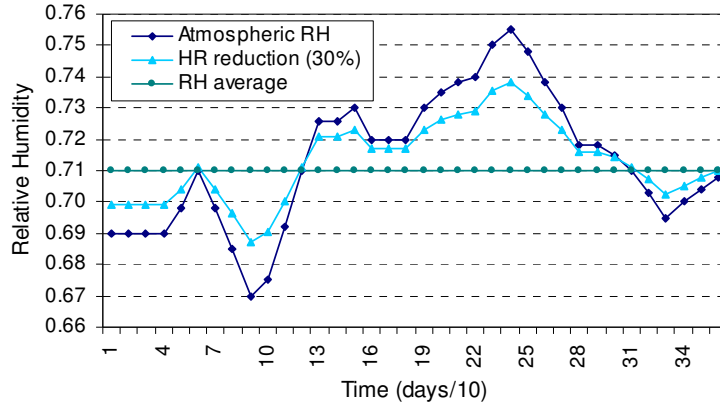


Fig. 10 – Example for RH reduction (30%).

## 5.2 Granular vs. Bituminous: parametric analysis

As mentioned in the previous section, the comparison between the Granular and the Bituminous sub-ballast solutions will be made by analyzing the amplitude of displacements calculated in points  $A_{\text{Granular}}$  and  $A_{\text{Bituminous}}$  for the different soils presented before and considering RH reductions mentioned in Tables 2 and 3. The maximum vertical displacements measured for each solution,  $\Delta_{\text{Granular}}$  and  $\Delta_{\text{Bituminous}}$ , can be considered to be the maximum amplitude of displacements observed in one year and are defined as the difference between the greatest deformation calculated: the difference between the maximum shrinking (volume decrease) and the maximum swelling (volume increase) observed in one year. An example is presented in Figure 11.

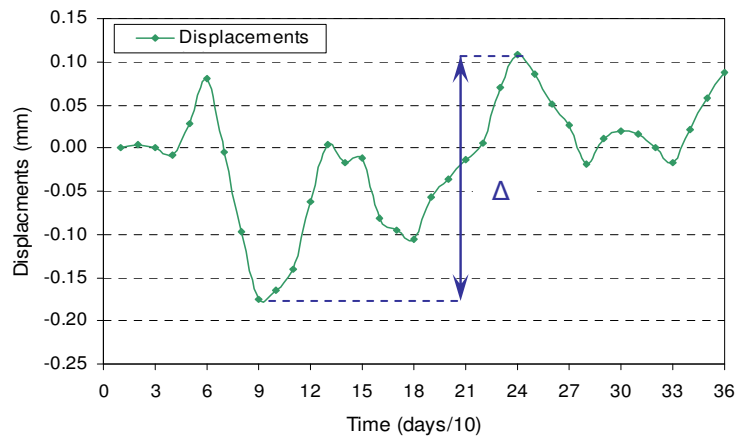


Fig. 11 – Example for Maximum amplitude of Vertical Displacements.

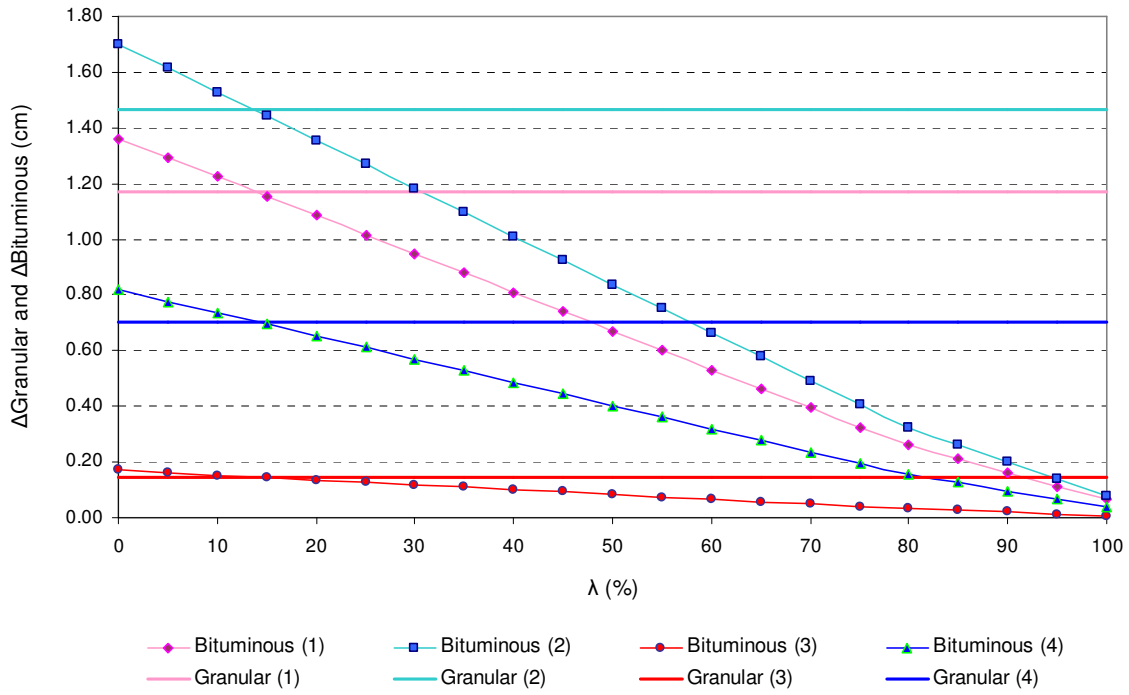
A parametric study in terms of the variable  $\lambda$  (reduction in the relative humidity provided by the Bituminous sub-ballast layer) and its effects on maximum vertical displacements (amplitude),  $\Delta$ , is performed. For each soil ((1), (2), (3) and (4)), it is considered that all layers bellow point A (Formation Layer, Subgrade 1 and 2) are composed by it and the total displacement is calculated with the correspondent  $k_s$ .

Figures 12, 13 and 14 register the results of this parametric study for the different climates considered (Tropical, Mediterranean and Subalpine). In these figures, the legends Granular (1) and Bituminous (1) correspond to the series that associate a given  $\Delta$ Granular and  $\Delta$ Bituminous, respectively, to each value of  $\lambda$  using the properties of soil (1). Once  $\Delta$ Granular is not dependent of the variable  $\lambda$ , a constant value is registered for each type of soil and is shown in the mentioned figures as a reference.

In this analysis it is intended to find:

- The RH reduction due to the adoption of a bituminous sub-ballast with different reduction factors,  $\lambda$ . The vertical displacements (amplitude) for different impervious properties considered for the bituminous will be compared with the granular one;
- The range of values for  $\lambda$  that leads to lower displacements (amplitudes) in the Bituminous sub-ballast cross section than the ones registered for Granular solution;
- Qualitative relations in terms of the  $\Delta$ Bituminous for the different climates.

(a)



(b)

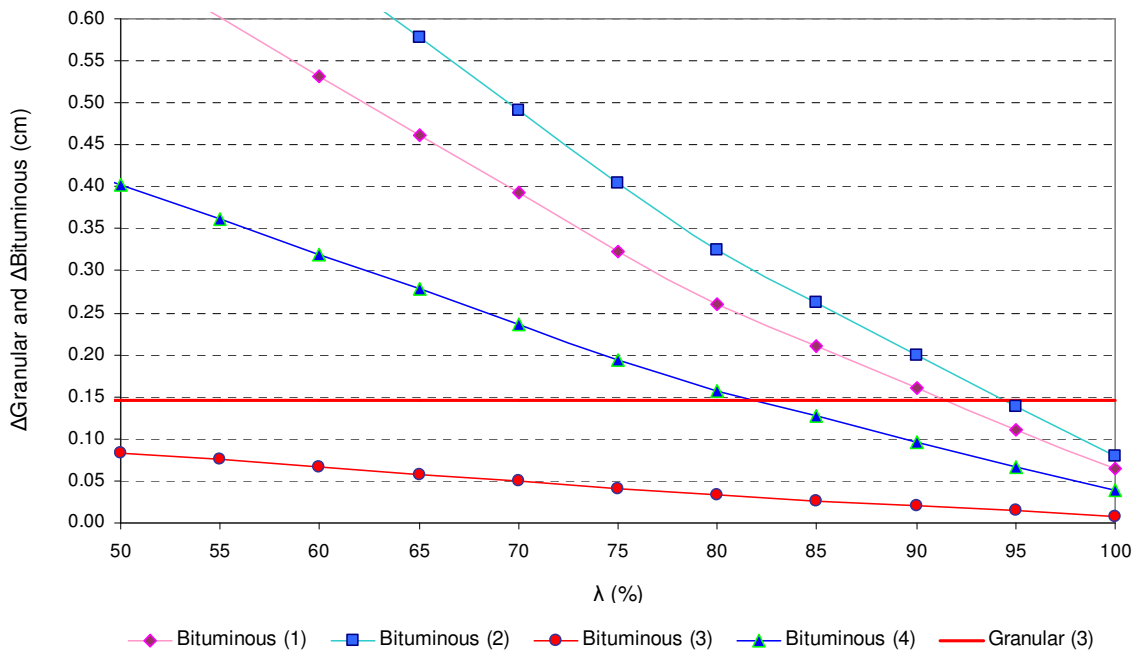
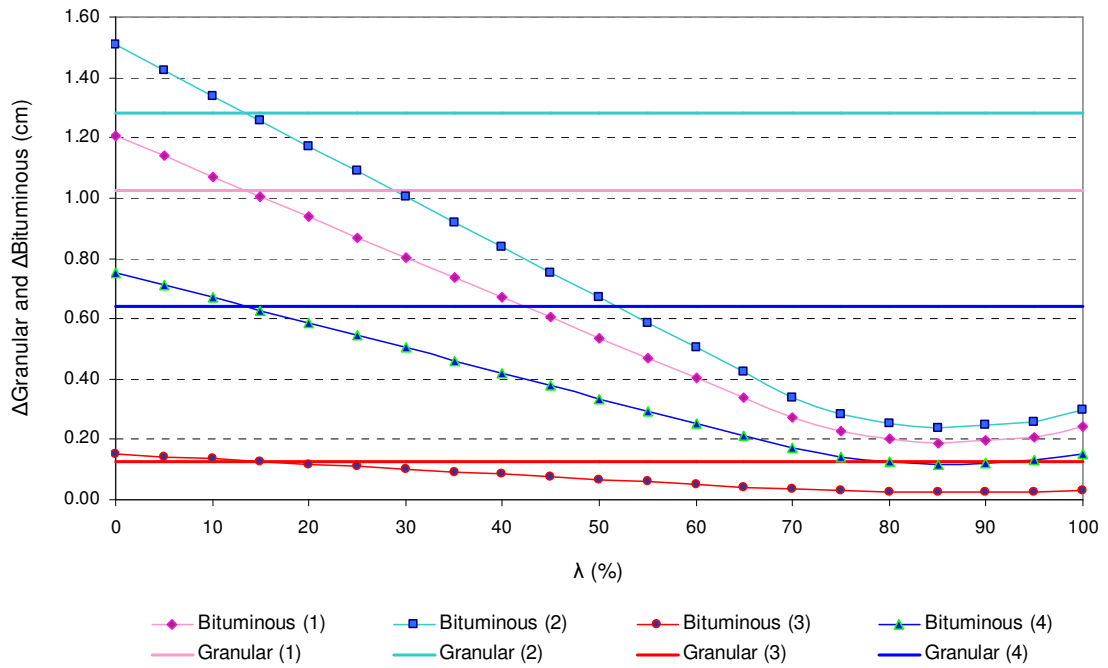


**Fig. 12 – Parametric Analysis for  $\lambda$  – Tropical (Moa, Cuba):**  
**(a)  $\lambda$ 's range 0-100%; (b)  $\lambda$ 's range 50-100%**

(a)



(b)

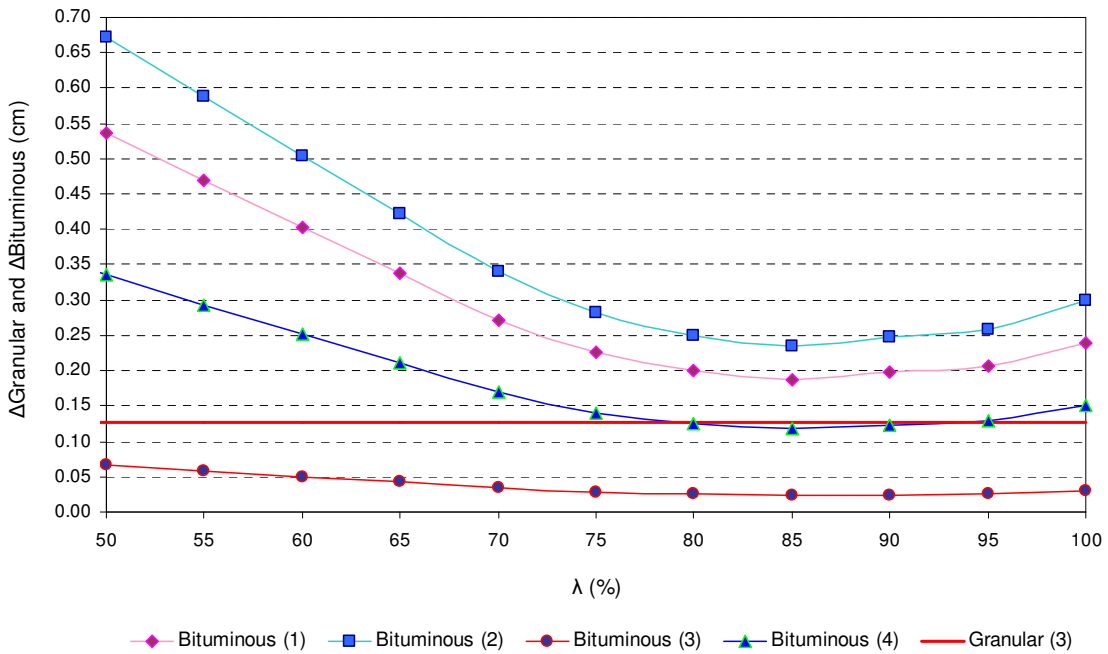


**Fig. 13 – Parametric Analysis for  $\lambda$  – Mediterranean (Tarragona):**  
(a)  $\lambda$ 's range 0-100%; (b)  $\lambda$ 's range 50-100%

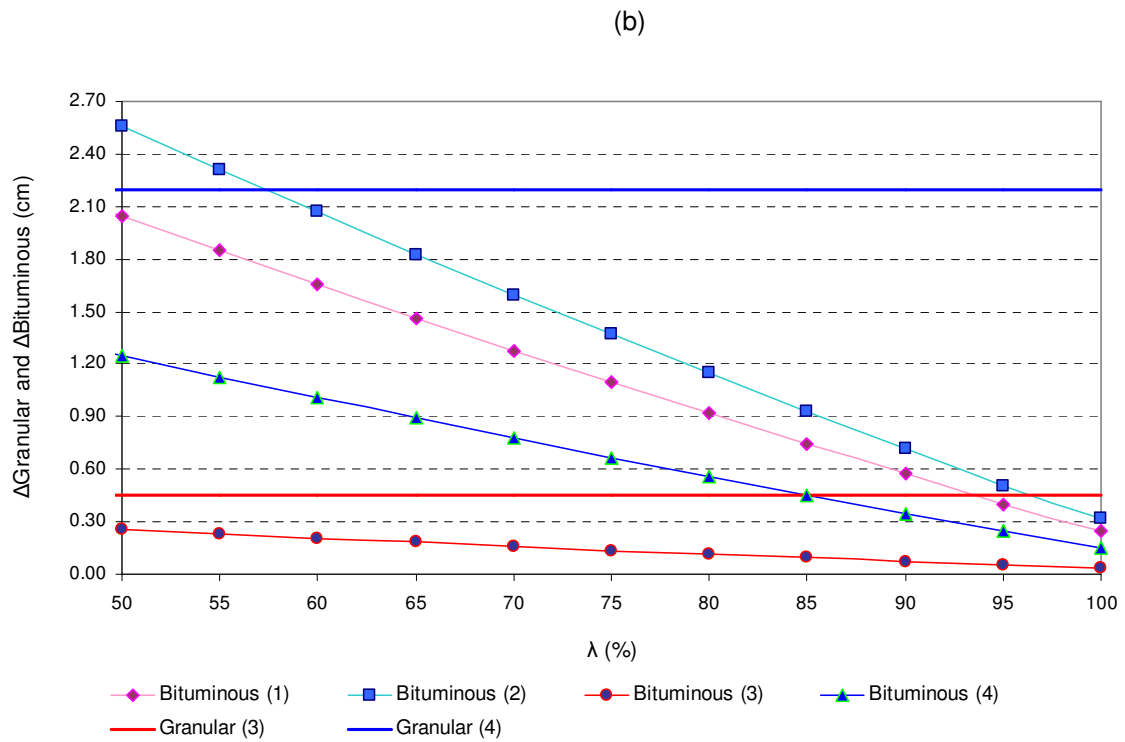
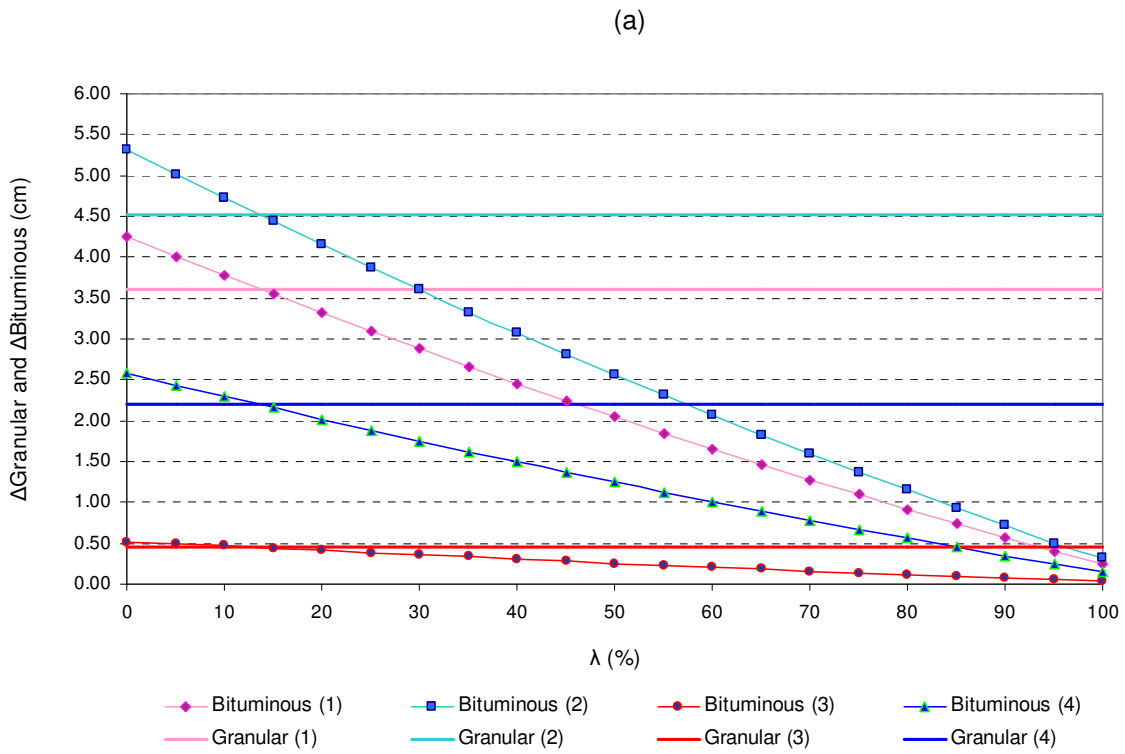


**Fig. 14 – Parametric Analysis for  $\lambda$  – Subalpine (Camprodón, Spain):**  
**(a)  $\lambda$ 's range 0-100%; (b)  $\lambda$ 's range 50-100%**

Concerning the results present in Figures 12,13 and 14, some comments can be made:

- The higher displacements registered for soils (1), (2), and (4) can be explained by their swelling properties since these soils are very sensitive to Relative Humidity changes. According to Table 1, Soil (1) has the lowest  $k_s$  and for this reason exhibits lower displacements than the other ones;
- For the Bituminous sub-ballast cross section, as expected, maximum vertical displacements (amplitude) calculated for each soil decreases as RH reduction,  $\lambda$ , increases; this fact is not observed in Figure 13 – Tarragona – where vertical displacements (amplitude) are minimized not for the highest value,  $\lambda=100\%$ , but for a lower one (85%), named  $\lambda_{opt}$  ( $\lambda_{opt} = 85\%$ );
- Considering all climates,  $\Delta$ Bituminous is equal to  $\Delta$ Granular for  $\lambda_0=15\%$  and will increase for lower  $\lambda$  values;
- It is possible to observe 50% of reduction in the displacements calculated with the bituminous sub-ballast (compared to those from the granular cross section) for the Mediterranean climate and for the Tropical and Subalpine ones considering the following values of  $\lambda$ :

$$\left. \begin{array}{l} \text{Mediterranean: } \lambda > 50\% \\ \text{Tropical and Subalpine: } \lambda > 55\% \end{array} \right\} \Delta\text{Bituminous} < \frac{1}{2} \Delta\text{Granular}$$

In Figures 12, 13 and 14, some quantitative differences between series associated to each soil can be observed. In spite of that, for each climate, all series described the same qualitative evolution. Thus, for each climate and in terms of the maximum amplitude of the displacements, it is possible to define a characteristic curve of their reduction when a bituminous cross section is adopted instead of a granular one. The efficiency of the bituminous solution can be measured in terms of the reduction of the displacements (amplitude) compared to those observed in the granular cross section. For its evaluation it is adopted a parameter named Bituminous reduction ( $Bit_{red}$ ) that relates the displacements (amplitude) measured in both cross sections.

$$Bit_{red} = \frac{\Delta Gran. - \Delta Bit.}{\Delta Gran} \quad (30)$$

According to Equation (30), if the Bituminous reduction is equal to zero, the vertical displacements are equal in both cross sections. If it is larger than zero, the adoption of a bituminous cross section will be more efficient since the vertical displacements are smaller than those found for the granular cross section and the opposite if it is smaller than zero.

The Bituminous reduction for varying impervious properties of the bituminous, quantified by  $\lambda$ , can be expressed by the curves presented in Figure 15. In spite of the efficiency loss in bituminous reduction in terms of the displacements (amplitude) for high values of  $\lambda$ , it may be considered that the percentage of reduction in vertical displacements performed by the bituminous sub-ballast is similar to the one associated to the increased of  $\lambda$ .

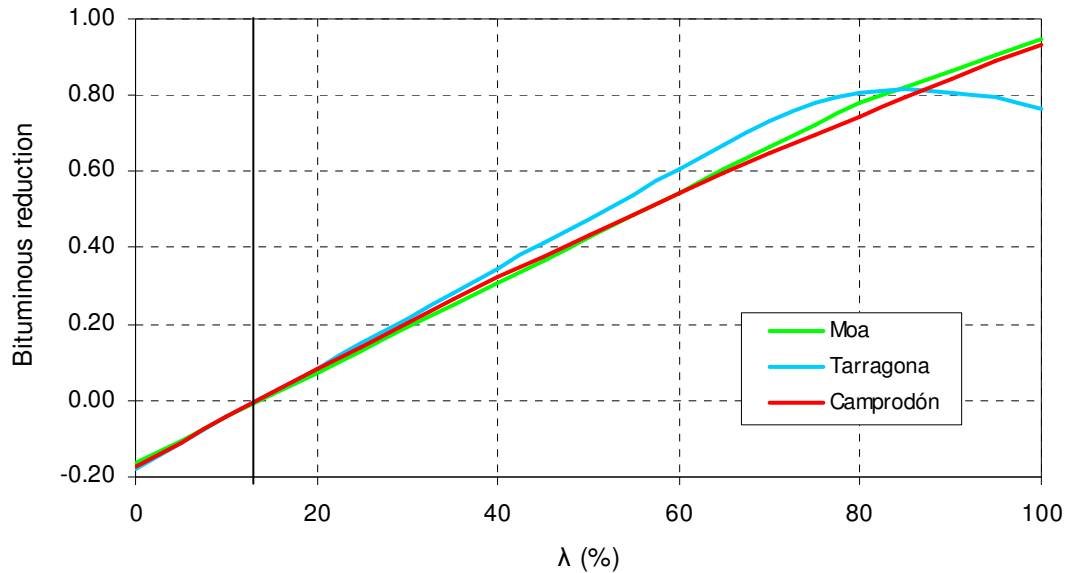


**Fig. 15 – Bituminous reduction for maximum vertical displacements**

According to Figure 15 and as mentioned before, the vertical displacements for the bituminous sub-ballast are equal to those found for the granular cross section (Bituminous reduction = 0) when  $\lambda = 15\%$ . Therefore it can be assumed that the adoption of bituminous sub-ballast, designed in order to guarantee a  $\lambda$  superior to 15%, is a better solution than the adoption of granular sub-ballast layers.

The bituminous reduction for maximum displacements registers a decrease for high values of  $\lambda$  represented by the decrease of the slope of the characteristic curves in Figure 15. For Tarragona climate, this loss has some relevance once it leads to an inversion of the slope in the associated characteristic curve. This inflexion point corresponds to the maximum reduction possible to achieve by changing the properties of the bituminous. According to Figure 15, this inflexion point is not visible neither for Moa (Tropical) or Camprodón (Subalpine) climates, as the maximum reduction in the vertical displacements is achieved for  $\lambda = 100\%$ . The existence of an inflexion point as observed for Tarragona (Mediterranean) climate indicates that it may exist an optimum value of  $\lambda$  ( $\lambda_{opt} = 85\%$  for the Tarragona climate) for which the efficiency of the design solution will be maximum. This indicates that the design of a bituminous solution should be focus to reach this maximum.

## 6. CODE\_BRIGHT description

### 6.1 Introduction

Weather affects the initial conditions of trackbed layers' soils (ballast, sub-ballast, formation layer and subgrade) and, as obvious, its effects reduce in depth. As previously mentioned in Chapter 2, it is necessary to have an adequate formulation to rule the exchanges of water in both vapour and liquid phases between soil and the environment. These exchanges are ruled by evaporation (therefore by temperature), by the amount of liquid water available (mainly from rain), by the soil water and air permeability that changes with the saturation degree, and by the soil water retention properties. Deformations of the compacted materials are expected as consequence of these changes and, due to the seasonal nature of them, fatigue and loss of strength take place. Trackbed layers are usually not-saturated and saturation is a limit condition that is often not attained. For this reason it is necessary to formulate, under general conditions, the transfer phenomena of water (liquid and vapour), air and temperature as well as mechanical equilibrium conditions in non-saturated soils.

This calculation is mathematically complex and requires the use of adequate computational tools. The finite element program CODE\_BRIGHT (Olivella et al., 1994, 1996; DIT-UPC, 2000) is chosen to perform the calculation of the evolution of water content, temperature and consequent deformation of the soil of the foundation of a railway trackbed. Long term behaviour can be analyzed in this simulation exercise once it is considered a period of 5 years.

CODE\_BRIGHT has been described by Olivella et al. (1994) and allows the solution of thermo-hydro-mechanical coupled problems in non-saturated soils assuming that they are deformable porous media. As input, it requires data concerning the mechanical and hydraulic properties of the materials, mechanical loading, restrains and others boundary conditions such as temperature and water inflow and outflow both in vapour and liquid phases. Calculation is performed with the equations that rule water and vapour flow (conduction and diffusion), thermal diffusion and heat flow, besides balance equations and the equilibrium of mass of solids, liquid, gas and energy. For mechanical constitutive model it is possible to choose BBM between some available laws.

The theoretical formulation used in CODE\_BRIGHT is presented in this Chapter. Modelling and appropriate calibration of the different solutions in study are described in Chapter 7. The results for the simulation exercise performed by this finite elements program will be presented in Chapters 8.

An analysis in terms of the RH reduction in depth is also performed with CODE\_BRIGHT. As mentioned before, an extension of the results presented in Chapter 8.2.2 is used for the parametric study presented before (Chapter 5) to define RH reduction values in depth.

## 6.2 Basic principles of the formulation

In this section, the basic principles of the formulation used in the analysis performed with CODE\_BRIGHT are described. They are: (i) Water Mass Balance; (ii) Air Mass Balance; (iii) Energy Balance and (iv) Equilibrium (mechanical) equations. The balance of solid mass is also included implicitly when the porosity changes in time are considered and its explanation can be found in detail in Olivella et al. (1994). Balance equations for water and air species are formulated considering the following basic phenomena:

### *Water and air flow*

- Liquid and gas flow in deformable porous media (Darcy's law generalized for unsaturated conditions);
- Vapour diffusion (Fick's law);
- Liquid – vapour phase changes (Perfect gases law / Psychometric law).

### *Heat flow*

- Conductive transport (Fourier's law);
- Advective transport in liquid and gas phases.

In the following relationships,  $\phi$  represents the porosity. Besides it appears explicitly in many equations, porosity is also hidden in variables that depend on it (e.g. intrinsic permeability). The other variables that will be presented in this work include a superindex to refer to species ( $h$  for solid mineral,  $w$  for water and  $a$  for dry air) and a subindex to represent the phases ( $s$  for solid,  $l$  for liquid and  $g$  for gas).

## 6.2.1 Water Mass Balance

Equation (31) represents the balance of the mass of water (in the liquid and gas phases):

$$\frac{\partial}{\partial t} (\theta_l^w S_l \phi + \theta_g^w S_g \phi) + \nabla \cdot (j_l^w + j_g^w + i_g^w) = f^w \quad (31)$$

where

$\theta_l^w (= \bar{\omega}_l^w \rho_l)$  - water mass per unit of volume in liquid phase (product of the mass fraction of that species,  $\bar{\omega}_l^w$ , and the bulk density of the phase,  $\rho_l$ ) [kg/m<sup>3</sup>];

$\theta_g^w (= \bar{\omega}_g^w \rho_g)$  - water mass per unit of volume of gas (vapour) (similar meaning as for the liquid phase) [kg/m<sup>3</sup>];

$S_l$  - gas volumetric fraction with respect to pore volume (degree of saturation);

$S_g$  - gas volumetric fraction with respect to pore volume ( $S_g = 1 - S_l$ );

$j_l^w$  and  $j_g^w$  - liquid and vapour water convective mass flow, respectively (kg/m<sup>3</sup>/s);

$i_g^w$  - vapour diffuse flow in air (kg/m<sup>3</sup>/s);

$f_w$  - water sources or sinks per total unit of volume (kg/m<sup>3</sup>/s).

To solve equation (31), the following constitutive relationships or thermodynamic equilibrium conditions are also necessary:

*Water density,  $\theta_l^w$*

$$\theta_l^w = \theta_l^w(T, p_l) = \bar{\omega}_l^w \rho_l \quad (32)$$

Water density, as present in Equation 32, depends on temperature,  $T$ , and liquid pressure,  $p_l$ . Temperature dependence ensures that convection phenomena associated with changes in density caused by temperature gradients are taken into account. This phenomenon is not expected to be significant when dealing with trackbeds, however.

*Vapour density,  $\theta_g^w$*

Changes in vapour density are determined by Equation (33) (Psychrometric Law):

$$\theta_g^w = (\theta_g^w)_0 \exp\left(\frac{-(p_g - p_l)M_w}{R(273.15 + T)\rho_l}\right) \quad (33)$$

where the influence of suction ( $s = p_g - p_l$  [MPa]: difference between gas and liquid pressure) and temperature  $T$  (K) are considered.  $(\theta_g^w)_0$  is the vapour density in contact with water at the reference pressure (atmospheric:  $p_g - p_l = 0$ ) and it is strongly dependent on temperature.  $M_w$  is the molecular mass of water ( $0.018 \text{ kg/mol}$ ) and  $R$  is the gas universal constant ( $R = 8.314 \text{ J/mol/K}$ ).

#### *Soil Water Retention Curve, WRC*

The WRC is necessary to calculate the storage term in Equation (31). It relates  $S_l$  (liquid saturation, as presented above) with suction,  $s$ , and to the stress state. It should be measured at a constant density although this aspect is frequently neglected in literature. Many empirical laws have been proposed for relationship  $S_l(s)$ . A frequently used relationship is Van Genuchten's (1980) described by Equation (34), which is the one used in this work. Hysteresis effects are not considered in the analysis.

$$S_e(s) = \frac{S_l - S_{lr}}{S_{ls} - S_{lr}} = \left( 1 + \left( \frac{s}{p_0} \right)^{\frac{1}{1-\lambda}} \right)^{-\lambda} \quad (34)$$

$S_{lr}$  - residual saturation (generally equal to 0);

$S_{ls}$  - maximum saturation (generally equal to 1);

$\lambda$  - model parameter;

$p_0$  - [MPa] is a parameter to introduce the effect of temperature in the retention curve.

In fact, if Laplace expression for capillary pressure is considered, which depends on water surface tension  $\sigma(T)$ , it can be proposed Equation (35). The variation of water surface tension with temperature is known.

$$p_0 = p_0 \frac{\sigma(T)}{\sigma_0(T_0)} \quad (35)$$

#### *Liquid water convective flow, $j_l^w$*

Darcy's law is expressed as function of the liquid density,  $\rho_l$ , and the flux of liquid,  $q_l$ , according to Equation (36),

$$j_l^w = \rho_l q_l = -\rho_l K_l / \nabla p_l + \rho_l \cdot g \nabla z \quad (36)$$

$g$  - gravity ( $=9.8 \text{ m/s}^2$ )

$\nabla z$  - difference in the water head ( $m$ )

$K_l = K \cdot k_{rl} / \mu_l$  is the water permeability (m/s) (Darcy's permeability generalized to unsaturated conditions). In this expression, the intrinsic permeability  $K(m^2)$  depends on soil porosimetry (voids size and geometry).  $\mu_l [Pa.s]$  is the water viscosity (depends on temperature) and  $k_{rl}$ , the relative permeability, that introduces the lack of saturation. Many empirical expressions have been proposed for  $k_{rl}$ . They relate  $k_{rl}$  with suction or degree of saturation (Alonso, Gens and Hight, 1987). The second option would be preferable as hysteresis is reduced. A wide group of empirical relationships for  $k_{rl}$  is coherent with Equation (37), where  $S_{lu}$ ,  $S_{lr}$ ,  $S_{ls}$  were defined above and  $n$  is a calibration parameter (usually it varies from 3 to 4).

$$k_{rl} = \left( \frac{S_l - S_{lr}}{S_{ls} - S_{lr}} \right)^n \quad (37)$$

Van Genuchten (1980) proposed an expression (Eq. (38)) to the relative permeability related to the retention curve (using the same parameters):

$$k_{rl} = S_l^{1/2} \left( 1 - \left( 1 - S_l^{1/\beta} \right)^\beta \right)^2 \quad (S_l \leq 1) \quad (38)$$

This "coherent" approximation, in the sense that it links both soil properties, has also been used by other authors (Fredlund et al., 1994).

#### Vapour diffusion through air, $j_g^w$

Fick's expression (Eq. (39)) is employed to calculate vapour flow in pores:

$$j_g^w = -D_g^w \nabla W_g^w = - \left( \phi \rho_g S_g \tau D_m^w I + \rho_g D_g' \right) \nabla W_g^w \quad (39)$$

$D_g^w$  - (tensor) dispersion coefficient;

$W_g^w (= \rho_v / \rho_g)$  - water mass fraction in gas;

$D_g'$  - mechanical dispersion that can be neglected if the gas flow is small;

$D_m^w$  - vapour molecular coefficient in the air - dependent on temperature (Eq. (40));

$\tau$  - tortuosity parameter;

$I$  - unit matrix

The moisture transfer mechanism in the vapour phase is important regarding temperature gradients, a situation widely documented. The generalized force that causes this flow is the vapour density gradient in soil pores.

$$D_m^w (m^2 / s) = 5.9 \times 10^{-12} \frac{(273.15 + T)^{2.3}}{p_g} \quad (40)$$

### 6.2.2 Air Mass Balance

Air mass balance is expressed by Equation (41):

$$\frac{\partial}{\partial t} (\theta_l^a S_l \phi + \theta_g^a S_g \phi) + \nabla \cdot (j_l^a + j_g^a + i_g^a) = f^a \quad (41)$$

where

$\theta_l^a$  and  $\theta_g^a (= \rho_a)$  - dry air masses per unit of volume of liquid and gas respectively;

$j_l^a$  and  $j_g^a$  - mass convective flows of air in liquid and gas phases;

$i_g^a$  - air diffusive flow in gas phase;

$f^a$  - external air source per unit of volume.

The terms from Equation (41) have the same units as the similar ones presented in Equation (31). Together with the balance condition of water mass, it is necessary to establish the following constitutive equations or thermodynamic equilibrium conditions:

*Air density,  $\theta_g^a$*

Generally it is a well-known function of temperature and gas pressure (ideal gases law):

$$\theta_g^a = \theta_g^a(T, p_g) \quad (42)$$

*Air mass dissolved in water,  $\theta_l^a$*

It is dependent of air mass fraction,  $w_l^a$ , and liquid density,  $\rho_l$  [kg/m<sup>3</sup>] as expressed in Equation (43):

$$\theta_l^a = w_l^a \rho_l \quad (43)$$

Air mass fraction is controlled by Henry's law (Eq. (44)):

$$w_l^a = \frac{p_a M_a}{H \cdot M_w} \quad (44)$$

$w_l^a$  - air mass fraction in water;

$p_a$  - partial air pressure [MPa];

$M_a$  - air molecular mass (0.02895 kg / mol);

$H$  - Henry constant (= 10000 MPa).

*Convective air flow (Darcy),  $j_g^a$*

It is described by a generalized Darcy's law (Eq. (45)):

$$j_g^a = \rho_a q_g = -\rho_a K_g (\nabla p_g + \rho_g g \nabla z) \quad (45)$$

where  $g$  and  $\nabla z$  were previously defined and  $K_g = K \cdot k_{rg} / \mu_g$  is the gas permeability (m/s). The relative permeability to gas is expressed through the relative permeability to water ( $k_{rg} = 1 - k_{rl}$ ). On the other hand, convective flow due to water movement is expressed as (transported dissolved air):  $j_l^a = q_l \theta_l^a$ .

*Air diffusion in gas phase,  $i_g^a$*

The purely dispersive flow is small. The diffusive flow, Fick type, is expressed in an analogy to the water vapour flow:

$$i_g^a = -(\phi \rho_g S_g \tau D_m^a) \nabla w_g^a \quad (46)$$

where  $D_m^a$  is the (tensor) dispersion coefficient and  $w_g^a (= \rho_a / \rho_g)$  the air mass fraction in gas. Since  $\rho_g = \rho_a + \rho_v$ ,  $\nabla(\rho_a / \rho_v) = -\nabla(\rho_v / \rho_g)$  and the previous flow Equation (46), balances vapour diffusion flow (assuming that the air and vapour molecular diffusion coefficients are equal).

All together, the dry airflow tends to have a lesser importance regarding the problems analyzed here, as air's high permeability usually guarantees a constant air pressure. In these cases the solution of the gas equation is not required. This was the procedure adopted in this work.

### 6.2.3 Energy Balance

Equation (47) expresses the energy balance:

$$\frac{\partial}{\partial t} (E_s \rho_s (1 - \phi) + E_l \rho_l S_l + E_g \rho_g S_g \phi) + \nabla \cdot (i_c + j_{El} + j_{Eg}) = f^E \quad (47)$$

$E_s, E_l, E_g$  - specific energies for each phase [J/kg];

$i_c$  - (non-advective) heat conduction term;

$j_{El}, j_{Eg}$  - advective terms for each of the existent flows (heat transfer convective terms through the liquid and gas phase, respectively) described by Equations (48) and (49) respectively:

$$-j_{El} = E_l \rho_l q_l \quad (48)$$

$$-j_{Eg} = E_g^w (j_g^w + i_g^w) + E_g^a (j_g^a + i_g^a) \quad (49)$$

$f^E$  - external energy contribution per unit of volume.

Usually, in heat transfer, conductive phenomena predominate and the influence of convective terms is generally small. In order to solve this balance equation other relationships, together with the ones already given, are necessary:

#### Specific energies, $E_s$

$E_s$  value depends on the mineral type (it is close to  $1000\Delta T$  (J/kg)). Regarding the liquid and gas phases, the following relationships expressed by Equations (50) and (51) are held:

$$E_l = E_l^w w_l^w + E_l^a w_l^a \quad (50)$$

$$E_g = E_g^w w_g^w + E_g^a w_g^a \quad (51)$$

where

$$E_l^w = 1180(\Delta T) \text{ (J/kg)};$$

$$E_l^a = 1006(\Delta T)$$

$$E_g^w = 2.5 \times 10^6 \cdot 1900(\Delta T) \text{ (water vaporization latent heat } (2.5 \times 10^6 \text{ J/kg)} \text{ is included.);}$$

$$E_g^a = 1006(\Delta T);$$

$w_\beta^\alpha$  - mass fraction of  $\alpha$  specie in phase  $\beta$ .

Thermal conductivity (Fourier's law),  $i_c$

Equation (52) is Fourier's law:

$$i_c = -\lambda \nabla T \quad [\text{Wm}^{-2}] \quad (52)$$

where  $\lambda$  [W/mK] is the global thermal conductivity, which can be expressed as a geometrical mean by Equation (53), where  $\lambda_s$ ,  $\lambda_l$ ,  $\lambda_g$  are the thermal conductivities for individual phases and  $\lambda_{sat} (= \lambda_s^{1-\phi} \lambda_l^\phi)$  and  $\lambda_{dry} (= \lambda_s^{1-\phi} \lambda_g^\phi)$  are the thermal conductivities in saturated and dry conditions respectively.

$$\lambda = \lambda_s^{(1-\phi)} \lambda_l^{\phi S_l} \lambda_g^{\phi(1-S_l)} = \lambda_{sat}^{S_l} \lambda_{dry}^{1-S_l} \quad (53)$$

### 6.2.4 Mechanical balance equations

Storage terms for balance Equations (31), (41) and (47) require the calculation of porosity variations ( $\phi$ ) and thus volumetric deformations. Flows and deformations are therefore coupled. Suction (associated with flow, or changes in liquid pressure) controls mechanical properties. In non-saturated materials it is convenient to work with two independent stresses as explained in BBM (Alonso et al., 1990) formulation presented before in Chapter 3. A convenient option is to considerer "net" mean stress (excess of total stress over air pressure:  $\sigma_{ij}^* = \sigma_{ij} - p_a \delta_{ij}$ ) and matric suction:  $s_{ij} = s \delta_{ij} = (p_g - p_l) \delta_{ij}$ . In saturated conditions,  $s = 0$ ,  $p_g = p_l$  and net stress become the effective stress.

The formulation of the mechanical problem requires equilibrium fulfillment expressed by Equation (54),

$$\nabla \cdot \sigma + b = 0 \quad (54)$$

(where  $\sigma$  [MPa] are the total stresses and  $b$  the corresponding mass forces) and some constitutive equations appropriate for compacted non-saturated soils.

A convenient formulation of constitutive equations for non-saturated soils may be put forward if volumetric deformations due to suction changes are imposed deformations (in the same way as thermal-dilatation or thermal contraction deformations are introduced in structural analysis); that is proposed by Equation (55):

$$d\epsilon = D^{-1} d\sigma + d\epsilon_0 \quad (55)$$

where  $d\epsilon_0$  are the volumetric deformations associated with suction changes,  $d\sigma^*$  is the change in net stress and  $D$  an appropriate tangent constitutive matrix (MPa). For its application in

finite elements, Equation (55) is alternatively expressed as an incremental equation (Eq. (56)) that provides stress changes caused, in each iteration, by strain increments:

$$d\sigma^* = D(d\varepsilon + d\varepsilon_0) \quad (56)$$

A simple approximation, convenient in some cases (suction paths that imply soil wetting), consists in formulating  $d\varepsilon_0$  by using state surfaces (Matyas and Radhakrishna, 1986; Lloret and Alonso, 1985); for instance the one presented by Equation (57):

$$\varepsilon_0 = a \ln p + b \ln s + c \ln p \cdot \ln s \quad (57)$$

where

$p$  - mean net stress;

$a, b, c$  – model parameters;

Equation (57) allows obtaining  $d\varepsilon_0$ .

For matrix  $D$ , linear and non-linear elastic formulations have been proposed (Alonso et al., 1988). If elastoplastic models are used, which are more accurate, Equation (57) should be expressed as follows in Equation (58):

$$d\sigma^* = D_{ep} d\varepsilon - h_{ep} ds \quad (58)$$

where  $D_{ep}$  and  $h_{ep}$  are the elastoplastic constitutive matrix and vector respectively. Alonso et al. (1990) proposed an elastoplastic model (BBM) for slightly expansive soils, which was described before. This model was then generalized by Gens and Alonso (1992) to expansive soils. A detailed description of the numerical formulation by the use of finite elements is available in Lloret and Ledesma (1993).

The thermal-caused deformation  $d\varepsilon_T$  can be introduced in the last formulation. Equation (55) would become as expressed in Equation (59):

$$d\sigma^* = D(d\varepsilon - d\varepsilon_0 - d\varepsilon_T) \quad (59)$$

where

$$d\varepsilon_T = \alpha_T dTI$$

$\alpha_T$  - thermal dilatation coefficient;

$I$  - unit matrix.

Finally, some of the phenomena and parameters are very important in order to understand or simulate coupled thermo-hydro-mechanical problems adequately. Concerning the design of trackbeds of roadways and railway infrastructures, the aspects that are more relevant in practice and that are assumed in this work are presented in Table 4 (Alonso, 1998). This table also indicates the manner in which significant constants and parameters can be obtained.

**Table 4 – Properties and parameters for flow, temperature and deformation analysis.  
(Alonso, 1998)**

<b>PHENOMENON/PARAMETER</b>	<b>DETERMINATION</b>	<b>RELATIVE IMPORTANCE</b>
<b>WATER FLOW</b>		
Liquid density	Physical constant	-
Vapour density	Physical constant	-
Vapour diffusion	Physical constant	High
Tortuosity	Special test	Low/intermediate
Vapour dispersion	Special test	Low/intermediate
Convective flow (Darcy)		
Intrinsic permeability	Test	Very high
Relative permeability	Test. Approximation from characteristic curve	Very high
Water viscosity (T)	Physical constant	Intermediate
Characteristic curve	Test. Approximation from grain size distribution?	Very high
<b>AIR FLOW</b>		
Gas density	Physical constant	
Air molecular diffusion	Physical constant	
Tortuosity	Special test	
Air dispersion	Special test	Generally low
Convective flow (Darcy)		
Relative permeability	Special test. Also from water relative permeability	
Air viscosity (T)	Physical constant	
<b>HEAT TRANSFER</b>		
Thermal conductivities	From physical constants; generally well-known	High
Specific heats	Physical constants	High
<b>MECHANICAL BEHAVIOUR</b>		
Thermal expansion coefficient	Special test	Intermediate/high
State surface for volume changes	Tests with controlled suction (oedometer, triaxial)	High
Elastic moduli	Tests with controlled suction	High

## 7. Models description and CODE\_BRIGHT calibration

### 7.1 Introduction

This chapter presents the numerical models of the two trackbed solutions analyzed in this work and their calibration for calculation with CODE\_BRIGHT. The models will be used to carry out sensitivity and evaluation studies for different physical phenomena that drive moisture changes in trackbed layers. These studies will be presented in the next chapters of this work.

### 7.2 Cross Sections

The design of the Granular and Bituminous sub-ballast cross sections used in this exercise is the same one presented in the BBM Application (Chapter 4). Figure 16 presents the Bituminous sub-ballast cross section and the finite element mesh adopted (triangular elements with 3 nodes).

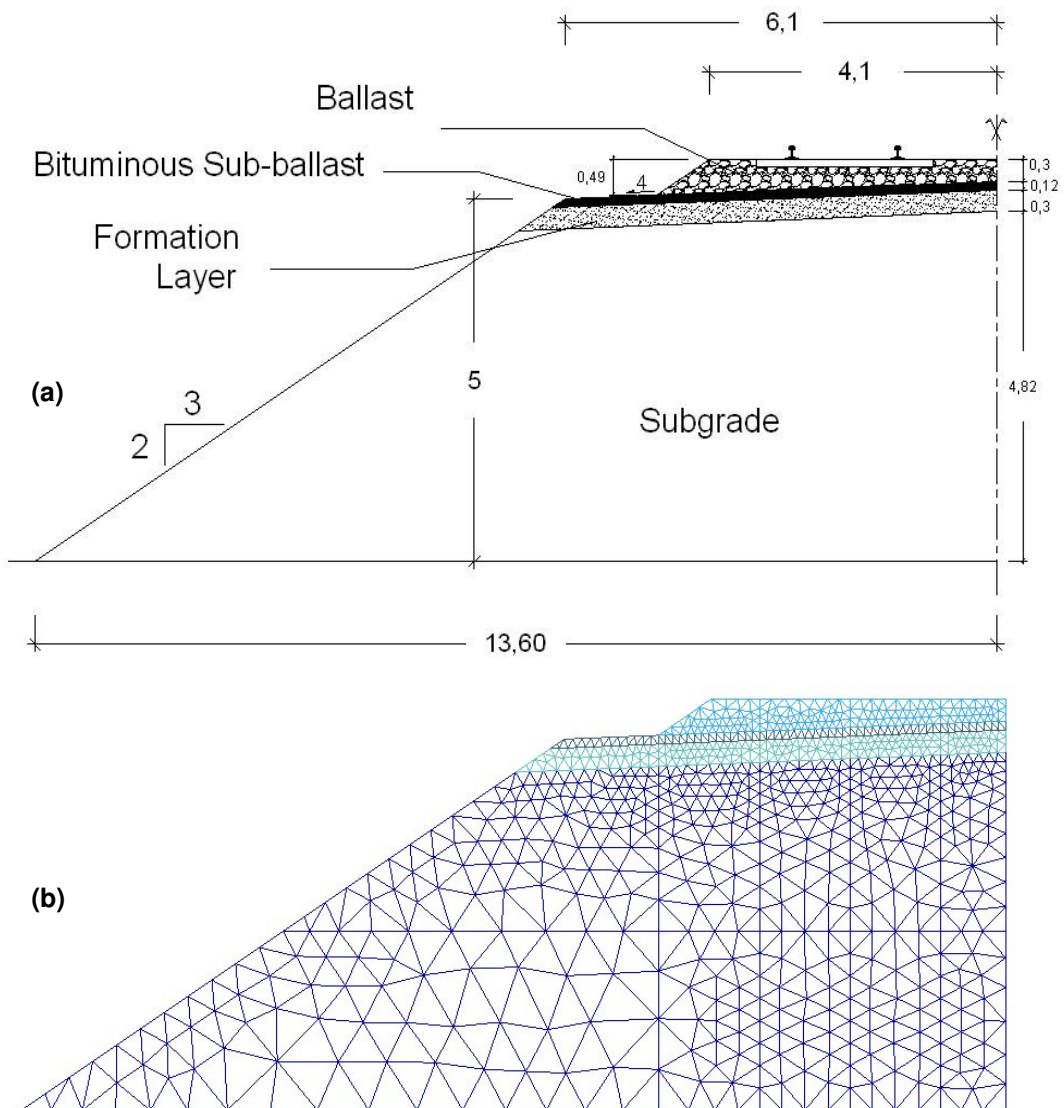


Fig. 16 – Bituminous sub-ballast cross section: (a) general design; (b) mesh (CODE\_BRIGHT).

As observed in Figure 16, major mesh density is adopted in the trackbed zone and near the rails axis line because this is considered to be the control zone. An adequate size to the finite elements within each layer is chosen.

A similar mesh is considered for the Granular sub-ballast cross section and is presented in Figure 17, where the geometry of this section is also shown. It can be observed that the geometry of this cross section is very similar to the one adopted for the Bituminous sub-ballast cross section except in the sub-ballast layer.

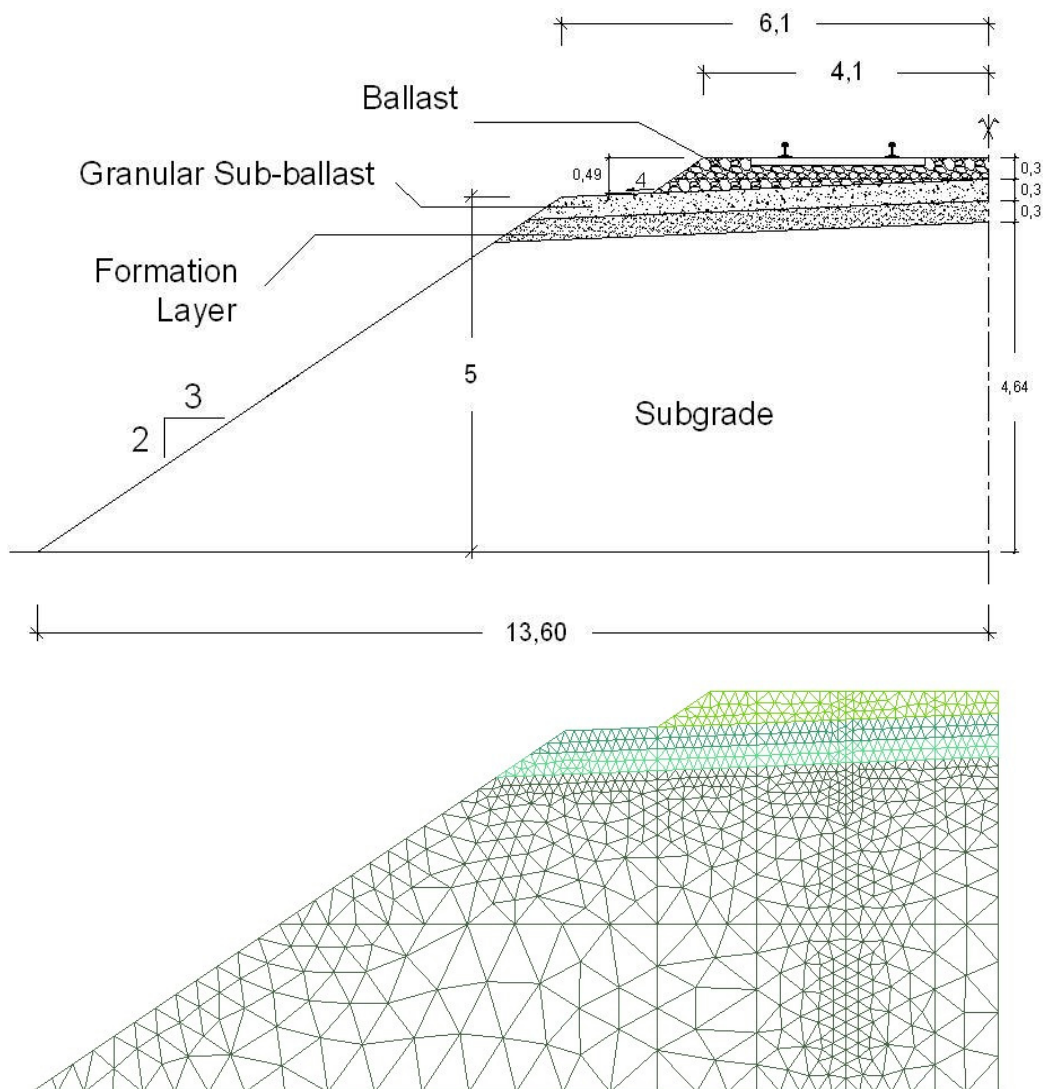


Fig. 17 – Granular sub-ballast cross section: (a) general design; (b) mesh (CODE\_BRIGHT).

### 7.3 Weather action considered

The weather actions considered in this analysis corresponds to the one from the city of Tarragona, Spain. It is a Mediterranean climate with well-defined wet and dry seasons, although it may be defined as an arid or semiarid climate. In order to carry out the simulation, a typical year is defined and is presented in Figure 18. The data (temperature variation, rainfall intensity and relative humidity) showed in Figure 18 concerns average values measured in 10 days intervals. For the purposes of the multiyear simulations performed, this average year is cyclically repeated along time (simulation for a period of 5 years – 1800 days).

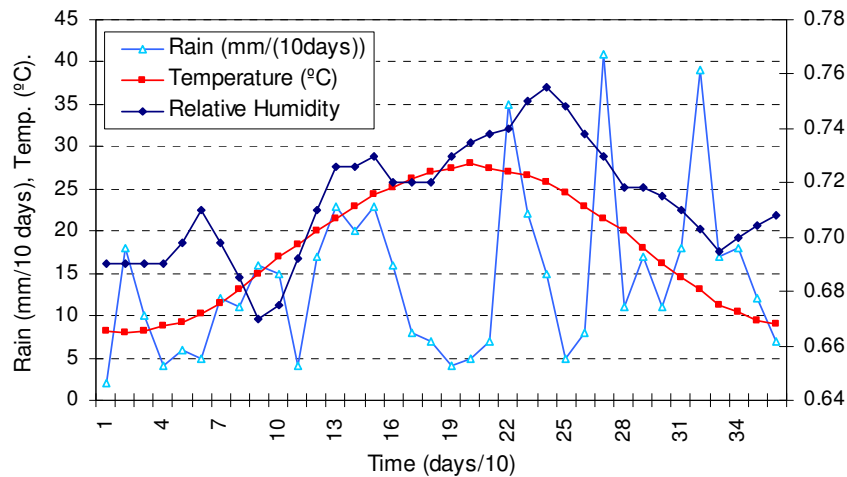


Fig. 18 – Atmospheric variables of average representative year in Tarragona, Spain.

### 7.4 Materials constitutive models calibration

Trackbed materials are described by means of the constitutive models and parameters given in Table 5. These properties were not measured in a real case but they can be assumed to adapt to the type of materials usually adopted in practice. The grading sizes of granular sub-ballast, formation layer and subgrade materials (silts, silts with clay, clayey sands and silty sands with clay, etc) correspond to dimensions smaller than the ones from ballast (gravel). The following comments may be made:

- Retention curve for ballast exhibits very small air entry pressure values (this property is controlled by parameter  $P_0$ ). Relative low suctions are capable of maintaining this material in dry conditions. These fine materials have a much higher entry pressure value than ballast. Bituminous sub-ballast has the highest value for air entry pressure to simulate its impermeability;

Table 5 – Material Models and Parameters

PROPERTY	MODEL	BALLAST	GRANULAR SUB-BALLAST	BITUMINOUS SUB-BALLAST	FORMATION LAYER	SUBGRADE	Legend
Retention curve	$S_e = \frac{S_l - S_{rl}}{S_{ls} - S_{rl}} = \left( 1 + \left( \frac{P_g - P_l}{P_0} \right)^{\frac{1}{1-\lambda}} \right)^{-1}$	$\lambda = 0.50$ $P_0 = 0.01MPa$ $S_{rl} = 0.0001$ $S_{ls} = 0.98$	$\lambda = 0.55$ $P_0 = 0.15MPa$ $S_{rl} = 0.05$ $S_{ls} = 0.80$	$\lambda = 0.50$ $P_0 = 0.35MPa$ $S_{rl} = 0.01$ $S_{ls} = 0.80$	$\lambda = 0.55$ $P_0 = 0.15MPa$ $S_{rl} = 0.05$ $S_{ls} = 0.80$	$\lambda = 0.55$ $P_0 = 0.15MPa$ $S_{rl} = 0.05$ $S_{ls} = 0.80$	$S_r$ : degree of sat. of liquid phase $P_l$ : liquid pressure $P_g$ : gas pressure
Liquid Flow	$q_l = \frac{k k_{rl}}{\mu_l} (\nabla P_l - \rho_l g)$ $k_{rl} = \sqrt{S_e} \left[ 1 - \left( \frac{1}{1 - S_e^2} \right)^{\lambda} \right]^2 \text{ or,}$ $k_{rl} = A(S_e)^\alpha$	$\lambda = 0.55$ $k = 1.0 \times 10^{-12} (m^2)$ $S_{rl} = 0.15$ $S_{ls} = 0.98$	$A = 1.0; \alpha = 3.0$ $k = 0.1 \times 10^{-19} (m^2)$ $S_{rl} = 0.01$ $S_{ls} = 0.98$	$\lambda = 0.55$ $k = 0.5 \times 10^{-15} (m^2)$ $S_{rl} = 0.15$ $S_{ls} = 0.98$	$\lambda = 0.55$ $k = 0.5 \times 10^{-15} (m^2)$ $S_{rl} = 0.15$ $S_{ls} = 0.98$	$\lambda = 0.55$ $k = 0.5 \times 10^{-15} (m^2)$ $S_{rl} = 0.15$ $S_{ls} = 0.98$	$\mu_l$ : liquid viscosity $\rho_l$ : liquid density $q_l$ : liquid advective flux $g$ : gravity
Conductive Heat Flow		$\lambda = 2(W / mK)$	$\lambda = 2(W / mK)$	$\lambda = 2(W / mK)$	$\lambda = 2(W / mK)$	$\lambda = 2(W / mK)$	$T$ : Temperature
Diffusion of Vapour	$D_m^w = - (n \rho_g (1 - S_r) D_m^w I \nabla \omega_g^w)$ $D_m^w = \mathcal{D}_0^w \left( \frac{T^r}{P_g} \right); S_g = 1 - S_r$	$t = 2.3; \tau = 1$ $D_0^w = 5.9 \times 10^{-6}$	$t = 2.3; \tau = 0.4$ $D_0^w = 5.9 \times 10^{-6}$	$t = 2.3; \tau = 1$ $D_0^w = 5.9 \times 10^{-6}$	$t = 2.3; \tau = 1$ $D_0^w = 5.9 \times 10^{-6}$	$t = 2.3; \tau = 1$ $D_0^w = 5.9 \times 10^{-6}$	$i_g^w$ : non-advective water mass flux in gas phase $n$ : porosity $\omega_g^w$ : mass fraction of water in gas phase
Deformation	Linear elastic (E, $\nu$ ) Strain due to suction and temperature changes: $\Delta \epsilon_v = 3a\Delta(P_l - P_g) + 3b\Delta T$	$E = 150MPa$ $\nu = 0.33$ $a = 0.0025$ $b = 0.55 \times 10^{-5}$	$E = 50MPa$ $\nu = 0.33$ $a = 0.0025$ $b = 0.55 \times 10^{-5}$	$E = 3000MPa$ $\nu = 0.33$ $a = 0.00$ $b = 0.55 \times 10^{-5}$	$E = 50MPa$ $\nu = 0.33$ $a = 0.0025$ $b = 0.55 \times 10^{-5}$	$E = 50MPa$ $\nu = 0.33$ $a = 0.0025$ $b = 0.55 \times 10^{-5}$	$\nu$ : Poisson Coefficient $E$ : Young Modulus

- Intrinsic permeability matches the grain size distribution expected for the trackbed materials. Subgrade permeability is also consistent with its retention curve. Ballast has a high value for permeability and Bituminous sub-ballast a smaller one, so the relative permeability properties of these two materials will be modeled;
- Water vapour flow is simulated by means of Fick's law. Equal calibration was used for all the materials due to the lack of information (diffusion vapour molecular coefficient  $D_0^w$ , constant  $t$  and tortuosity parameter  $\tau$  – Eq. (39));  $D_0^w$  depends on temperature, and controls the intensity of vapour mass transfer;
- A linear elastic stress-strain relationship is adopted (the discussion concerning the elastic behaviour of the soil when subjected to suction cycles was done in Chapter 3, section 2, when BBM was presented). This assumption means that the stress/suction paths are within the region limited by the LC and the SI curves in plane  $(p, s)$ . A linear law is also used for strain calculation due to suction and temperature changes, which is given in Table 5. For the calibration of this law it is assumed that Ballast and Bituminous sub-ballast are very stiff against suction changes ( $a = 0.00$ ) because they do not present swelling potential. The subgrade and the granular materials, which are assumed to have some mass percentage of fines, however, can change its volume under suction changes (it swells or shrinks). Assuming compacted materials with good quality therefore with small swelling potential, a small value for the stiffness against suction changes was adopted ( $a = 0.0025$ );
- All the trackbed layers dilate or contract when subjected to temperature changes ( $b = 0.55 \times 10^{-5}$ );
- Due to insufficient information, for all materials it is assumed standard values for thermal conductivity,  $\lambda$ .

## 7.5 Boundary Conditions

The initial water content corresponds to an equilibrium situation consistent with the water level located at the lowest boundary of the discretized domain. Boundary conditions are given in Figure 19.

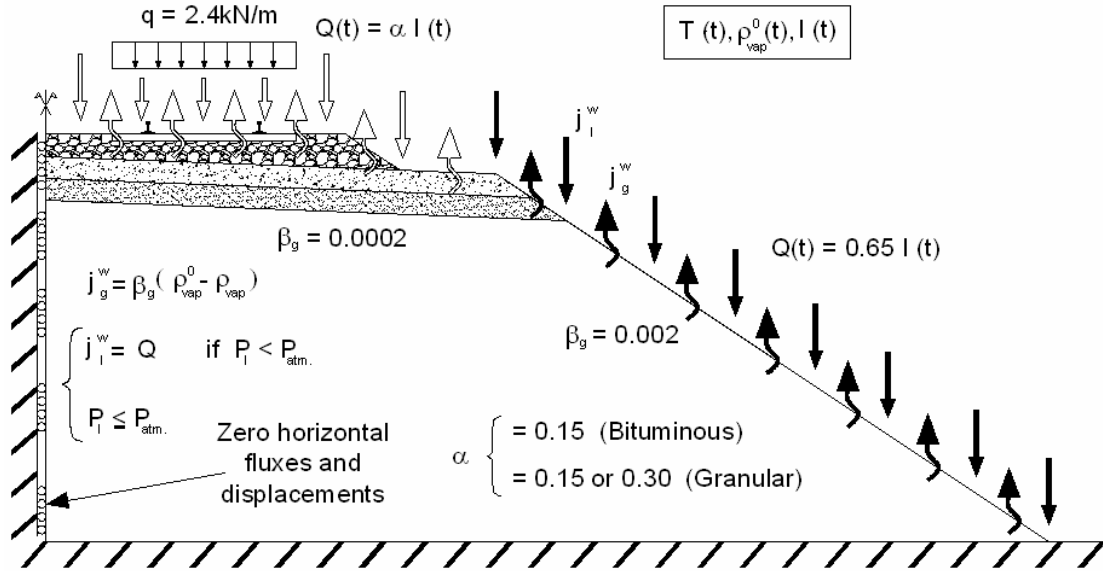


Fig. 19 – Boundary flow rate conditions.

Providing that the water pressure in the boundaries does not reach the atmospheric value, it is assumed that only a given percentage of rain intensity infiltrates into the trackbed layers. This percentage is related with rain's infiltration as well as the quantity of water that is not drained and is assumed to depend on the surface exposed to rain. Alonso (1998) adopted the value of 15% and 65% to the bituminous and to slope coefficient, respectively. Similar values were adopted in this work, but with small changes. For the slope boundary (non-paved area) a constant coefficient of 65% is adopted. For the upper boundary it is adopted the value  $\alpha$  (presented in Figure 19), which depends on the trackbed material. In fact, due to its hydraulic characteristics, it is expected that Bituminous sub-ballast exhibits better behaviour in terms of drainage than granular sub-ballast. Therefore, less quantity of water is available on the top of the platform when bituminous is used. This indicates that the  $\alpha$  adopted for the bituminous should be inferior to the one adopted to the granular material (for upper boundary it is assumed  $\alpha=15\%$  for the Bituminous and  $\alpha=30\%$  for the Granular). However it is also analyzed  $\alpha=15\%$  for the Granular for comparison purposes with the Bituminous.

Water vapour flow at the boundaries is controlled by the linear law expressed in Equation (60):

$$j_g^w = \beta_g (\rho_{vap}^0 - \rho_{vap}) \quad (60)$$

which specifies that the evaporative flux is proportional to the difference between vapour density computed at the upper boundaries of the trackbed and water vapour at the atmosphere (given as part of the climate variables). It is considered  $\beta_g = 0.0002$  in the upper boundary and  $\beta_g = 0.002$  in the slope.

To simulate the surcharge of rails and sleepers, a weight of  $6kN$  per linear meter of rail is considered. In a sleeper with  $2.5m$  length this surcharge is equivalent to a load of  $2.4kN/m$ .

As mentioned before, this simulation concerns the evolution in a period of 5 years – 1800 days – of Temperature, Relative Humidity, and Rain intensity. Using CODE\_BRIGTH (Olivella et al., 1994, 1996; DIT-UPC, 2000) it is necessary to input for each time interval (10 days) these prescribed climate data as a boundary condition “flow rate”.

- Temperature

Temperature is prescribed for each time interval in  $^{\circ}C$ .

- Relative Humidity

This software allows the input of the Relative Humidity for each time interval by prescribing the Vapour Mass Fraction,  $\omega_g^w$ . Temperature and RH are used to calculate Vapour Mass Fraction as follows:

Vapour pressure for a given Temperature,  $T(^{\circ}C)$ , is calculated as (Eq. (61)):

$$p_v = 136075 \exp\left(\frac{-5239.7}{273.15 + T}\right) \quad (MPa) \quad (61)$$

and the corresponding density is (Eq. 62):

$$\rho_v = \frac{p_v M}{R(273.15 + T)} = \frac{3536 Pa \times 0.018 kg/mol}{8.3143 J/mol/K \times (273.15 + T)K} \quad (kg/m^3) \quad (62)$$

Vapour Mass Fraction for a given Relative Humidity,  $HR$ , and a fixed Gas Density  $\rho_g = 1.12 kg/m^3$  (specific from CODE\_BRIGTH) is calculated as follows (Eq. (63)):

$$\omega_g^w = \frac{HR \cdot \rho_v}{\rho_g} \quad (kg/kg) \quad (63)$$

- Rainfall

As mentioned before, different percentages of rain infiltration are considered for upper and slope boundaries. The prescribed liquid flow is calculated using Equation (64):

$$j_l = \frac{\alpha \cdot I(\text{mm}/10\text{days})}{86400(\text{s})} \quad (\text{kg} / \text{s}) \quad (64)$$

Other numerical values for boundary flow rate, common to all time intervals, needed to be defined to run the program and are presented in Table 6:

**Table 6 – Numerical values for boundary flow rate.**

Prescribed Liquid Pressure - $P_l$	(MPa)	0.10
Gamma for Liquid - $\gamma_l$	(kg / s / MPa)	-100
Liquid Density - $\rho_l$	(kg / m <sup>3</sup> )	1000
Gamma for Heat - $\gamma_e$	(J / s / C)	10
Smoothing parameter - $\delta$		0.01

Finally, it should be said that no longitudinal drainage is assumed within the model. This could represent an assumption of track structure under poor drainage conditions. The impact of this limitation on the results obtained will be discussed in Chapter 8.

## 7.6 Initial Unknowns

Some initial values have to be assumed for porosity (or void ratio) and initial suction. For initial suction it is assumed 3MPa which seems to be a realistic value for the compaction procedures usually adopted in embankment construction (Alonso, 1994). Table 7 presents the values adopted for the initial porosity and void ratio of materials as well as the initial temperature and confining stress:

**Table 7 – Initial unknowns: Porosity, Liquid Pressure, Temperature and Stress.**

	Porosity - $n = \frac{e}{1+e}$	Void ratio - $e$
Ballast	0.50	1.00
Granular sub-ballast	0.40	0.67
Bituminous sub-ballast	0.10	0.11
Formation Layer	0.40	0.67
Subgrade	0.40	0.67

Liquid Pressure - $P_l$	Temperature - $T$	Stress - $\sigma_x = \sigma_y$
- 3MPa	18° C	- 0.01MPa

## 8. Study on the performance of the two trackbed solutions for five years under poor drainage conditions

### 8.1 Introduction

This chapter presents the calculation with CODE\_BRIGHT of the models described in Chapter 7. These models were defined to simulate two different railway trackbed solutions named Granular and Bituminous cross sections. The analysis performed is likely to be representing cases of poor drainage conditions, since no drains will be considered on the model. The displacements calculated in several points (Figure 20) of the two design solutions analyzed will be compared to evaluate their performance. As explained in Chapter 7, section 5, a given percentage of rain intensity named  $\alpha$  is adopted in the pavement area (upper boundary) and is different for both trackbed solutions. The cases analyzed are  $\alpha=15\%$  for the Bituminous and Granular cross sections, to allow a direct comparison between both designs; it is also considered  $\alpha=30\%$  for Granular cross section, to take into account its hydraulic characteristics when compared with the Bituminous one. The results for all cases are presented in this chapter as well as the results from calculation used to validate it, namely the seasonal evolution in time of the temperature, degree of saturation and relative humidity.

Some changes are introduced in the models previously presented in Chapter 7.2 (Original designs) to evaluate the influence of the geometry adopted for the calculation. This analysis is important to evaluate the influence of the water flow under poor drainage conditions. It is simulated an embankment lower than the first one (named Lower design) and an embankment similar to the Original one but with a larger platform (named Extended design). Their inclusion aimed to compare the influence of the water exchanges between the embankment shoulders and the atmosphere in terms of displacements under the rail axis. Both cross sections are analyzed for these two alternative designs. Materials, boundary conditions (except in particular cases that will be mentioned) and initial conditions are identical to those considered in the Original sections.

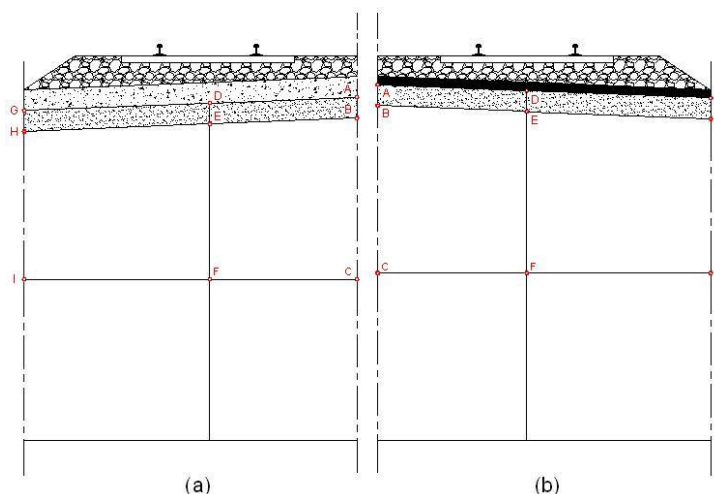
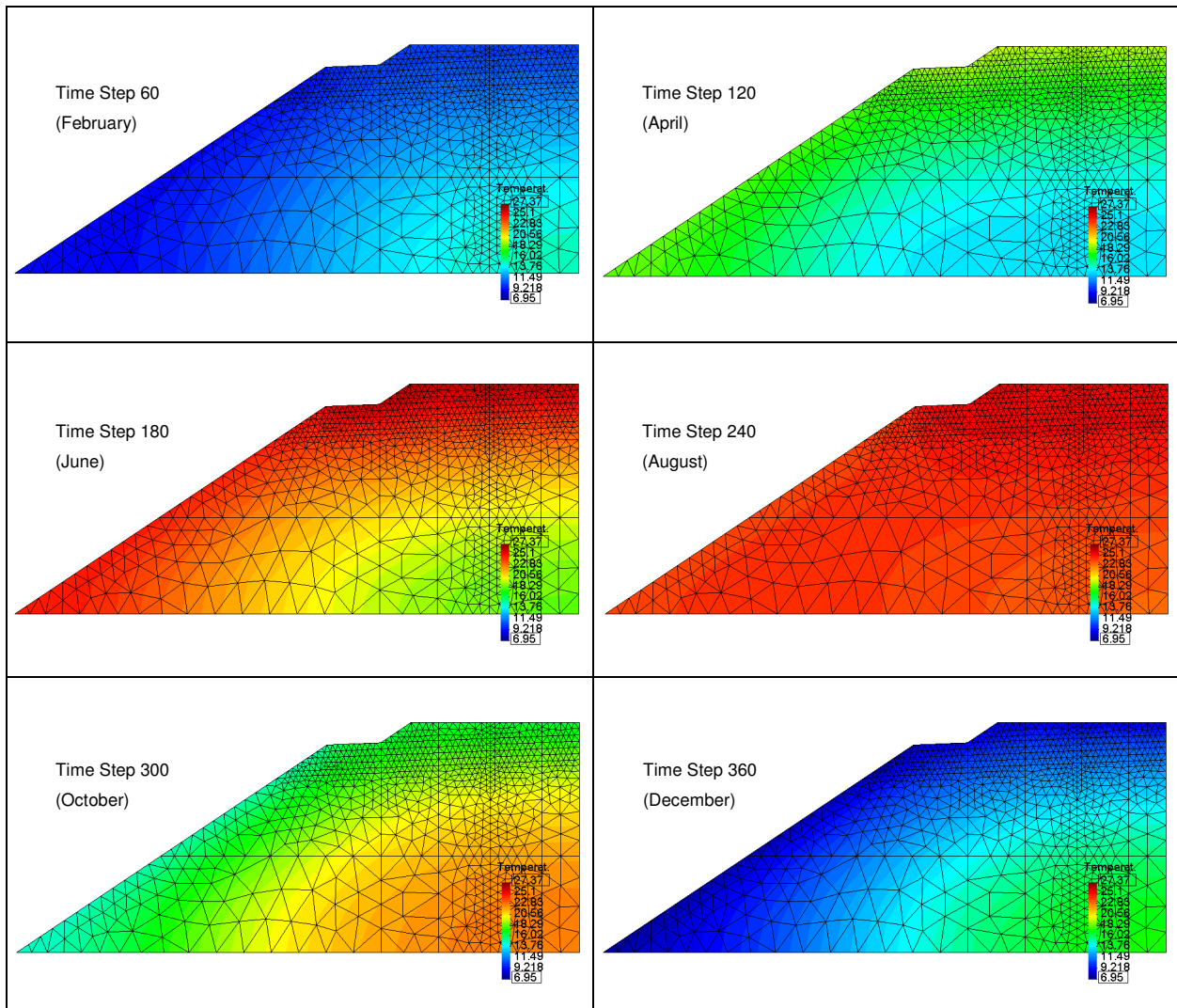


Fig. 20 – Control Points: (a) Granular Sub-ballast; (b) Bituminous Sub-ballast.

## 8.2 Results for Bituminous and Granular sub-ballast designs

### 8.2.1 Temperature

Temperature is one of the climate variables analyzed. The following sequence of images in Figure 21 shows the evolution of the Temperature during the first year for the Granular cross section using  $\alpha = 15\%$ . Similar results were found for the Bituminous one since the properties of all the materials concerning the temperature are identical (presented in Table 5 from Chapter 7, section 4).



**Fig. 21 – Temperature evolution during first year (Original Granular cross section  $\alpha = 15\%$ )**

The evolution of the Temperature calculated in Points D, E and F during the five years can be observed on Figure 22, showing that the average value is the same and corresponds to the average temperature of Tarragona ( $18^{\circ}\text{C}$ ). Seasonal Temperature evolution corresponding to summer (high temperatures) and winter (low temperatures) is well demarked. The differences in depth observed in Figures 21 and 21 result from the delay of Temperature

distribution (usually called thermal inertia) since the deepest layers are colder than the ones at the upper surface in summer, and warmer in winter. A reduction with deep of the Temperature range is also observed in Figure 22; as expected, the upper layers are more sensible to temperature changes than the deeper ones.

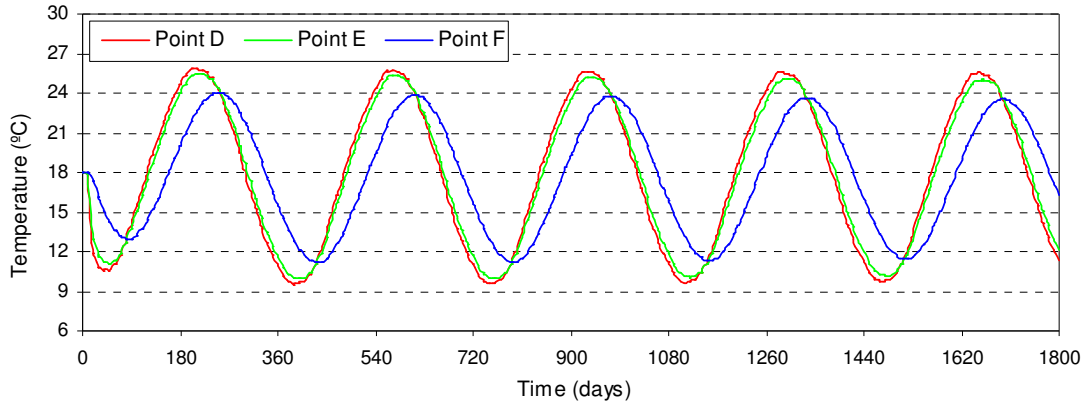


**Fig. 22 – Temperature evolution on Points D, E and F along five years  
(Original Granular cross section)**

### 8.2.2 Relative Humidity

Considering the same points analyzed for Temperature (D, E and F), Figure 23 presents the evolution of Relative Humidity inside the embankment during the 5 years of the simulation.

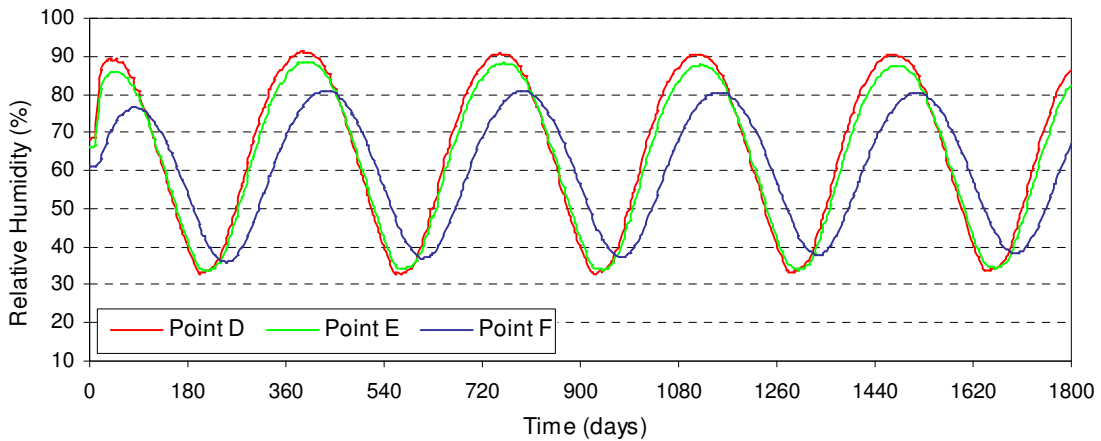


**Fig. 23 – Relative Humidity evolution on Points D, E and F during five years  
(Original Granular cross section ( $\alpha = 15\%$ ))**

In Figure 23, the lag between the RH calculated in each control point indicates that the total amount of water does not reach depth once the Relative Humidity calculated on point F in the subgrade has smaller values than those calculated in the more superficial layers. As well as Temperature, it is possible to observe a seasonal behaviour in RH evolution: low values corresponding to summer periods and relatively high values for winter. The range for Relative

Humidity values inside the embankment registered in Figure 23 is larger than the one presented for atmospheric RH in climate data (Figure 18). This fact is due to the complex interaction between temperature, rainfall, atmospheric RH and water accumulation inside the embankment.

From Figure 23 it is possible to obtain the relation between RH values and correspondent reductions of the different layers for the granular sub-ballast cross section ( $\alpha = 15\%$ ). An adequate procedure to found these relations was described in Chapter 5, considering a greater number of control points over the rail axis line according to Figure 8.

### 8.2.3 Liquid Saturation

The impervious properties of the bituminous are well known and are assumed to be the most important advantage of the use of this material for trackbed construction instead of granular materials. This assumption can be verified by comparing the evolution of the degree of saturation in both design solutions.

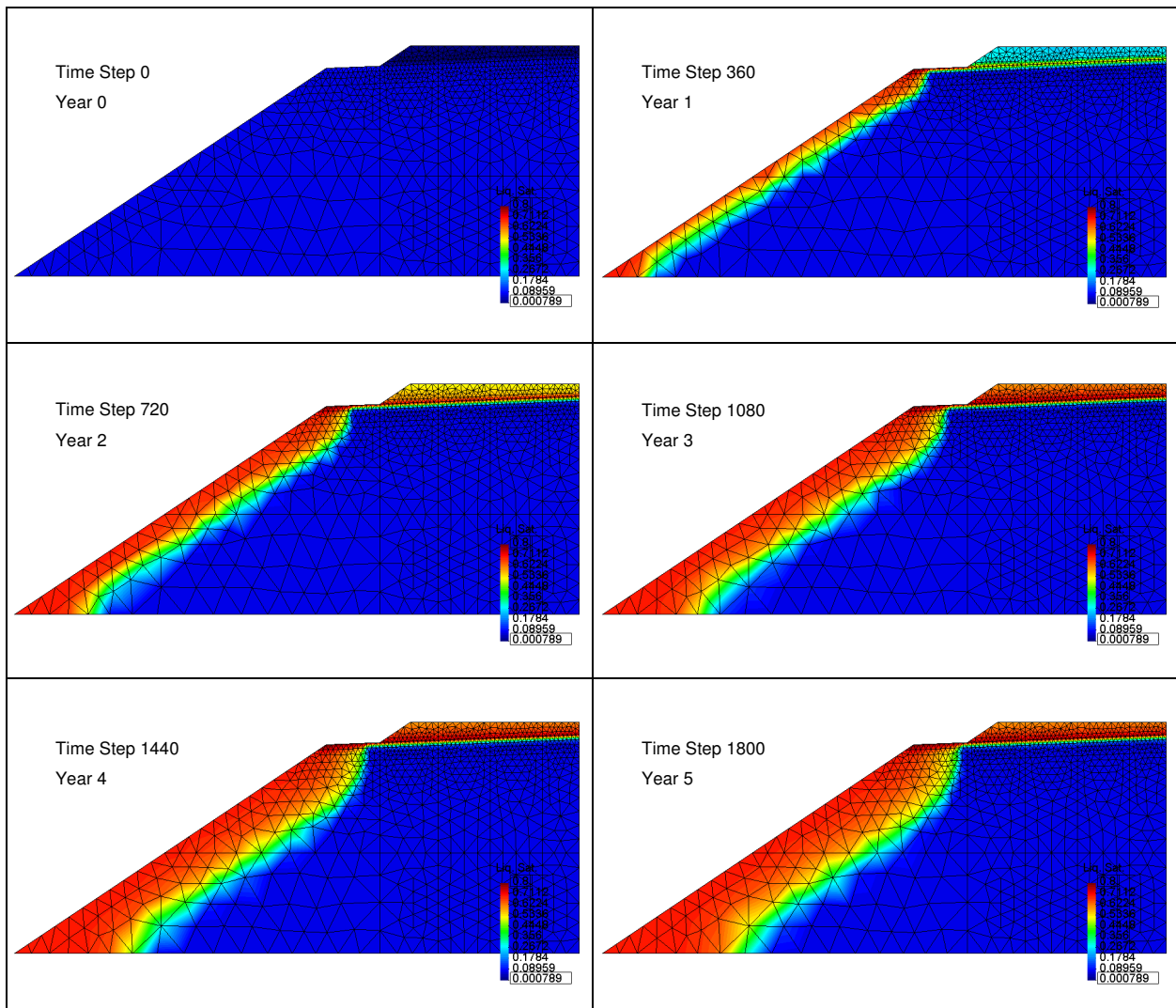
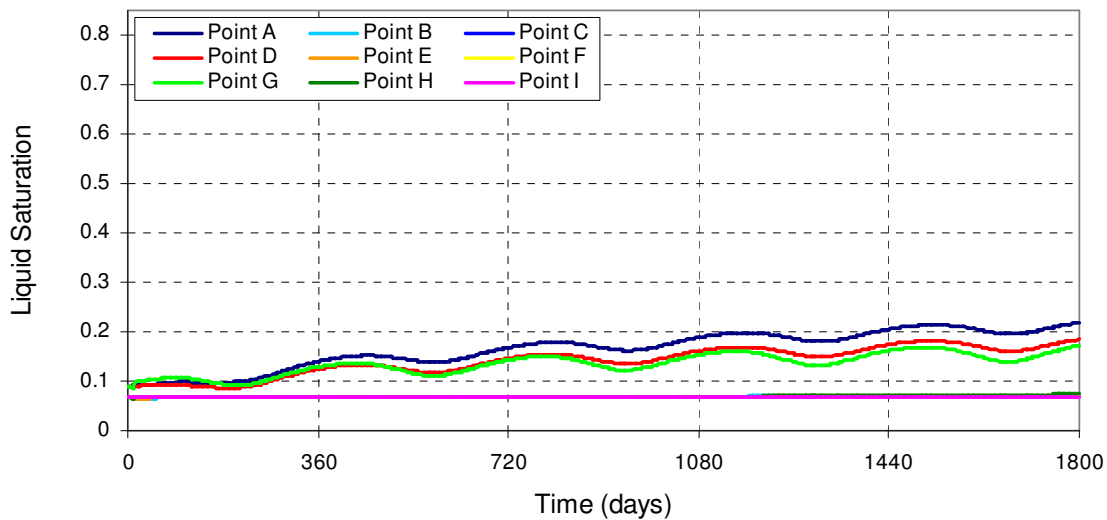


Fig. 24 – Liquid Saturation evolution during 5 years (Original Bituminous cross section ( $\alpha = 15\%$ ))

Figure 24 shows the evolution of the Liquid Saturation during five years for the Bituminous sub-ballast cross section (for this material it was assumed the percentage of rain intensity  $\alpha = 15\%$  ).

Figure 25 presents the evolution of the Liquid Saturation in the control points of the Bituminous sub-ballast cross section, along all simulation time – 1800 days.



**Fig. 25 – Liquid Saturation evolution on control points (Original Bituminous cross section ( $\alpha = 15\%$ )).**

In Figure 24 the geometric distribution of liquid water inside the embankment clearly shows the Bituminous sub-ballast working as a barrier against water infiltration. This almost impermeable layer is responsible for water accumulation in the ballast.

Cyclic (elastic) phenomena are well demarked in points A, D and G (Figure 25), the ones more affected by environmental changes in terms of Liquid Saturation due to its proximity to the Bituminous sub-ballast. The maximum degree of saturation calculated in the five years is relatively low (less than 25%, in point A). Maximum values are attained in the upper control points. The deepest ones are barely affected.

Lateral infiltration leads to a constant increase of liquid saturation and water flow near the slope boundary. This problem, as well as water accumulation in ballast, is due to the absence of drains in the model (this question will be discussed in section 5).

The results from the calculation of the evolution in time of the Liquid Saturation in the Granular sub-ballast cross sections are presented in the following figures. Two percentages of rain intensity,  $\alpha = 15\%$  and  $\alpha = 30\%$  , were analyzed. Figures 26 and 27 show the evolution of the liquid saturation inside the embankment for  $\alpha = 15\%$  . Figures 28 and 29 show it for  $\alpha = 30\%$  .

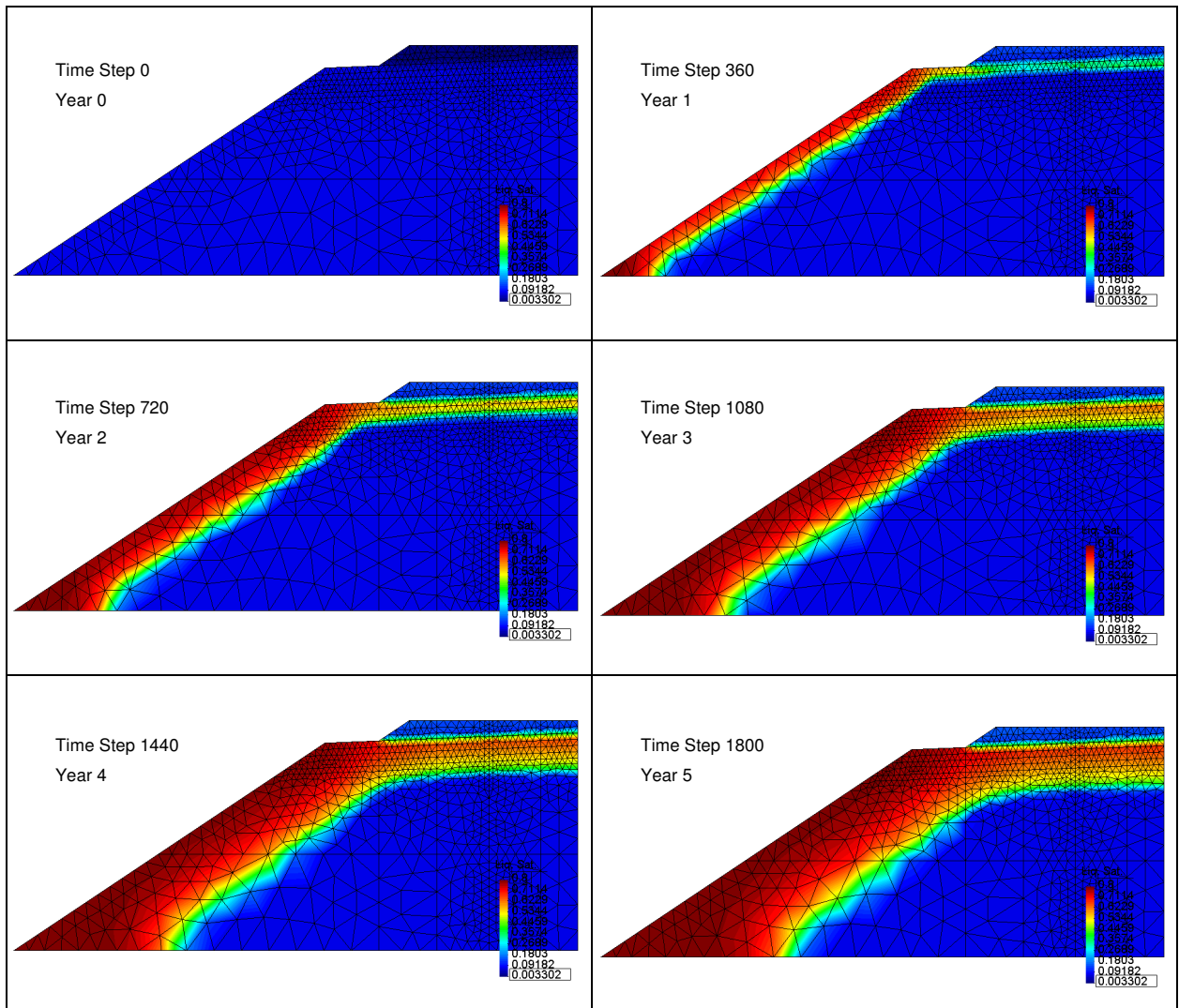


Fig. 26 – Liquid Saturation evolution during 5 years (Original Granular cross section ( $\alpha = 15\%$ ))

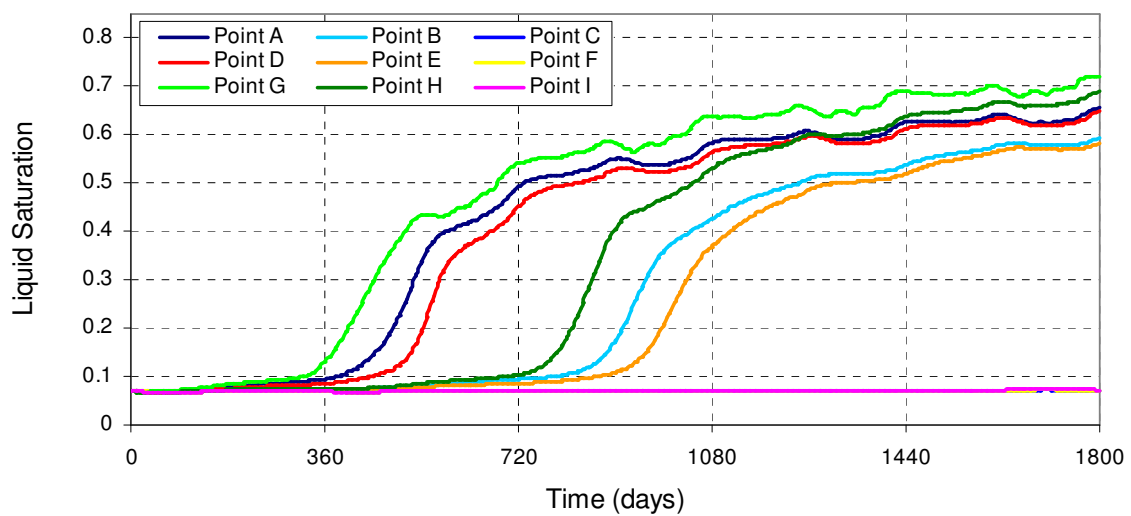
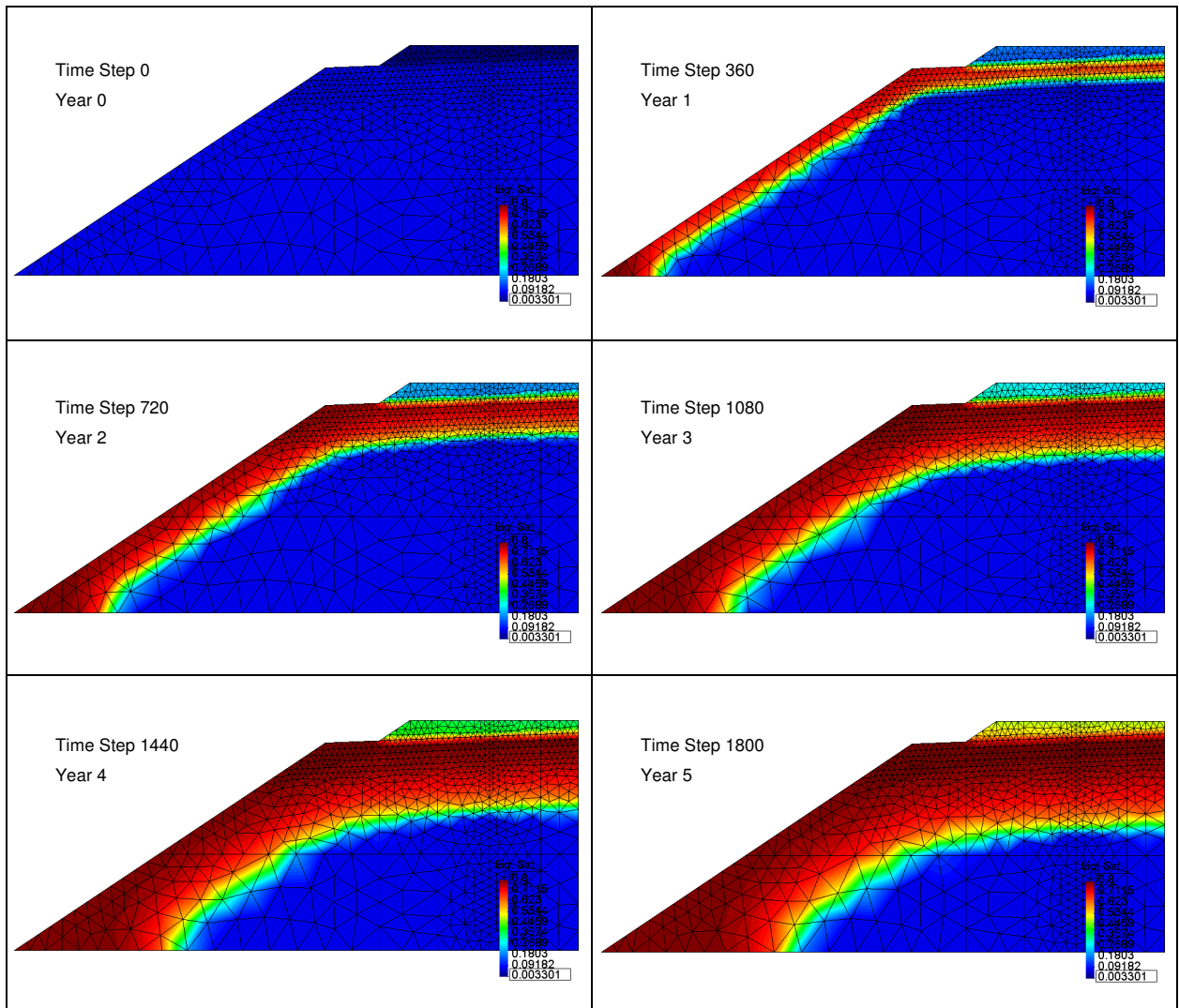
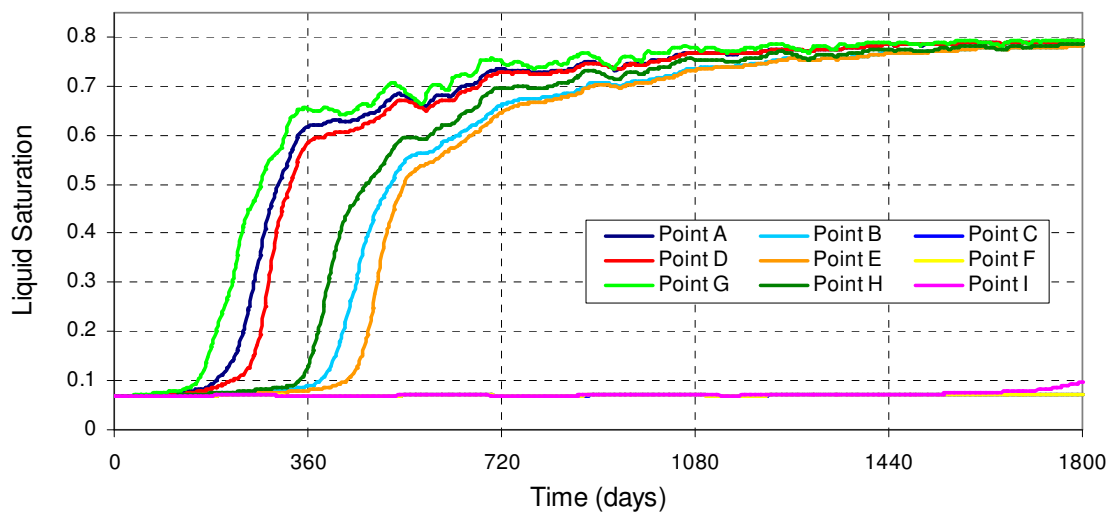


Fig. 27 – Liquid Saturation evolution on control points (Original Granular cross section ( $\alpha = 15\%$ )).



**Fig. 28 – Liquid Saturation evolution during 5 years (Original Granular cross section ( $\alpha = 30\%$ ))**



**Fig. 29 – Liquid Saturation evolution on control points (Original Granular cross section ( $\alpha = 30\%$ ))**

Granular sub-ballast allows water flowing through it, in opposite to what happens for the Bituminous one. This can be observed by comparing the Liquid Saturation increase in depth under the platform in Figures 26 and 28, for the Granular cross sections, and in Figure 24 for the Bituminous cross section (the same scale was adopted in Figures 24, 26 and 28). The permeability of the Granular sub-ballast allows a gradual increase of water inside the embankment. As expected, for a coefficient of infiltration  $\alpha=30\%$ , the advance in liquid saturation is greater than for  $\alpha=15\%$ .

The accumulation of water in the ballast is insignificant for  $\alpha=15\%$  (Figure 26), although, for greater percentages of rain infiltration the excess of water is not drained.

As registered for the Bituminous sub-ballast cross section, for the Granular cross sections analyzed there is a constant increase of liquid saturation and water flow in the slope boundary due to the absence of drains.

The evolution of the Liquid Saturation calculated in the upper control points for  $\alpha=15\%$  (Figure 27), shows a gradual increasing in time (with a maximum of 60 - 70%) and without reaching steady values after five years. For  $\alpha=30\%$  (Figure 29) the Liquid Saturation increases faster than the observed for  $\alpha=15\%$  and reaches a steady value (80%) after two years. This value corresponds to the maximum allowed for soil water retention and was imposed when the Retention Curves of the materials were defined (Table 5, Chapter 7, section 4). As expected, independently from the cross section and from the rain intensity adopted in the Granular trackbed design solution, the points at the deepest layers (F and I) are not affected by the water infiltration.

## 8.2.4 Vertical Displacements

Environmental changes in Temperature, Relative Humidity and Rain lead to deformations defined by the law presented in Table 5. Computations with CODE\_BRIGHT allow the calculation of Vertical Displacements for the cross section designs previously presented.

Figures 30, 31 and 32 show the Vertical Displacements calculated along the five years. As before, the values presented were found for the representative points from Figure 20 for the Bituminous and Granular sub-ballast cross sections considered in this analyzes. The two different coefficients of water infiltration,  $\alpha$ , were analyzed for the Granular sub-ballast cross section.

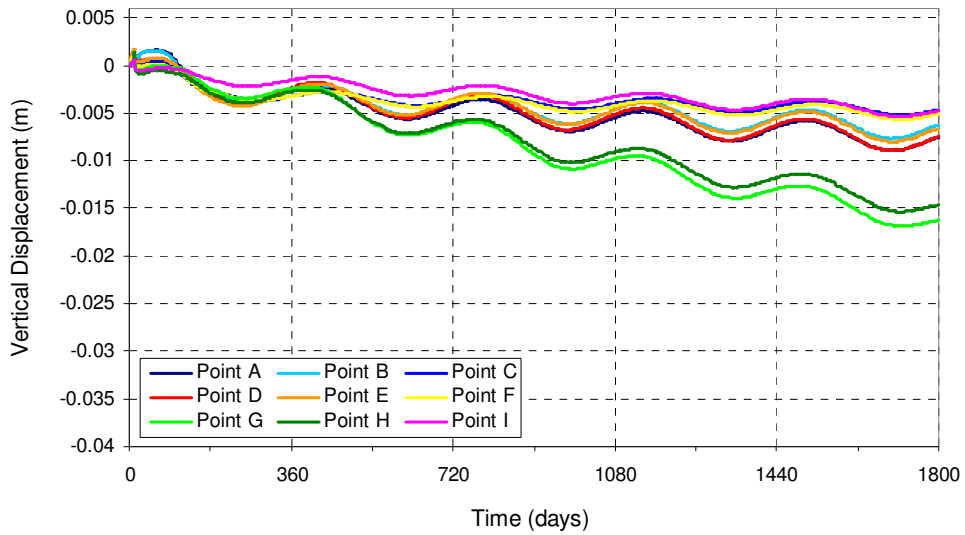


**Fig. 30 – Vertical Displacements variation on control points (Original Bituminous cross section ( $\alpha = 15\%$ )).**

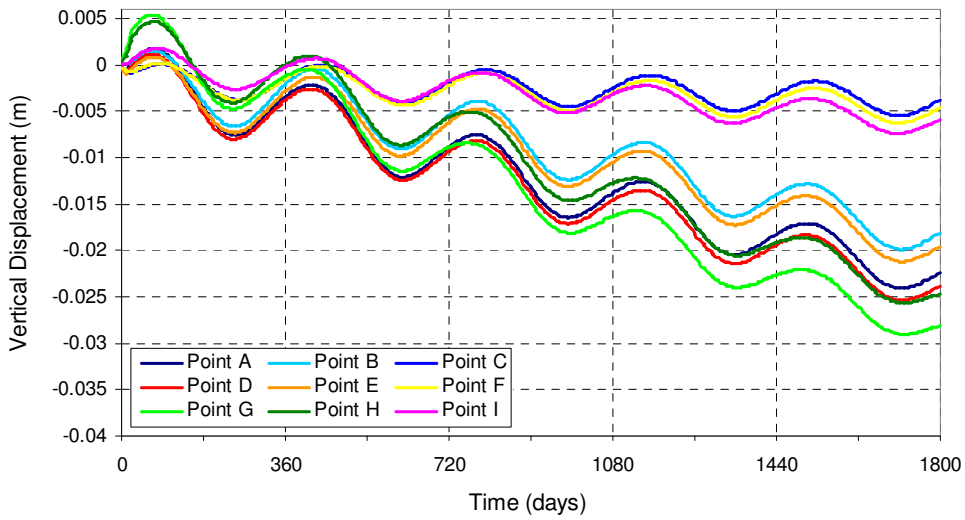


**Fig. 31 – Vertical Displacements variation on control points (Original Granular cross section ( $\alpha = 15\%$ )).**

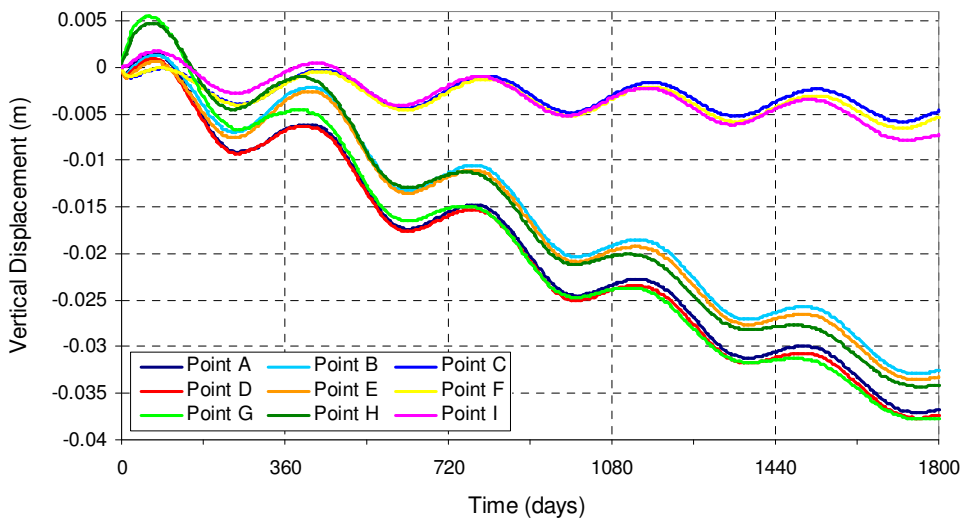


**Fig. 32 – Vertical Displacements variation on control points (Original Granular cross section ( $\alpha = 30\%$ )).**

The evolution of the Vertical Displacements found for all sections are very similar, however smaller displacements are registered for the Bituminous cross section. Independently from the cross section analyzed, the displacements measured are very small for the deepest points (Points C, F and G). In all cases, cyclic (elastic) phenomena can be observed since a bimodal curve is obtained in the calculation of each year and is repeated every year. It is possible to define an average variation associated to the range of the vertical displacements registered which is decreasing in all cases, indicating a progressive settlement of layers.

For the Bituminous cross section (Figure 30), the control points located above the bituminous layer (points A and D) and below it (points B and E) show similar paths of displacements. Points C, F and I, also show similar paths and have in common their deeper position. Points G and H show the highest displacements which can be explained by their location near the slope, having a relatively low protection against water flow from this boundary. It is possible to distinguish relevant differences in the Vertical Displacements calculated in the control points located above (A and D) and below (B and E) the bituminous sub-ballast layer, which may be explained by the impervious effect of this material.

The analysis of the cyclic pattern of the Vertical Displacements observed for the Bituminous cross section is presented in Table 8. This table presents the Vertical Displacements calculated in the control points at the end of the five years (1800 days) and also the maximum amplitude of its variation (the difference between the maximum and the minimum displacements found in each year).

**Table 8 – Vertical Displacements (Original Bituminous cross section ( $\alpha = 15\%$ )).**

Points	Vertical Displacement 1800 days (mm)	Approximated Amplitude of the Vertical Displacements (mm)
A D	7.5	3 - 4
B E	6.2 - 6.5	3 - 4
G H	14.3 - 16.2	4 - 5
C F I	4.5 - 5.1	2

Vertical Displacements associated to the end of 5 years are the greatest ones registered for all simulation time and correspond to the winter season.

The impervious protection given by the bituminous is clearly detected when comparing the results obtained in this cross section with those found for the Granular sub-ballast cross sections (Table 9). For these last ones, the points below the sub-ballast are strongly affected by the environment and the Vertical Displacements from these sections are higher than those found for the Bituminous cross section. Another consequence of the higher permeability of the granular materials compared to the one of the bituminous is that the cyclic variation of the displacements is not so well demarked and the settlements increase more in time, showing a marked accumulation. Figures 31 and 32 present the displacements found for the Granular sub-ballast cross sections, showing a significant aggravation when  $\alpha = 30\%$ . As for Table 8, Table 9 presents the displacements calculated in the control points at the end of five years (1800 days) and their maximum amplitude.

**Table 9 – Vertical Displacements (Original Granular cross section ( $\alpha = 15\%$  and  $\alpha = 30\%$ )).**

Points	Vertical Displacement		Approximated Amplitude of the	
	1800 days (mm)		Vertical Displacements (mm)	
	$\alpha = 15\%$	$\alpha = 30\%$	$\alpha = 15\%$	$\alpha = 30\%$
A D	22.5 - 24.0	37.0 - 37.5	7 - 10	8 - 11
B E	18.0 - 20.0	32.5 - 33.5	6 - 8	7 - 10
G H	24.5 - 28.0	34.0 - 38.0	9 - 12	7 - 11
C F I	4.0 - 6.0	5.0 - 7.5	5	5

A qualitative reduction performed by the bituminous sub-ballast (Bituminous reduction) when compared with the granular one can be established by the same relation presented in Eq. (30) presented in Chapter 5.2 and using  $\Delta_{Bit}$  for the displacements calculated on the Bituminous cross section (Table 8) and  $\Delta_{Gran}$  for the displacements calculated on the Granular cross section (Table 9). The values found, converted into percentage, are presented in Table 10.

**Table 10 – Ranges for Qualitative reduction performed by bituminous sub-ballast – Displacements.**

Points	Vertical Displacement Reduction		Average Amplitude of the	
	1800 days (%)		Vertical Displacements (%)	
	$\alpha = 15\%$	$\alpha = 30\%$	$\alpha = 15\%$	$\alpha = 30\%$
A D	66 - 70	80	40 - 70	50 - 70
B E	64 - 69	81	30 - 60	40 - 70
G H	34 - 49	52 - 62	40 - 70	30 - 60
C F I	$\approx 0$	$\approx 0$	60	60

Table 10 shows that bituminous sub-ballast performs a significant reduction in terms of the values registered for Vertical Displacements and their amplitude during a year. As expected, this reduction is higher for  $\alpha = 30\%$  than for  $\alpha = 15\%$ . For example, analyzing points A and D and considering  $\alpha = 15\%$ , bituminous sub-ballast performs a reduction in Vertical Displacements in a range of 66% to 70% as well as a reduction in terms of the amplitude of these displacements in a range of 40% to 70% when compared with the granular one. For  $\alpha = 30\%$ , the reduction in Vertical Displacements due to the bituminous sub-ballast considering the same points is 80% and the range of reduction for correspondent amplitudes is 50% to 70%.

These facts indicate that the adoption of a bituminous sub-ballast allows a better performance of the railway infrastructure for fatigue and other negative impacts caused by the occurrence of cyclic displacements due to weather actions. Seasonal distributions in displacements, as well as their irregular evolution are responsible for great implications in the railway maintenance costs.

## 8.3 Geometry influence in the hydraulic boundary conditions

### 8.3.1 Models considered

The results of the evolution in time of the Liquid Saturation and Vertical Displacements in several control points located under the railway track could be explained by the water infiltration and accumulation inside the embankment. The absence of drains in the numerical model can be the main reason for this accumulation, however the values calculated in the external control points immediately above the bituminous layer of the Bituminous cross section (points G and H from Figure 20) are superior to those expected due to the impervious property of the bituminous. This fact indicates that the water exchanged in the slope (hydraulic boundary condition) also affects these points leading to higher Vertical Displacements. In this section, two alternative solutions will be studied to clarify the influence of the geometry of the embankment in the displacements measured. Only the exposed area of the slopes was changed in these new solutions. The materials and their calibration, the initial conditions, climate data, loads and boundary conditions of these alternative numerical models are identical to those adopted for the Original cross sections analyzed and presented in Chapter 7.

An alternative design is an extension of the first one by eliminating the slope. This solution, named Extended cross section, is an extreme case, where there is no interference of the slope boundary conditions in the results. Figure 33 shows the Extended Granular sub-ballast cross section and the correspondent mesh (a similar one is considered for Extended Bituminous sub-ballast cross section).

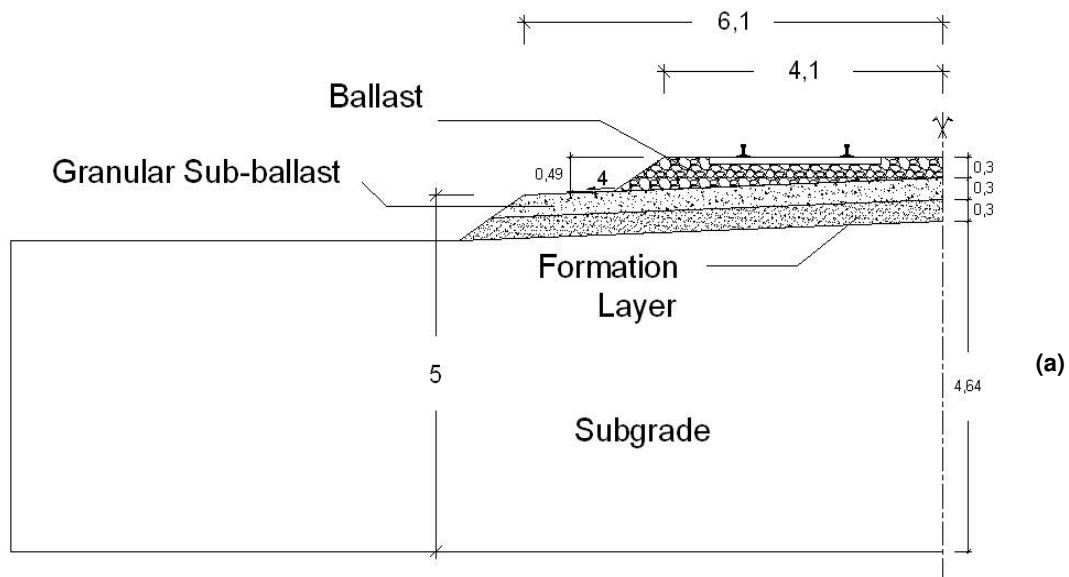
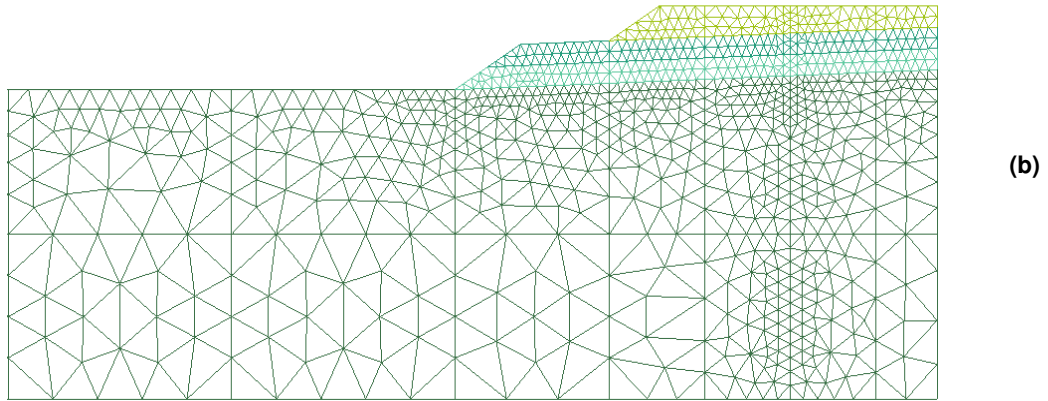


Fig. 33 (a) – Extended granular sub-ballast cross section: general design.

**Note:** the embankment was extended more than is represented.



**Fig. 33 (b) – Extended granular sub-ballast cross section: mesh (CODE\_BRIGHT).**

The other design solution consists on reducing the height of the embankment. The new embankment has 2.6 meters tall (approximately half height of the first one) and will be named Lower embankment. Correspondent Lower Bituminous sub-ballast cross section and associated mesh are represented in Figure 34 (a similar one is considered for Lower Granular sub-ballast cross section).

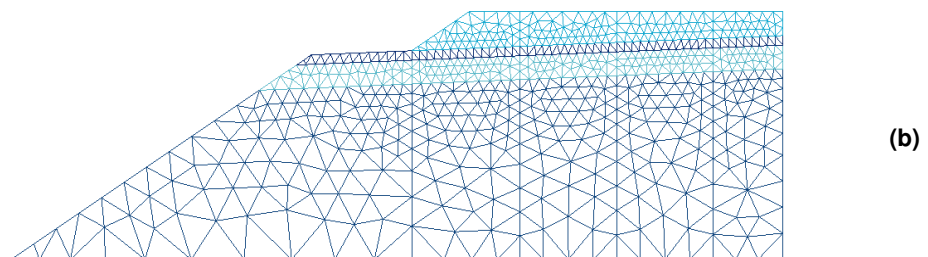
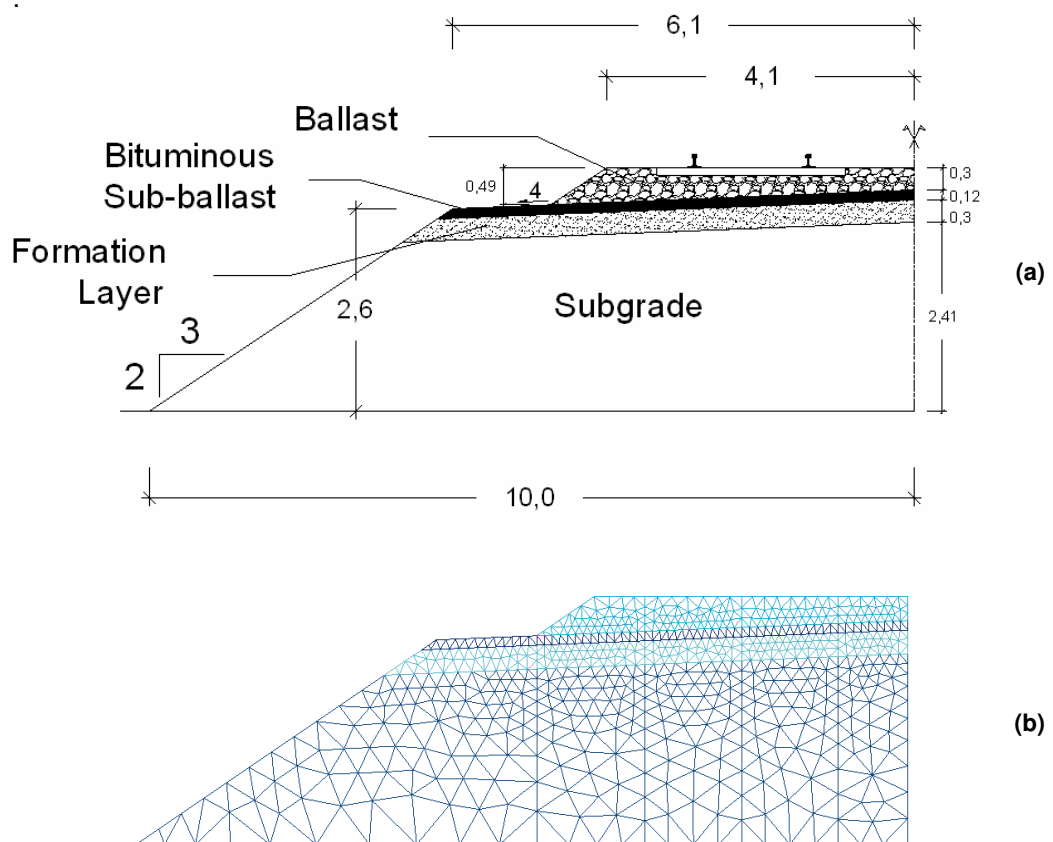


**Fig. 34 – Low bituminous sub-ballast cross section: (a) general design; (b) mesh (CODE\_BRIGHT).**

The analysis of these alternative Bituminous and Granular sub-ballast cross sections considers the same control points mentioned before (Figure 20).

The following analysis is similar to the one made for the Original design solutions and the results for Liquid Saturation, as well as for Vertical Displacements, will be presented, discussed and compared. The figures showing the results are presented in Chapter 12 – Annexes.

### **8.3.2 Extended cross sections**

Figure A1 presents the evolution of the Liquid Saturation inside the embankment, considering the Extended Bituminous sub-ballast cross section. The evolution of the Liquid Saturation along the 5 years (1800 days) on the control points of this cross section is presented in Figure A2.

Comparing Figures 24 (Original Bituminous cross section) and A1, the evolution of the Liquid Saturation inside the embankment is very similar. Figure A1 shows that the bituminous sub-ballast prevents water flow below the platform area (the trajectory of the water flow in the Extended cross section is vertical and it was curved from the slope boundary towards the interior of the embankment in the Original cross sections analyzed) so this area is not affected by the gradual advance of the Liquid Saturation front. This leads to the concentration of the infiltrated water far from the bituminous layer where the control zone is. According to Figure 24, the water accumulated near the slope boundary does not affect directly any control point, explaining the low differences in the values and paths found for the evolution of the Liquid Saturation shown in Figures 25 (Original Bituminous cross section) and A2.

The accumulation of water in ballast, cyclic (elastic) phenomena and a relatively low degree of saturation, less than 25%, are registered in both designs.

For the Extended Granular sub-ballast cross section, different percentages of rain infiltration in the upper layer are considered, as made for the Original Granular cross section. Figures A3 and A4 present the results for  $\alpha = 15\%$  and Figures A5 and A6 for  $\alpha = 30\%$ . As considered for slope boundary in the Original design, a constant percentage of 65% is assumed for rain infiltration in the subgrade extension.

As obtained in the comparison of both Bituminous cross sections designs, this Extended design for the Granular cross section does not give different results from those obtained for the Original design (Figures 27 and 29). The accumulation of water near the subgrade extension is also verified. The calculations of the Liquid Saturation in the control points are not affected by this geometry change and similar distributions of water are found.

Figures A7, A8 and A9 present the results found for the variation of the Vertical Displacements during the five years for the Extended Bituminous and Granular sub-ballast cross sections (with different coefficients of water infiltration,  $\alpha$ ). As before, the same representative points (Figure 20) are used.

According to Figures A7, A8 and A9 for the Extended sections, and figures 30, 31 and 32 for the Original ones, only points G, H and I (near slope in the first design) are slightly affected. This can be explained by the changes in the accumulation of water near these points previously mentioned. The comparison of the performances observed in the Extended cross sections and the ones of the Original cross sections is done in section 4.

Using the same procedure presented for the Original design, maximum values found at the end of the five years (1800 days), as well as the maximum amplitudes registered on control points of the Extended Bituminous and Granular cross sections are shown in Tables 11 and 12. Table 13 presents the ranges for qualitative reduction performed by the bituminous sub-ballast when compared with the granular one.

**Table 11 – Vertical Displacements (Extended Bituminous cross section ( $\alpha = 15\%$ )).**

Points	Vertical Displacement		Approximated Amplitude of the	
	1800 days (mm)		Vertical Displacements (mm)	
A D	7.7 – 8.4		3.0 – 3.5	
B E	6.7 – 7.0		2.5 – 3.0	
G H	11.6 – 13.3		3.0 – 4.0	
C F I	1.8 – 4.8		1.5 – 2.0	

**Table 12 – Vertical Displacements (Extended Granular cross section ( $\alpha = 15\%$  and  $\alpha = 30\%$ )).**

Points	Vertical Displacement		Approximated Amplitude of the	
	1800 days (mm)		Vertical Displacements (mm)	
	$\alpha = 15\%$	$\alpha = 30\%$	$\alpha = 15\%$	$\alpha = 30\%$
A D	23.5 – 24.5	38.0	6.0 – 10.0	7.0 – 11.0
B E	19.0 – 20.0	34.0	6.0 – 9.0	7.0 – 11.0
G H	21.5 – 25.0	31.5 – 35.5	6.0 – 11.0	7.0 – 12.0
C F I	3.0 – 4.5	3.5 – 5.0	3.0 – 4.0	2.5 – 3.5

**Table 13 – Ranges for Qualitative reduction performed by bituminous sub-ballast – Displacements (Extended cross section)**

Points	Vertical Displacement Reduction		Average Amplitude of the	
	1800 days (%)		Vertical Displacements (%)	
	$\alpha = 15\%$	$\alpha = 30\%$	$\alpha = 15\%$	$\alpha = 30\%$
A D	64 – 68	78 – 80	42 – 70	50 – 73
B E	63 – 67	79 – 80	50 – 72	57 – 77
G H	38 – 54	58 – 67	33 – 73	43 – 75
C F I	0 - 60	0 - 63	33 - 63	20 – 57

### 8.3.3 Lower cross sections

Figure A10 presents the evolution of the Liquid Saturation inside the embankment for the Lower Bituminous sub-ballast cross section. The evolution of the Liquid Saturation along the 5 years (1800 days) in the control points in this cross section is presented in Figure A11.

As verified for the Extended Bituminous sub-ballast cross section, there are no significant changes in the evolution of the Liquid Saturation when comparing this design cross section with the Original one (embankment with 5 meters tall). A small reduction in Liquid Saturation, less than 1%, is registered in the upper control points.

Figures A12, A13, A14 and A15 present the results of the calculation of the Granular sub-ballast cross sections in terms of Liquid Saturation and its evolution in time. As before, different percentages of rain intensity,  $\alpha$ , are considered to allow a direct comparison with the results presented for other designs.

As observed in the analysis of the Extended design solution, no significant changes are observed inside the embankment. However the Lower Granular cross section for  $\alpha = 30\%$  shows that the Liquid Saturation is similar in all points of the embankment at the end of the 5 years. This is due to the water accumulation inside the embankment.

Figures A16, A17 and A18 show the evolution in time of the Vertical Displacements, calculated in the control points for the Lower cross sections analyzed.

The results found for the Lower cross sections (Figures A16, A17 and A18) have some differences from those found for the Original design cross sections (Figures 30, 31 and 32). Due to its geometric nature a reduction in the values of the Vertical Displacements when compared with the ones of Original design was expected. Also as obtained for the Original cross sections analyzed, the Lower Granular sub-ballast cross sections present higher Vertical Displacements than those calculated for the Lower Bituminous solution, however with similar evolution in time.

It is important to notice that the cyclic (elastic) variations of the settlements are not very significant for the Lower Granular cross sections, especially to the one with  $\alpha = 30\%$  (Figure A18). This can be explained by the fact that this entire Lower cross section had the same Liquid Saturation (80%). This high saturation degree is very stable and can only be reduced by evaporation. It would be necessary an extreme dry environment to reduce this saturation degree so the seasonal effects could affect the water distribution inside the embankment.

**Note:** for the Lower designs, the lower points C, F and I do not exist.

Tables 14 and 15 present the results for Vertical Displacements and the associated amplitudes on control points of Lower Bituminous and Granular cross sections. Table 16 shows the ranges for qualitative reduction performed by the bituminous sub-ballast when compared with the granular one.

**Table 14 – Vertical Displacements (Lower Bituminous cross section ( $\alpha = 15\%$ )).**

Points	Vertical Displacement	Approximated Amplitude of the
	1800 days (mm)	Vertical Displacements (mm)
A D	2.4 – 3.1	2.0 - 2.5
B E	1.4 – 1.7	2.0 - 2.2
G H	10.1 – 11.8	2.6 – 3.0

**Table 15 – Vertical Displacements (Lower Granular cross section ( $\alpha = 15\%$  and  $\alpha = 30\%$ )).**

Points	Vertical Displacement		Approximated Amplitude of the	
	1800 days (mm)		Vertical Displacements (mm)	
	$\alpha = 15\%$	$\alpha = 30\%$	$\alpha = 15\%$	$\alpha = 30\%$
A D	16.5 - 17.5	33.0	4 - 8	7 - 9
B E	12.5 - 13.5	29.0	5 - 7	6 - 8
G H	18.5 - 22.0	28.0 - 31.5	4 - 8	7 - 9

**Table 16 – Ranges for Qualitative reduction performed by bituminous sub-ballast – Displacements (Lower cross section).**

Points	Vertical Displacement Relation		Approximated Amplitude of the	
	1800 days (%)		Vertical Displacements (%)	
	$\alpha = 15\%$	$\alpha = 30\%$	$\alpha = 15\%$	$\alpha = 30\%$
A D	81 - 87	90 - 93	38 - 75	64 - 78
B E	86 - 90	94 - 95	56 - 71	63 - 75
G H	37 - 54	58 - 68	25 - 68	57 - 71

By comparing the Vertical Displacements of the Lower design solutions with those calculated for the Original design (embankment with 5 meters) it can be seen smaller displacements in the Lower design one. The comparison of the performances observed in the Lower cross sections and the ones of the Original design is done in section 4.

## 8.4 Conclusions about the performance of Original, Lower and Extended cross sections

The previous sections of this chapter presented the results in terms of Vertical Displacements and Liquid Saturation for the different designs considered: Original, Lower and Extended cross sections. This section presents the main conclusions concerning the results obtained.

The control points A, B and C – symmetry axis of the embankment, and D, E and F – rail axis line, will be the ones analyzed in this section. They were chosen since they are not so sensitive to geometry changes (and its influence in boundary conditions) as the external ones and their location above the platform allow a direct comparison between bituminous and granular sub-ballast. In terms of maintenance of the railways and its cost, the displacements registered on the interior points assume an extreme importance. Tables 17 and 18 summarize the results obtained for the different designs using bituminous (Table 17) and granular sub-ballast (Table 18). As it can be seen by comparing the values from each column and for the same geometry, the vertical displacements obtained for the cross sections with the bituminous sub-ballast are lower than those found for the granular ones. Concerning the liquid saturation, the values found are higher for the granular cross sections because, as discussed before, they are less impervious as the bituminous ones.

**Table 17 – Ranges for Vertical Displacements and Liquid Saturation on interior control points (Bituminous cross sections ( $\alpha = 15\%$ )).**

	Points	Vertical Displacement	Average Amplitude of the	Maximum
		1800 days (mm)	Vertical Displacements (mm)	Liquid Saturation (%)
Original	A D	7.5	3 – 4	18 – 22
	B E	6.2 – 6.5	3 – 4	6 – 7
	C F	4.5 – 5.1	2.0	6 – 7
Extended	A D	7.7 – 8.4	3.0 – 3.5	18 – 22
	B E	6.7 – 7.0	2.5 – 3.0	6 – 7
	C F	1.8 – 4.8	1.5 – 2.0	6 – 7
Lower	A D	2.4 – 3.1	2.0 – 2.5	20 – 24
	B E	1.4 – 1.7	2.0 – 2.2	6 – 7

**Table 18 – Ranges for Vertical Displacements and Liquid Saturation on interior control points (Granular cross sections ( $\alpha = 15\%$  and  $\alpha = 30\%$ )).**

	Points	Vertical Displacement		Average Amplitude of the		Maximum	
		1800 days (mm)		Vertical Displacements (mm)		Liquid Saturation (%)	
		$\alpha = 15\%$	$\alpha = 30\%$	$\alpha = 15\%$	$\alpha = 30\%$	$\alpha = 15\%$	$\alpha = 30\%$
Original	A D	22.5 – 24.0	37.0 – 37.5	7.0 – 10.0	8.0 – 11.0	65	80
	B E	18.0 – 20.0	32.5 – 33.5	6.0 – 8.0	7.0 – 10.0	60	80
	C F	4.0 – 6.0	4.5 – 7.5	5.0	5.0	8	10
Extended	A D	23.5 – 24.5	38.0	6.0 – 10.0	7.0 – 11.0	65	80
	B E	19.0 – 20.0	34.0	6.0 – 9.0	7.0 – 11.0	60	80
	C F	3.0 – 4.5	3.5 – 5.0	3.0 – 4.0	2.5 – 3.5	8	10
Lower	A D	17.0 – 18.0	33.0	4.0 – 8.0	7.0 – 9.0	65	80
	B E	12.5 – 13.5	29.0	5.0 – 7.0	6.0 – 8.0	60	80

Table 19 presents the ranges for qualitative reduction performed by the bituminous sub-ballast cross section taking the results from the granular one for each type of section as reference. As before, for evaluate the efficiency of the bituminous solution it was used the parameter named Bituminous reduction defined by Eq. (30) in Chapter 5.2.

**Table 19 – Ranges for Qualitative reduction performed by bituminous sub-ballast Displacements and Liquid Saturation**

	Points	Vertical Displacement 1800 days (mm)		Average Amplitude of the Vertical Displacements (mm)	
		$\alpha = 15\%$	$\alpha = 30\%$	$\alpha = 15\%$	$\alpha = 30\%$
		Original	A D	65 – 70	80
B E	65 – 70		80	30 – 60	40 – 70
C F	≈ 0		≈ 0	60	60
Extended	A D	65 – 70	80	40 – 70	50 – 70
	B E	60 – 70	80	50 – 70	60 – 80
	C F	0 – 60	0 – 65	30 – 60	20 – 60
Lower	A D	80 – 90	90 – 95	40 – 75	60 – 80
	B E	85 – 90	95	55 – 70	60 – 75

From the perspective of the railway maintenance costs, the amplitude of Vertical Displacements is the main variable (column named Average Amplitude of the vertical displacements). The cyclic nature of the displacements leads to fatigue problems in the infrastructure as well as an increase in the number of maintenance operations once these seasonal recoverable displacements may be considered irreversible (plastic) for small periods of time (associated to maintenance intervals). Thus, it is desirable to adopt the design solution that will lead to small vertical displacements amplitude, as is the case of the bituminous sub-ballast cross section as observed in the previous tables and as will be explained as follows.

Considering the same percentage of water infiltration,  $\alpha = 15\%$ , for both sub-ballast solutions (Bituminous and Granular) and for original and extended geometries, the results indicate that the bituminous sub-ballast reduces the amplitude of Vertical Displacements from 45% to 70% (column average values, points A and D in table 19). The reduction slightly increases from 50% to 70% if the differences in drainage behaviour between both sub-ballast solutions are taking into account ( $\alpha = 15\%$  and  $\alpha = 30\%$  for bituminous and granular solutions respectively). This indicates an increase in 5% in the efficiency of the bituminous solution if the granular solution is less impervious ( $\alpha = 30\%$  instead of  $\alpha = 15\%$ ).

Analyzing the ranges of reductions for the bituminous sub-ballast cases at the end of the 5 years, it was found reductions from 60% to 90% (average values) for the upper points (A, B, D and E) if  $\alpha = 15\%$  is considered for Granular sub-ballast design. These values are higher for  $\alpha = 30\%$ , where reductions from 80% to 95% can be achieved for the upper points.

The main conclusion from this analysis is that, taking the granular sub-ballast performance as reference for the embankment geometries considered, bituminous sub-ballast may allow an important reduction in the seasonal vertical displacements, higher than 50%.

The efficiency of the Bituminous sub-ballast solution also depends on the geometry of the embankment, as shown by the analysis performed for the low and extended embankments. A relation ( $\Delta_{\text{Extended}}/\Delta_{\text{Original}}$  or  $\Delta_{\text{Lower}}/\Delta_{\text{Original}}$ ) between the displacements found for each case ( $\Delta_{\text{Extended}}$  and  $\Delta_{\text{Lower}}$ , respectively) with those found in the original embankment ( $\Delta_{\text{Original}}$ ) allows the comparison of their performance. Values higher than the unity indicate that the displacements found in that point for the alternative solution are higher than those found, in the same point, for the original one. For points D, E and F, the values found in time for this relation are presented in Figure 35.

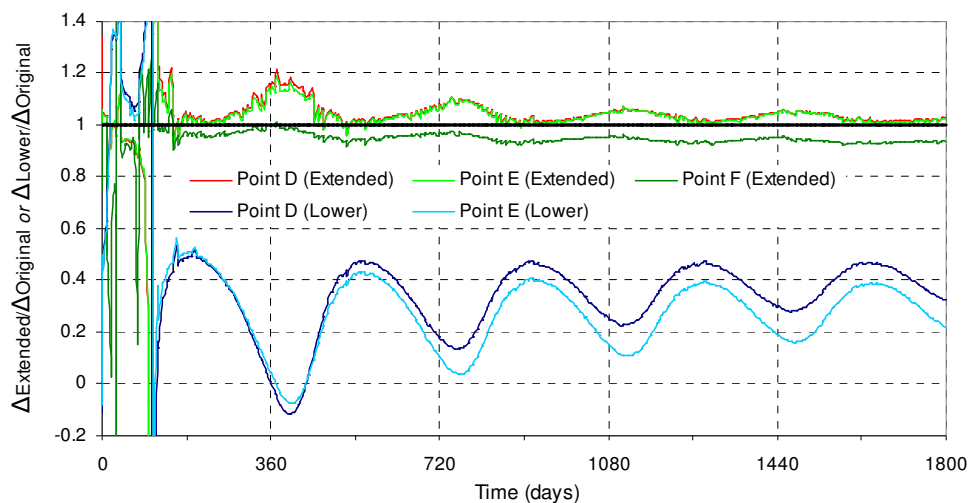


**Fig. 35 – Relation between original and alternative designs using bituminous sub-ballast**

According to Figure 35 there are no significant differences between the displacements calculated for the Original and for the Extended cross sections. Upper points (D and E) from the Extended design registered higher displacements [0% – 10%] than the correspondent points from the Original design; but considering point F (deeper), lower displacements are registered.

Analyzing the performance of the Lower Bituminous cross section design in the upper points (D and E), Figure 35 shows a reduction higher than 50% on when compared with the Original Bituminous cross section.

As previously discussed, besides the fact that higher embankments have higher deformations if compared with small embankments made of the same materials, the amount of water inside the embankments with different geometries depends on the hydraulic boundaries and they include not only the platform where the bituminous layer is, but also the slopes. The highest ranges of reduction found in the study of the three geometries with the bituminous sub-ballast correspond to the Lower solution (Table 19 and Figure 35), the one with less area not protected from rain (and evaporation). This result expresses the importance of the weight of the embankment as it has associated an area not protected. This study confirms that impervious solutions, such as vegetable cover, geotextile or other protections for covering the slopes should be adopted, as they usually are in design practice.

## 8.5 Considerations on the drainage system

The constant increase of Liquid Saturation indicating water accumulation can be explained by water infiltration from the boundaries and from the slope in particular. This is observed for all the cross sections analyzed, being more reduced for the ones with bituminous material due to its low permeability. The absence of drains in the numerical models can explain the water accumulation.

The adoption of a rain intensity coefficient (named  $\alpha$ ) for the slopes and the platforms intended to compensate this absence since it would correspond to the percentage of rain that would be allowed to infiltrate in the soil. The excess of rain would be drained in the boundary, without being considered in the calculation. This is a reasonable assumption for modeling. Probably it would be necessary to perform a better calibration of parameter  $\alpha$  to avoid this problem however there is no enough data available in the bibliography.

The rain intensity coefficient,  $\alpha$ , is not the only numerical parameter that can be used to control the accumulation of water inside the embankment. Besides liquid water, the calculation also considers exchanges of water in the vapour phase. As mentioned when CODE\_BRIGTH modeling was described (Chapter 7.5) the flow of water in the gas phase at the boundaries is controlled by a linear law (Eq. (60)):

$$j_g^w = \beta_g (\rho_{vap}^0 - \rho_{vap}) \quad (60)$$

where  $\beta_g$  represents the relative importance assumed for water vapour flow in the simulation. This flux is zero ( $\beta_g = 0$ ) when an impervious to gas layer is considered and a higher value must be assumed when evaporation is admitted to be significant.

In this work, it is considered  $\beta_g=0.0002$  in the upper boundary (platform) and  $\beta_g=0.002$  in the slope. For granular layers, higher values for  $\beta_g$  should be considered once it allows a superior water vapour flow. Bituminous layers, considering their impervious properties, should have an inferior value for  $\beta_g$ , simulating a low rate of evaporation when compared with granular ones. A solution to avoid water accumulation should be the increasing of evaporation by using higher values for  $\beta_g$  but numerical problems arise when higher values are considered.

Finally, numerical tools can be used to simulate drainage however they require a careful calibration of the parameters, which is not an easy task especially when there is no data available. To allow an accurate analysis, drains should be considered. The results concerning the accumulation of water had shown that the location of drains should be in the ballast boundary and in the subgrade shoulders, which are the places usually adopted in design practice.

## 9. Considerations regarding the Geometric Quality of high-speed railway track

In previous chapters, an alternative design which incorporates a bituminous sub-ballast layer was examined in order to understand its advantages when compared with the conventional one (granular sub-ballast). However, after project design and construction, the various railway system components start operating, wear begins to appear and, after a certain time, maintenance becomes necessary. Track maintenance decisively affects both train safety and passenger comfort. Track maintenance expenses represent a significant percentage of total railway network expenses.

Therefore, track maintenance expenses should be kept as low as possible while ensuring, for a specific operation speed, that running safety and passenger comfort remain acceptable at all times. With respect to safety, maintenance should be preventive; regarding comfort, maintenance should be corrective; and finally, as regards the financial aspects of the matter, an optimum solution should be achieved, so as to ensure a satisfactory safety margin and prevent an irreparable degradation of track quality.

The above objectives depend on two fundamentally different classes of parameters: on the one hand geometrical parameters, the degradation of which is usually reversible: and on the other, mechanical parameters which in most cases cannot be restored without parts replacement (rails, fastenings, sleepers, welds, etc.). Geometrical parameters, however, degrade much faster, about 5 – 15 times, than mechanical parameters.

Deviations between the real and theoretical values of geometrical track characteristics are termed *track defects* and their restoration is done through track maintenance mainly tamping works.

In terms of comfort and safety, the geometrical quality of the railway track must fulfill some requisites quantified through specific parameters. Among them, the most important are:

- **Track gauge** (mm): distance between the inner sides of the rails; according to UIC (International Union of Railways) it is measured 14 mm below the rolling surface (Figure 36);
- **Horizontal defect** (mm): horizontal deviation of the real position of the track from its theoretical (project) position (Figure 36);
- **Longitudinal defect** (mm): distance defined by the difference of level between the rolling surface and the theoretical plan (Figure 36);
- **Transverse defect** (mm): difference between the theoretical and the real value measured for the superelevation of the external rail in relation to the inner rail (cant), (Figure 36);
- **Local distortion** (mm/m): considering four points of the track lying on two transverse sections they must lie in the same plane; local distortion is defined as the deviation of one point from the plane defined by the other three (Figure 36).

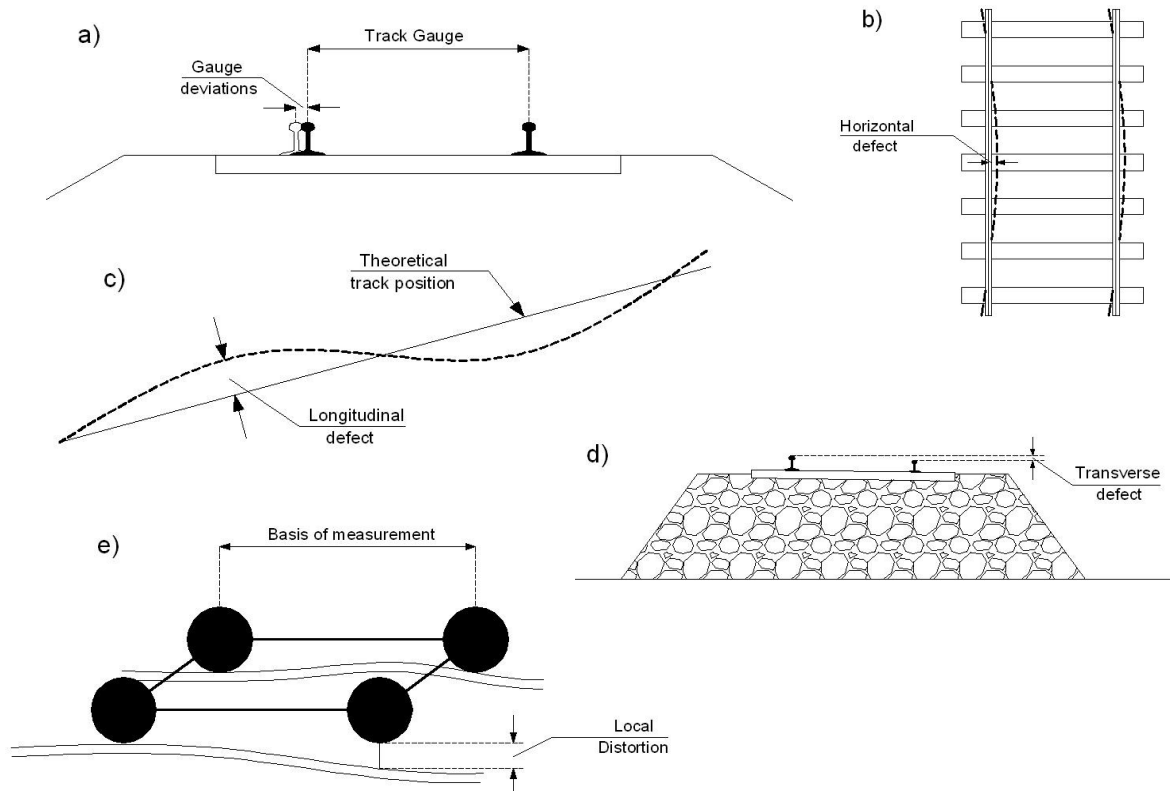


**Fig. 36 – Track defects: a) Track gauge; b) Horizontal defect; c) Longitudinal defect; d) Transverse defect; e) Local distortion**

In recent years, modern railway technology is using recording vehicles traveling the track at specified intervals to detect track defects (Figure 37). These vehicles are provided with recording equipment which measure the values of the various track defects in accordance with a specific basis of measurement (for conventional lines, in order of 10m for longitudinal, transversal and horizontal defects and in the order of 2.5-3m for local distortion; in high speeds long wavelengths defects should also be assessed).

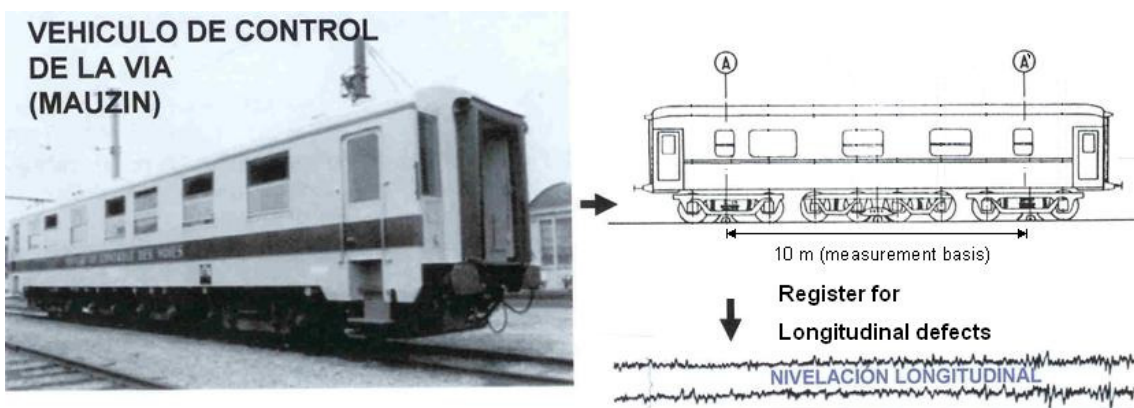


**Fig. 37 – Recording vehicle (Mauzin) – register for the longitudinal defects**

The distribution of the various types of defects is of a stochastic nature and can be approximated with the aid of spectral analysis. Thus, it can be calculated for each class of defects, their frequency of occurrence, the wavelength to which they correspond, their relation to train speed, etc. A first, and simplest, analysis approach is to calculate the mean values of a defect as well as its maximum discrete values over a particular length.

However, at medium, high, and very high speeds, the decisive parameters are those determining passenger comfort. At these speeds, ensuring a high level of passenger comfort also ensures traffic safety. Consequently, as indices of track quality at the above speeds, the processed values of the various types of defects are used (obtained from the values recorded by the recording vehicle). Most important characteristic of these processed values is the standard deviation of a particular type of defect over a specific length, which reliably measures the differential value of the defect in question. According to SNCF (Société Nationale des Chemins de Fer) criteria, Table 20, it is possible to evaluate the influence of speed in the limits/tolerances for corrective operations required to guarantee an adequate geometric quality:

**Table 20 – Limits for corrective operations – Influence of speed in Geometric Quality.**

Parameter	Conventional	High-Speed		
	Reference	Current	Isolated	Standard Deviation
	Value	defect	defect	in 300 m (mm)
Track gauge	+30/-5 mm	±2.5	±6	0.9/1.0
Horizontal defect	±5 mm	±3.5	±6	1.0/1.7
<b>Longitudinal defect</b>	<b>±5 mm (base 10 m)</b>	<b>±2.5</b>	<b>±5</b>	<b>0.8/1.0</b>
Transverse defect	±5 mm	±2.0	±4	0.6/0.8
Local distortion	2/3 mm/m (base 3 m)	1.5 mm/m	3 mm/m	-

The longitudinal defect is the principal factor in determining the magnitude of the track maintenance expenses.

Currently, the analysis of the geometric parameters allows defining three quality correction levels for a railway line:

- Quality **QN 1**: implies normal maintenance (recording);
- Quality **QN 2**: implies maintenance operations in the short term;
- Quality **QN 3**: not desirable situation (however admissible).

From UIC (International Union of Railways) recommendations: 50% of a railway line must achieve a quality higher than QN 1; 40% of the line between qualities QN 1 and QN 2; 10% between QN 2 and QN 3 qualities.

Table 21 shows the standard deviation and maximum isolated values allowed for longitudinal defects depending on geometric quality:

**Table 21 – Longitudinal defects – Standard deviation and Maximum values on isolated points.**

Speed (km/h)	QN 1		QN 2	
	Maximum value (mm)	Standard deviation (mm)	Maximum value (mm)	Standard deviation (mm)
$v \leq 80$	12.0	2.3	16.0	2.6
$80 < v \leq 120$	8.0	1.8	12.0	2.1
$120 < v \leq 160$	6.0	1.4	10.0	1.7
$160 < v \leq 200$	5.0	1.2	9.0	1.5
$200 < v \leq 300$	4.0	1.0	8.0	1.3

The control of the displacements and their annual amplitude plays a central role when high-speed railway lines are considered. From a trackbed design perspective, the use of a bituminous sub-ballast as an alternative to the granular one, may improve the geometric performance of the railway infrastructure and contribute to an effective reduction of track maintenance needs.

Figure 38 shows a given register for the longitudinal defects due to the weather actions and associated to a granular sub-ballast cross section. Assuming that the bituminous sub-ballast may perform a reduction in the order of 50% in terms of the displacements and their annual amplitude (as supported by the results in Chapters 5.2 and 8.4), it would imply a reduction for the longitudinal defects as also shown by Figure 38. Considering  $LD_{current}^{gran.}$  the current value for longitudinal defect registered for the granular sub-ballast and  $\Delta_{gran.}$  its seasonal amplitude, the correspondent values registered for the bituminous sub-ballast would be  $LD_{current}^{bit.} = 0.5 \times LD_{current}^{gran.}$  and  $\Delta_{bit.} = 0.5 \times \Delta_{gran.}$ . Lower displacements and amplitudes performed by the bituminous sub-ballast in each cross section would lead to a reduction in Current ( $LD_{current}$ ) and Standard Deviation ( $\delta_{bit.} < \delta_{gran.}$ ) values for the longitudinal defects.

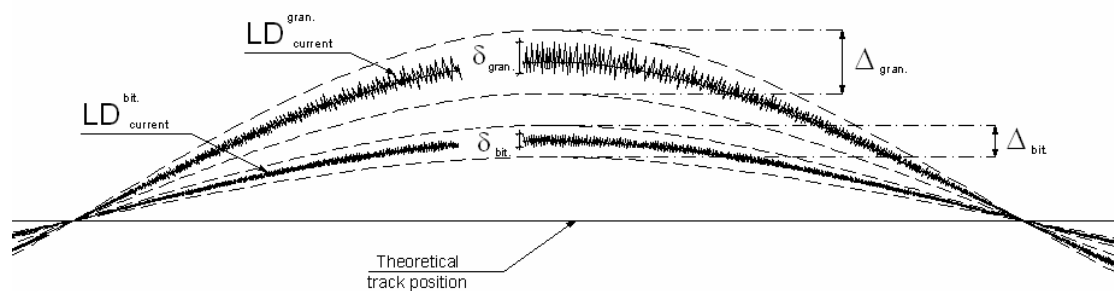


**Fig. 38 – Register for Longitudinal defects: Granular vs. Bituminous**

## 10. Conclusions and Current Research

This work discussed the possible improvements of conventional high-speed trackbed design. An alternative solution to the widely used granular sub-ballast was presented. The possible interest of using a bituminous sub-ballast layer was analyzed and, from a theoretical point of view, a comparison between its performance and the granular one was carried out.

The first approach was made by recurring to the Barcelona Basic Model, BBM, which considers the behaviour of partially saturated soils. Using the deformations due to suction variations in the elastic domain of the  $(p, s)$  space and assuming that each layer of the cross section design provided a given reduction of the atmospheric relative humidity, a parametric study was developed to analyze the sensibility of the bituminous sub-ballast reduction.

In this parametric analysis, the comparison between the granular and bituminous sub-ballast solutions was made in terms of the maximum amplitude of vertical displacements registered in a specific point during a year. Three climates data corresponding to the cities of Moa, Tarragona and Camprodón were analyzed as well as four different types of soil composing the embankment layers. The cross section design was defined in order to simulate a 5 m high embankment and was based in typical geometry and thicknesses of trackbed layers.

From the obtained results it is possible to conclude that:

- lower displacements are associated to low values of suction compressibility,  $k_s$ ;
- generally, maximum amplitude of vertical displacements decreases as the bituminous reduction for relative humidity increases;
- the adoption of bituminous sub-ballast, designed in order to guarantee a relative humidity reduction superior to 15%, is a better solution than the adoption of granular sub-ballast layers;
- it is observed a 50% reduction in the displacements (amplitude) performed by the bituminous solution considering a reduction in the relative humidity higher than 50% for Tarragona climate and 55% for Moa and Camprodón;
- for each climate it is possible to define a characteristic curve of reduction provided by the bituminous sub-ballast layer. This curve evidences the loss of efficiency for high values of relative humidity reduction performed by the bituminous sub-ballast;
- the percentage of reduction in vertical displacements (amplitude) provided by the bituminous sub-ballast is similar to the one associated to the increased of relative humidity reduction;
- the efficiency loss may lead to an inversion of the slope in the associated characteristic curve. The existence of an inflexion point as observed for Tarragona climate indicates that it may exist an optimum value for the relative humidity reduction associated to the maximum efficiency of the design solution.

The use of adequate formulation is necessary to rule the exchanges of water in both vapour and liquid phases between soil and the environment. Once this calculation is mathematically complex, the second approach for the bituminous sub-ballast analysis was performed by the finite elements program CODE\_BRIGHT. Its formulation considers the hydraulic constitutive equations, the conductive, heat, diffusive and dispersive fluxes as well as the intrinsic permeability. This allowed an accurate description of the problem.

Using this program, a simulation exercise concerning a period of 5 years was performed to allow the study of the cross sections long term behaviour. The Tarragona climate data was the one simulated in this exercise. The trackbed materials were described by constitutive models and parameters and assumed to be adapted to the type of materials usually adopted in practice. In order to understand the influence of cross section geometry in the hydraulic boundary conditions, the Original design was also compared with alternative geometric solutions: Extended and Lower. Different percentages of rain in filtration were considered in the upper boundary for both solutions (bituminous and granular sub-ballast).

The comparison between the bituminous and granular sub-ballast solutions was made by recurring to the evolution of liquid saturation, vertical displacements and their amplitude in several points of control. From the perspective of the railway maintenance costs, the amplitude of vertical displacements is the main variable.

The registered results allow the following comments:

- considering the same percentage of rain infiltration, 15%, for both sub-ballast solutions (bituminous and granular), it is possible to assume a range of reduction in the amplitude of vertical displacements from 45% to 70% (average values) performed by the bituminous sub-ballast;
- if the differences in drainage behaviour between both sub-ballast solutions are taking into account (bituminous and granular percentages of rain infiltration of 15% and 30% respectively), then a range of reduction from 50% to 75% (average values) is obtained by using the bituminous sub-ballast;
- analyzing the ranges of reductions performed by bituminous sub-ballast in terms of displacements at the end of the 5 years (under poor drainage conditions), it can be assumed reductions from 60% to 90% or 80% to 95% (average values) on the upper points for rain's infiltration percentages of 15% and 30% respectively;
- in terms of liquid saturation, bituminous sub-ballast helps maintaining low levels of the moisture content along the year in opposite to the granular solution;
- a comparison in terms of displacements registered at the end of the 5 years between the different designs using the bituminous sub-ballast solution shows that Lower design may perform a reduction higher than 50% on the upper points when compared with the Original one; no significant differences are observed between Original and Extended designs.

From both approaches performed to analyze the possible interest of a bituminous sub-ballast as an alternative to the conventional granular ones, the main conclusion is that bituminous sub-ballast may allow an important reduction in the seasonal vertical displacements, up to 50% or more under poor drainage conditions.

The amplitude of the displacements is related with their cyclic nature and leads to fatigue problems in the infrastructure as well as an increase in the number of maintenance operations once these seasonal recoverable displacements may be considered irreversible (plastic) for small periods of time (associated to maintenance intervals).

Considering a given register for the longitudinal defects due to the weather actions, if a given reduction in the displacements and their amplitudes is assumed to be performed by the bituminous sub-ballast layer, it would mean a reduction in maximum, current and standard deviation values for the longitudinal defects.

The results presented in the study correspond to an unfavourable situation of poor drainage conditions. Further research will aim at introducing on the model different drainage assumptions in order to get deeper on the evaluation of the impact of using bituminous sub-ballast on track deformation.

In a parallel way, in-situ measurements on both the variations on relative humidity and the resulting settlement of railway embankments should help to confirm the interest of the bituminous layers for high-speed tracks. In relation to this issue, Spanish Railways are proceeding to the instrumentation of a trial with bituminous sub-ballast in a section of the Barcelona – French Border high-speed line under construction, to evaluate its behaviour and compare it with sections with granular sub-ballast. The interpretation of these results together with ongoing research on the assessment of the geometric quality of tracks with bituminous sub-ballast (in Italy) will help quantifying in what conditions this solution can contribute to an effective reduction of track life cycle costs.

## 11. Bibliographic References

- Alonso, E. E., Gens, A. And Josa, A. (1990) – *A constitutive model for partially saturated soils*, Géotechnique 40, No. 3, pp. 405-430, 1990.
- Alonso, E. E. – *Suction and moisture regimes in roadway bases and subgrades*, Simposio Internacional: Drenaje Interno de Firmes y Explanadas, pp. 57-104, 1998.
- Fredlund and Rahardjo (1974), Fredlund, D.G. Rahardjo, H., *Soil mechanics for unsaturated soils*, Wiley, 1974.
- Loret et Khalili (2002) Benjamin Loret, Nasser Khalili - *An effective stress elastic-plastic model for unsaturated porous media*, Mechanics of Materials, 34, pp. 97–116, 2002.
- Olivella, S. – *Manual user for CODE\_BRIGTH - thermal-hydro-mechanical finite elements program*, 1994, 1996 DIT - Universitat Politècnica de Catalunya, 2000.
- Profillidis, V.A. (2000) – *Railway Engineering*, second edition, Textbook, ISBN 0-7546-1279-1, Greece, 2000.
- Sivakumar and Wheeler (2000) V. Sivakumar & S.J. Wheeler - *Influence of compaction procedure on the mechanical behaviour of an unsaturated compacted clay*. Part 1: wetting and isotropic compression. Géotechnique, 50, pp. 359-368, 2000.
- Teixeira, P. F., A. López Pita, C. Casas, A. Bachiller and F. Robusté (2006) "*Improvements in high-speed ballasted track design: benefits of bituminous sub-ballast layers*". Transportation Research Record: Journal of the Transportation Research Board N° 1943, 2006, pp.43-49, ISSN 0361-1981, ISBN 0-309-09425-9.
- Teixeira, P. F., A. – *Apontamentos da disciplina de Caminhos de Ferro, DEC – Instituto Superior Técnico*, Technical University of Lisbon, 2006.
- Toll (1990) Toll D.G. - *A Framework for Unsaturated Soil Behaviour*, Géotechnique, 40(1), pp. 31-44, 1990.
- Van Genuchten, (1980) Van Genuchten, M. T. – *A closed-form equation for predicting the hydraulic conductivity of unsaturated soils*. Soil Sci. Soc. Am. J. 44: 892-898, 1980.

Vanapalli, et al. (1996) Vanapalli, S.K., Fredlund, D. G., Pufahl, D. E., and Clifton, A. W - *Model for the prediction of shear strength with respect to soil suction*, Canadian Geotechnical Journal, 33(3), pp. 379-392, 1996.

Wheeler (1991) Wheeler, S J I – *An Alternative Framework for Unsaturated Soil Behaviour*, Géotechnique, 41(2), pp. 257-261, 1991.

## 12. Annexes

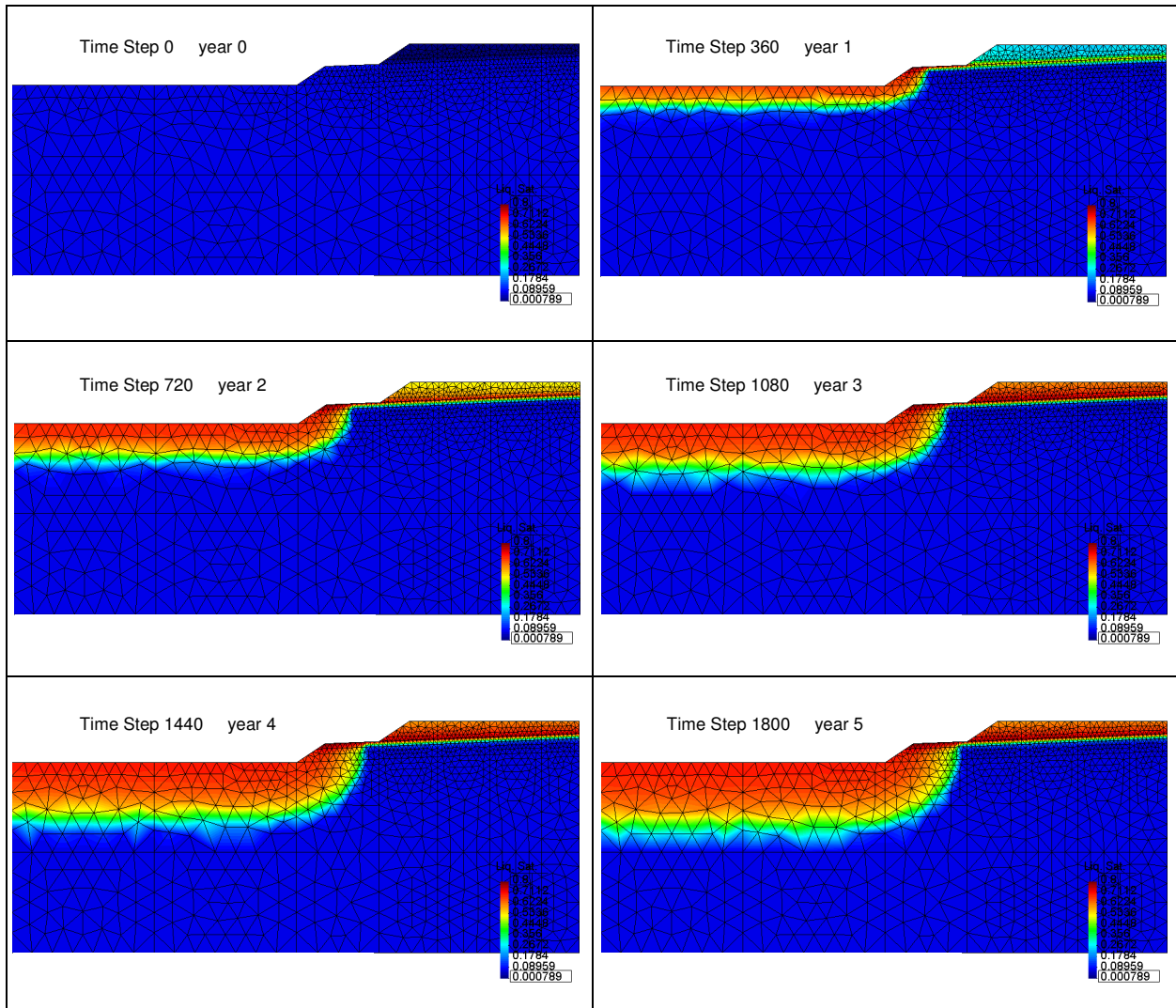


Fig. A1 – Liquid Saturation evolution along 5 years (Extended Bituminous cross section ( $\alpha = 15\%$ ))

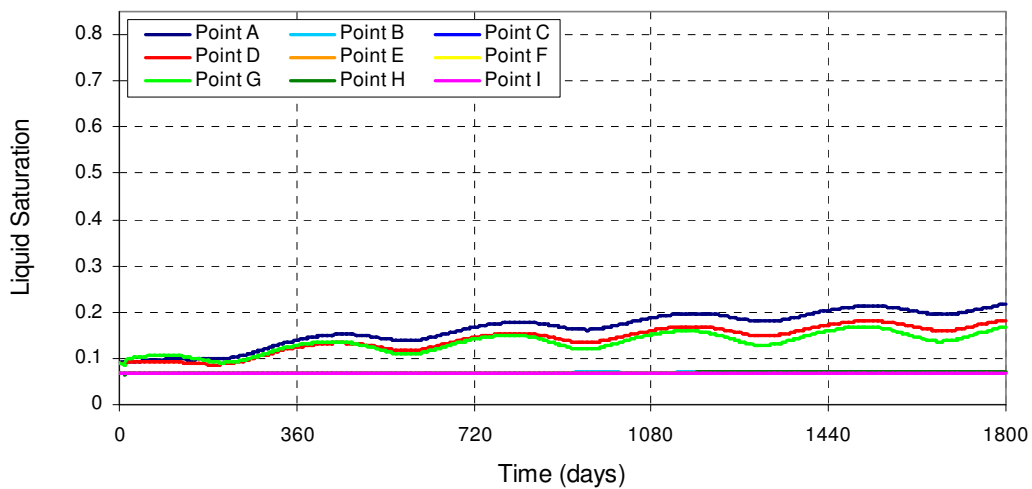


Fig. A2 – Liquid Saturation evolution on control points (Extended Bituminous cross section ( $\alpha = 15\%$ )).

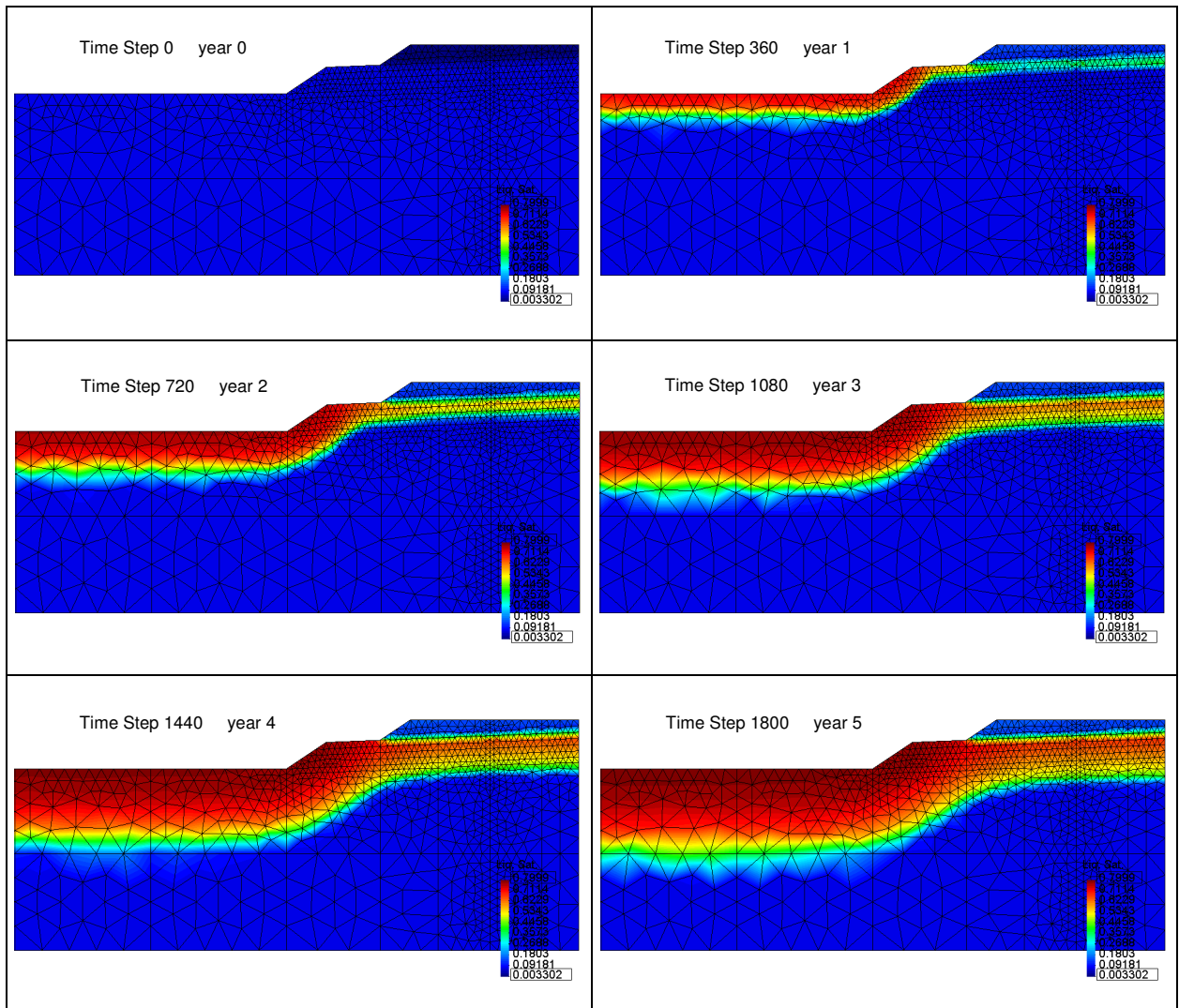


Fig. A3 – Liquid Saturation evolution during 5 years (Extended Granular cross section ( $\alpha = 15\%$ )).

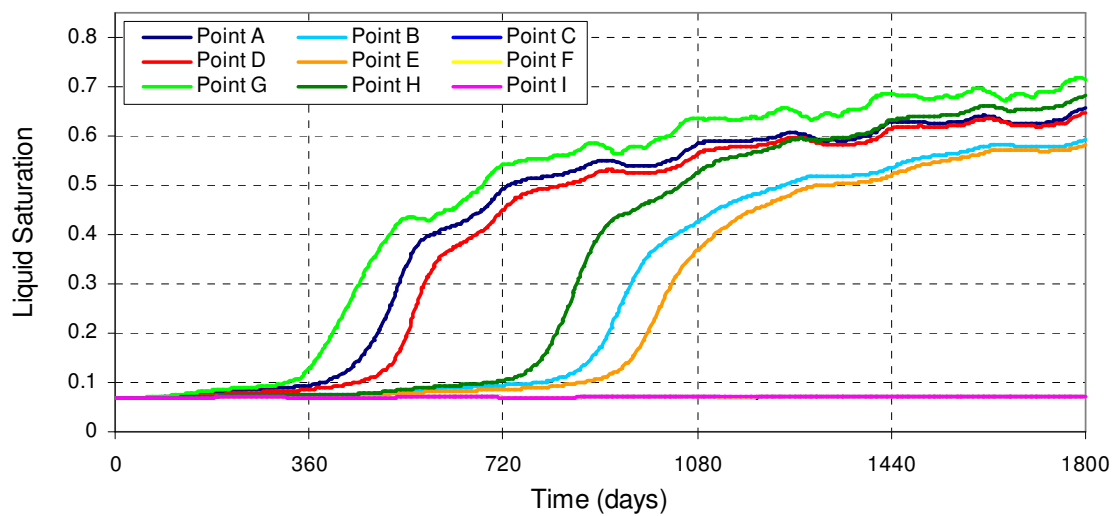


Fig. A4 – Liquid Saturation evolution on control points (Extended Granular cross section ( $\alpha = 15\%$ )).

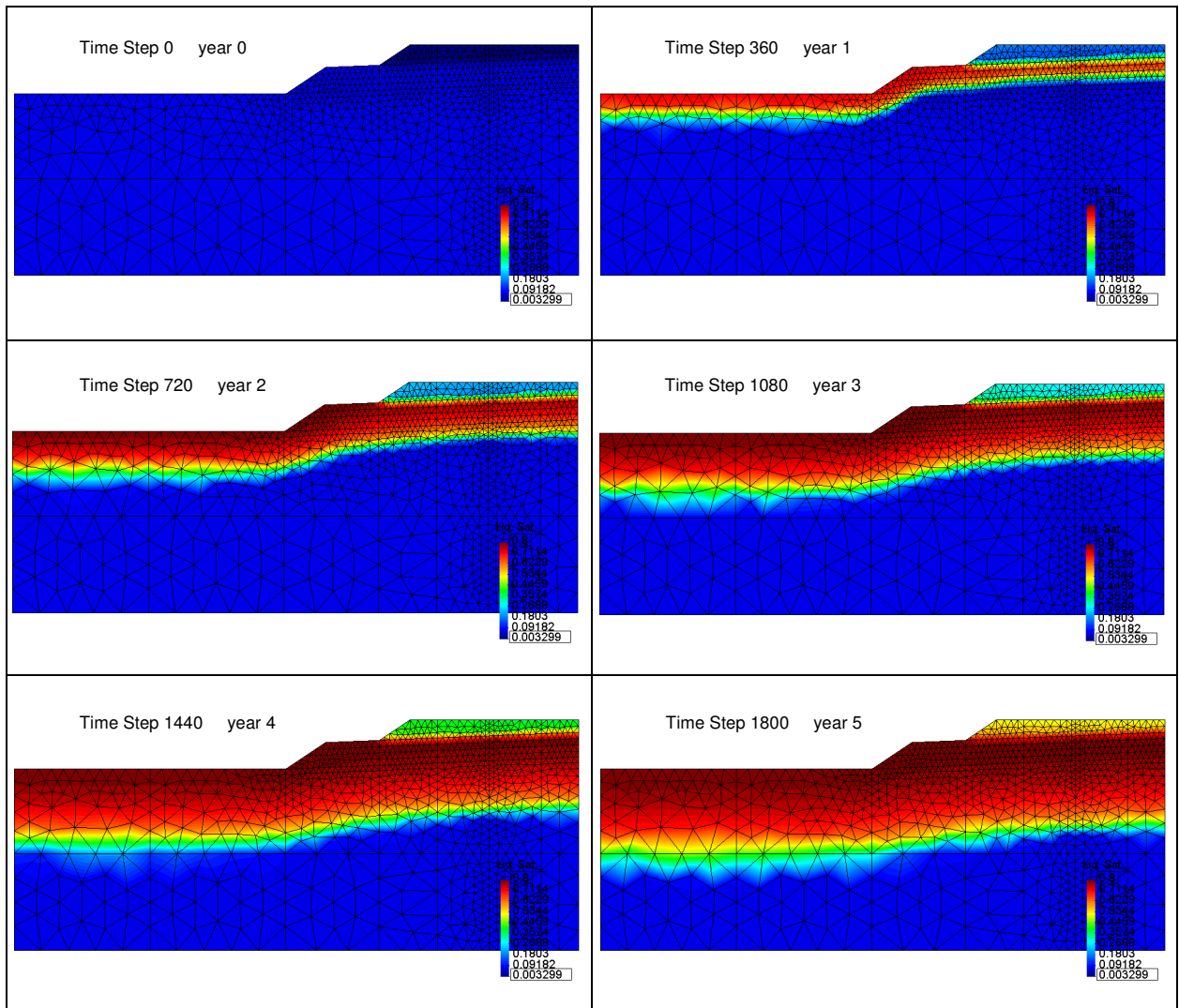


Fig. A5 – Liquid Saturation evolution during 5 years (Extended Granular cross section ( $\alpha = 30\%$ )).

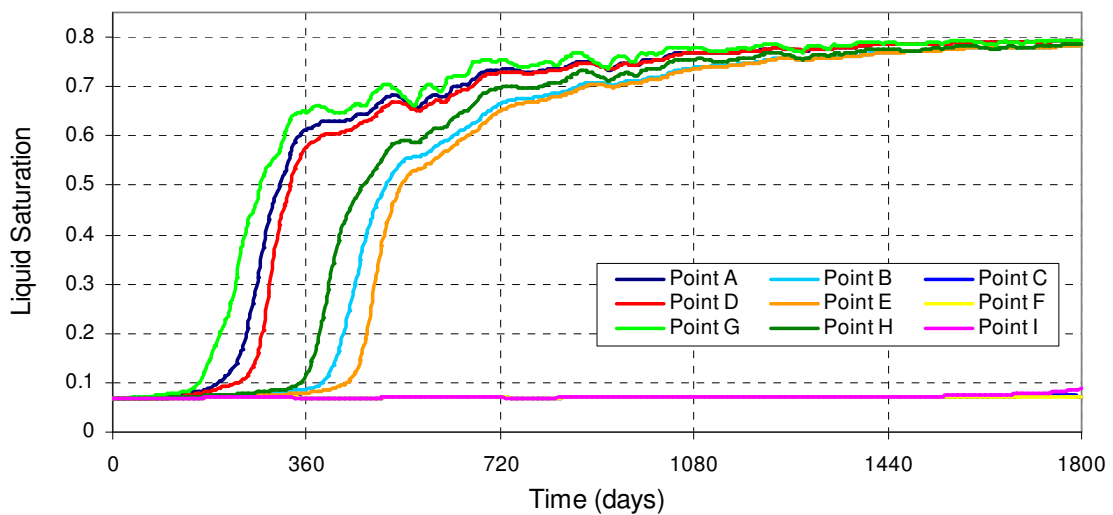
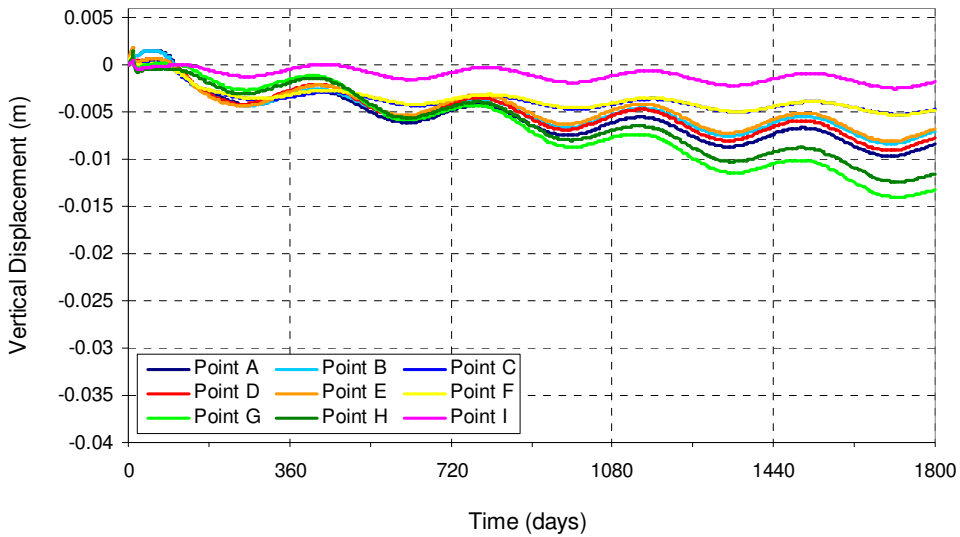
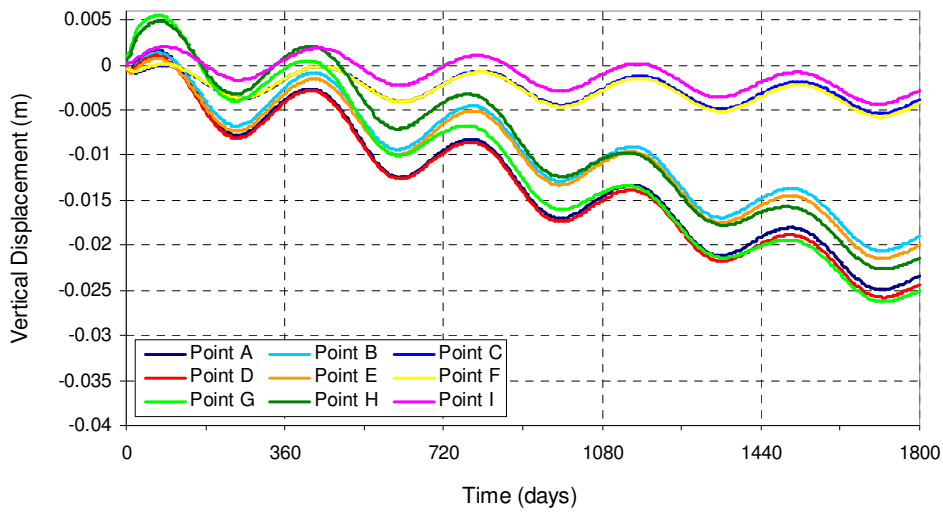


Fig. A6 – Liquid Saturation evolution on control points (Extended Granular cross section ( $\alpha = 30\%$ )).



**Fig. A7 – Vertical Displacements variation on control points (Extended Bituminous cross section ( $\alpha = 15\%$ )).**



**Fig. A8 – Vertical Displacements variation on control points (Extended Granular cross section ( $\alpha = 15\%$ )).**

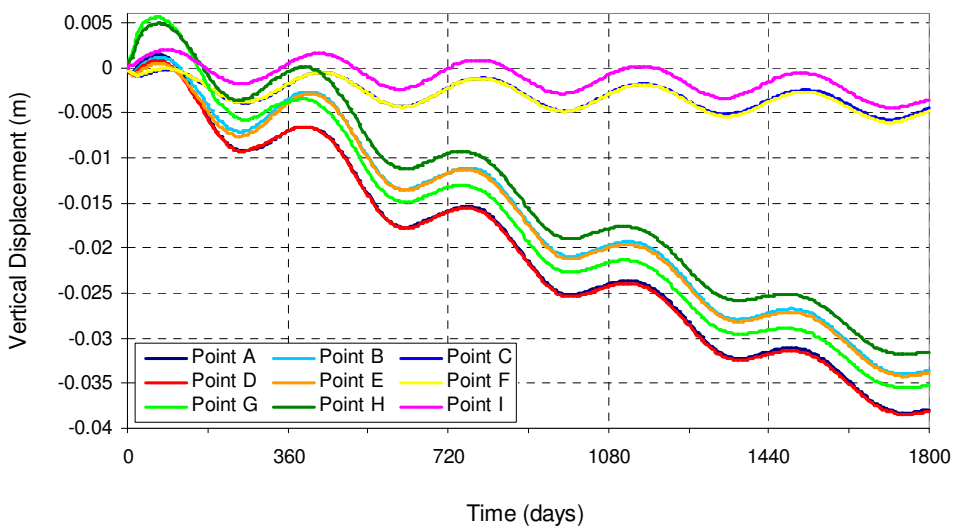


**Fig. A9 – Vertical Displacements variation on control points (Extended Granular cross section ( $\alpha = 30\%$ )).**

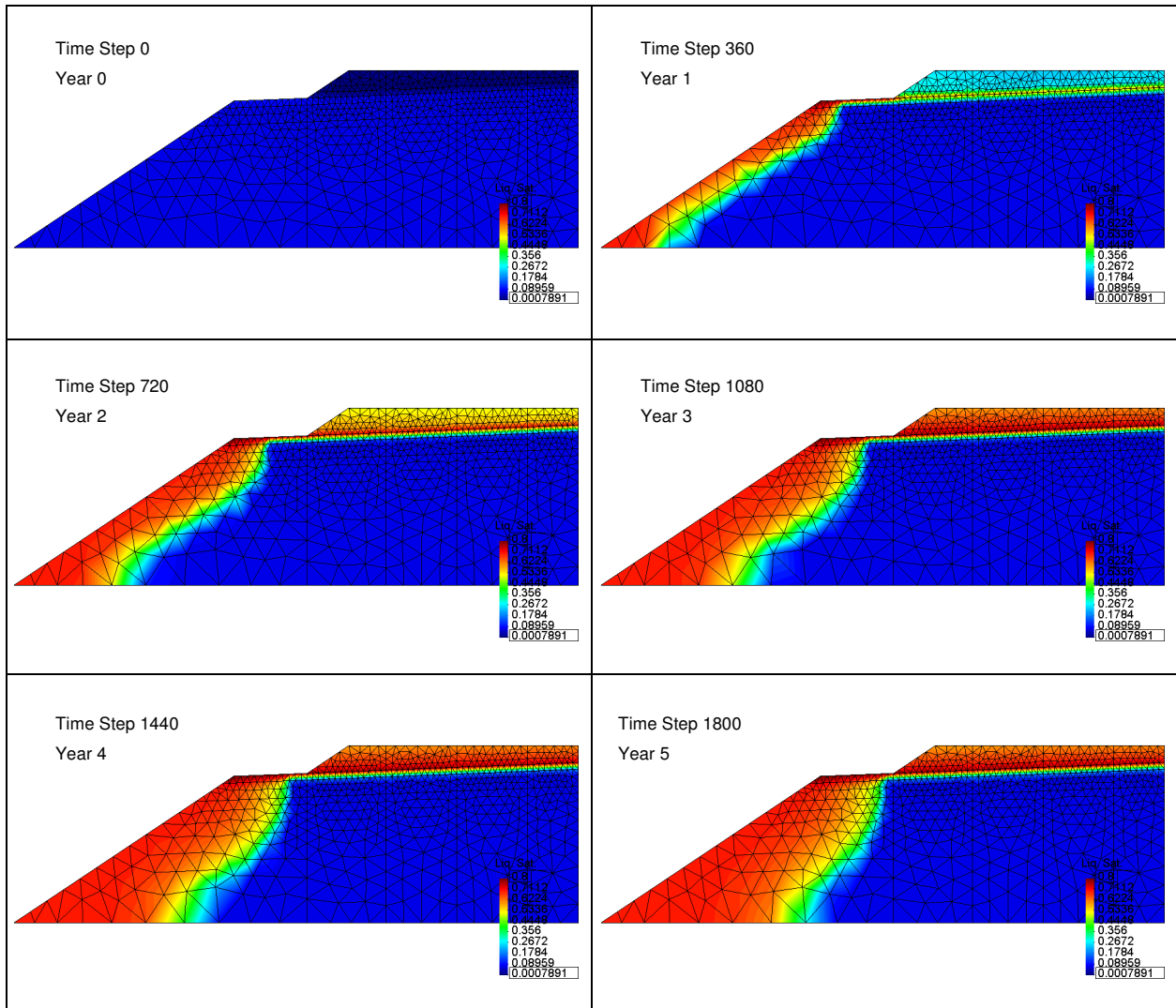


Fig. A10 – Liquid Saturation evolution along 5 years (Lower Bituminous cross section ( $\alpha = 15\%$ )).

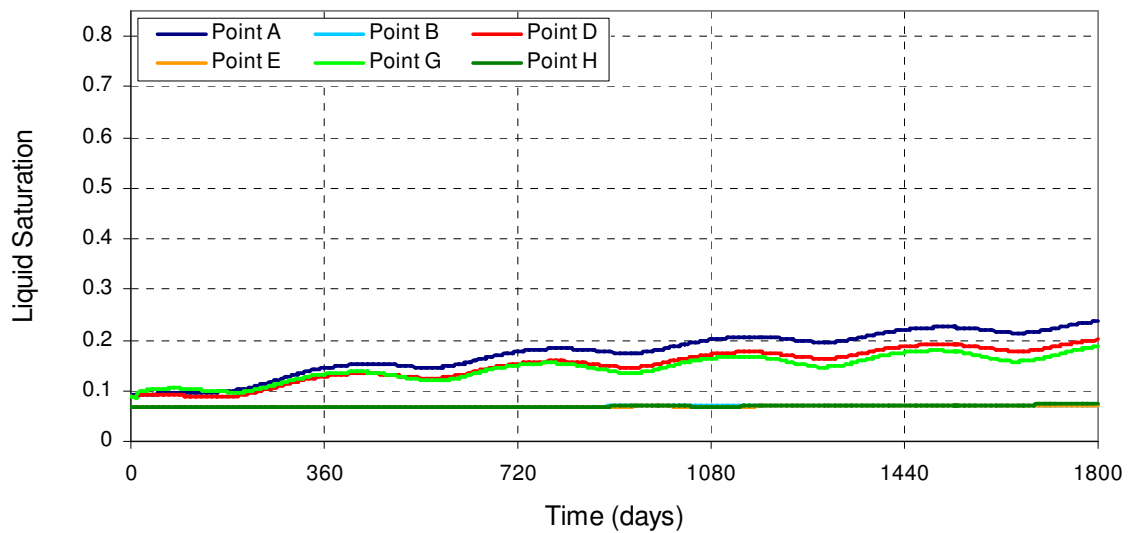


Fig. A11 – Liquid Saturation evolution on control points (Lower Bituminous cross section ( $\alpha = 15\%$ )).

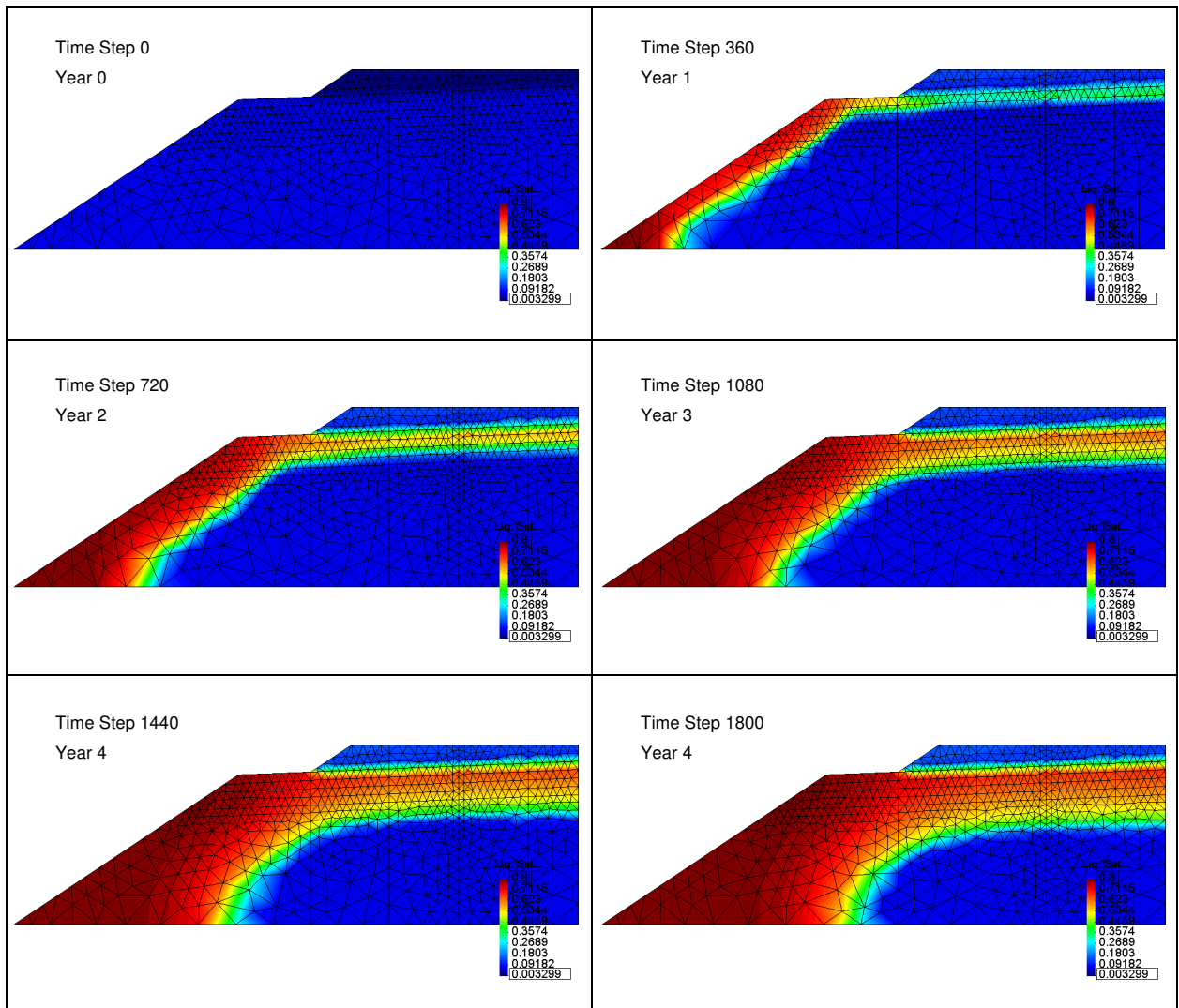


Fig. A12 – Liquid Saturation evolution during 5 years (Lower Granular cross section ( $\alpha = 15\%$ )).

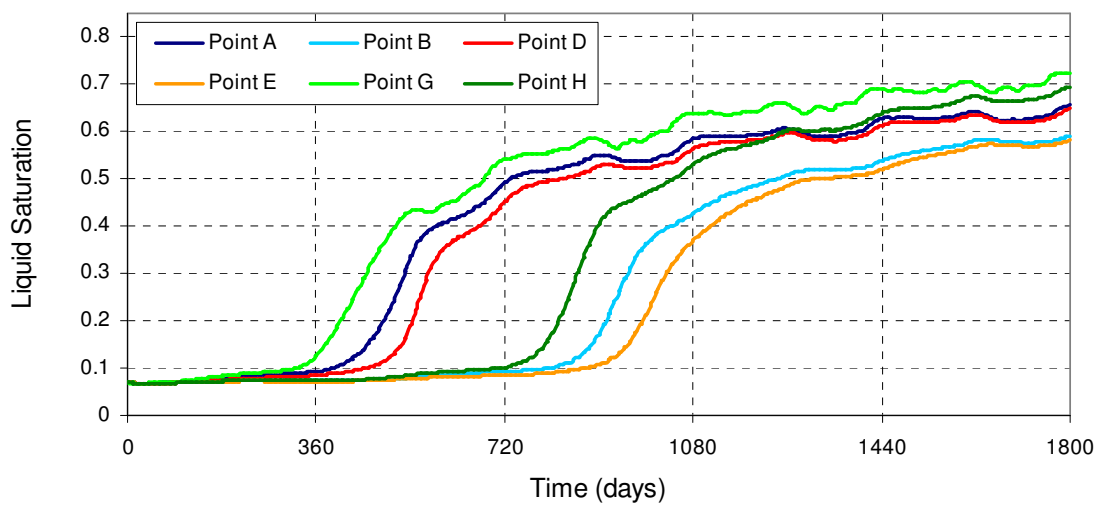


Fig. A13 – Liquid Saturation evolution on control points (Lower Granular cross section ( $\alpha = 15\%$ )).

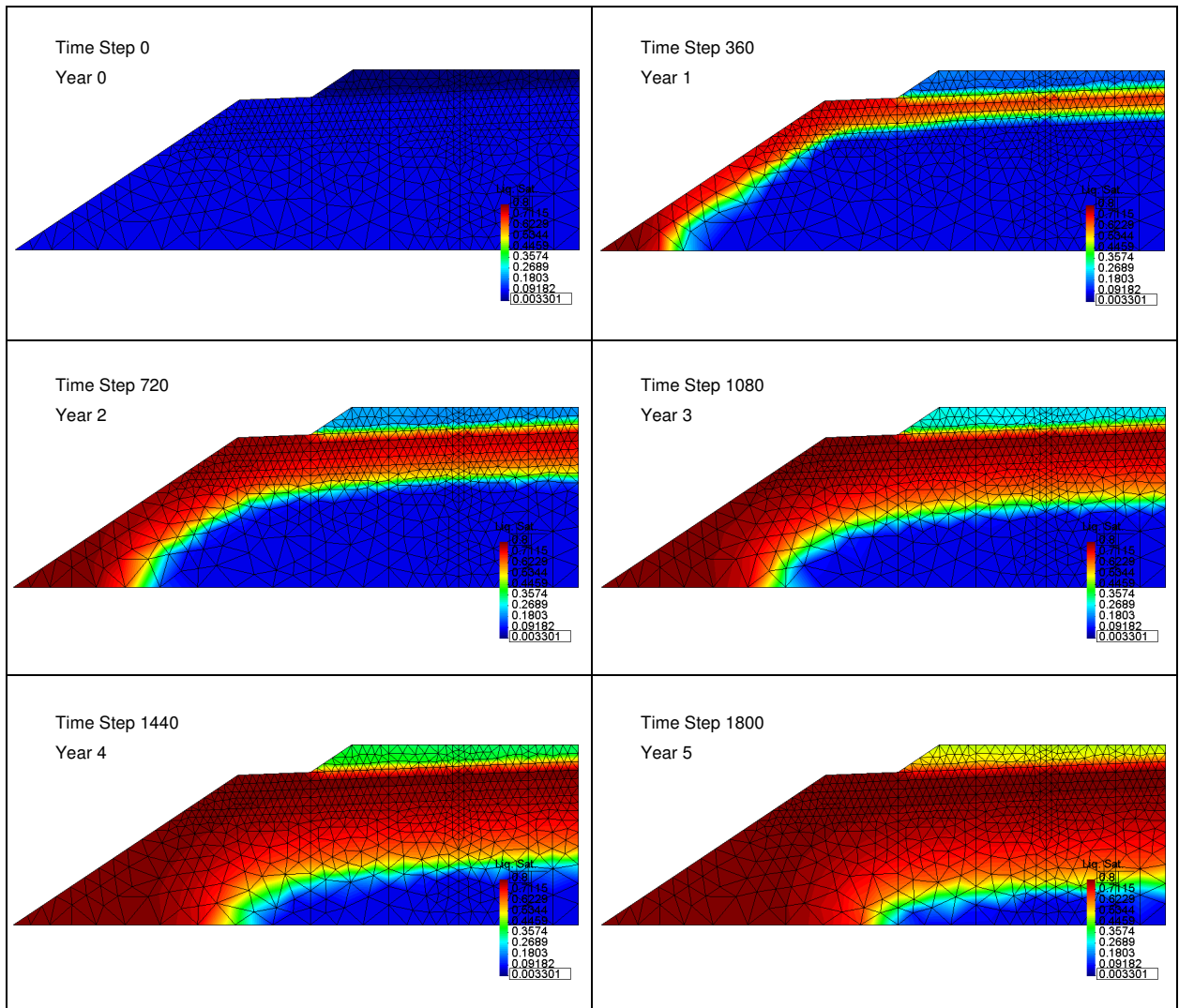


Fig. A14 – Liquid Saturation evolution during 5 years (Lower Granular cross section ( $\alpha = 30\%$ )).

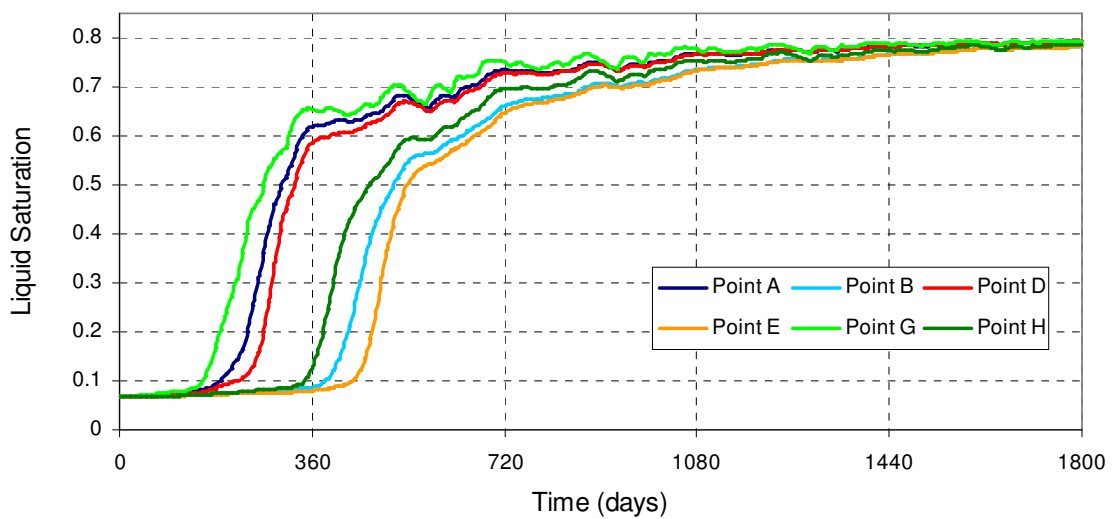


Fig. A15 – Liquid Saturation evolution on control points (Lower Granular cross section ( $\alpha = 30\%$ )).

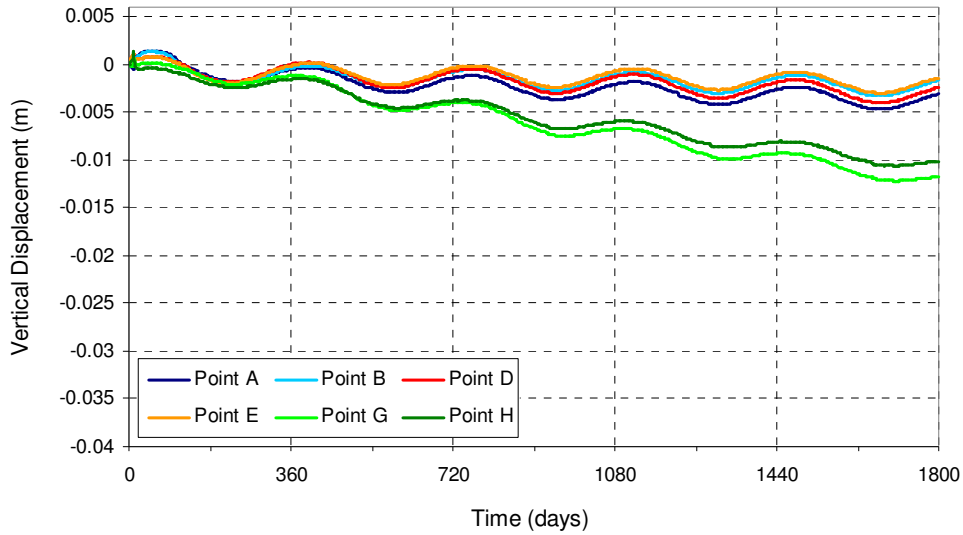


Fig. A16 – Vertical Displacements variation on control points (Lower Bituminous cross section ( $\alpha = 15\%$ )).

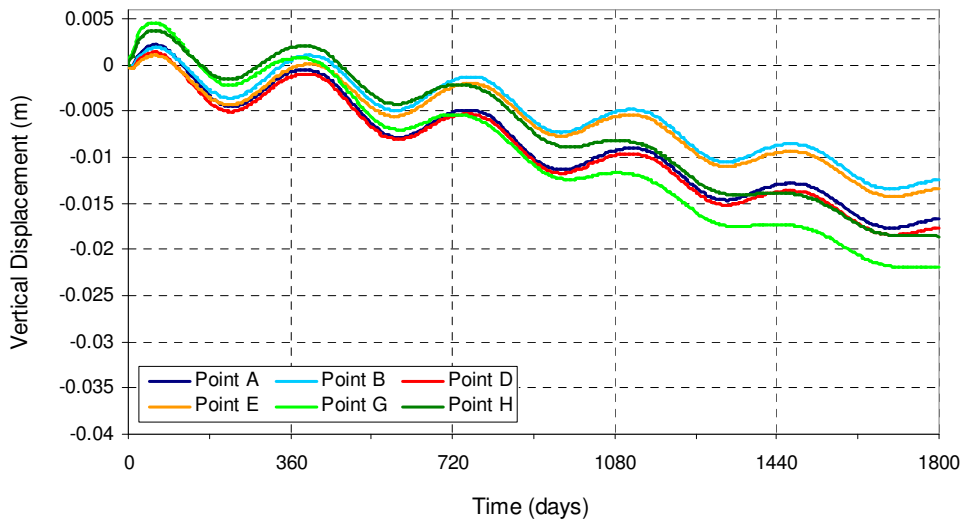


Fig. A17 – Vertical Displacements variation on control points (Lower Granular cross section ( $\alpha = 15\%$ )).

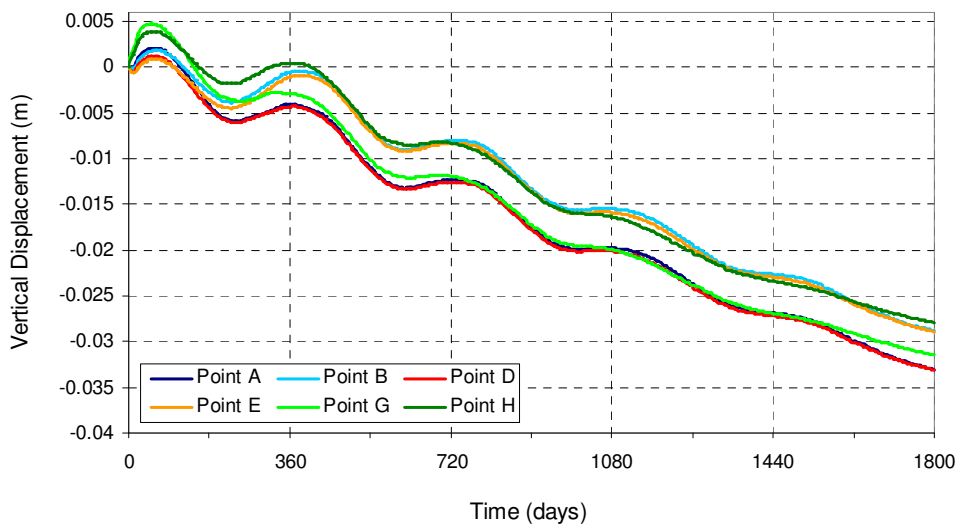


Fig. A18 – Vertical Displacements variation on control points (Lower Granular cross section ( $\alpha = 30\%$ )).